

Exploring the mid-infrared SEDs of six AGN dusty torus models II: the data

OMAIRA GONZÁLEZ-MARTÍN,¹ JOSEFA MASEGOSA,² ISMAEL GARCÍA-BERNETE,³ CRISTINA RAMOS ALMEIDA,^{4,5}
 JOSÉ MIGUEL RODRÍGUEZ-ESPINOSA,^{4,5} ISABEL MÁRQUEZ,² DONAJI ESPARZA-ARREDONDO,¹ NATALIA OSORIO-CLAVIJO,¹
 MARIELA MARTÍNEZ-PAREDES,^{1,6} CÉSAR VICTORIA-CEBALLOS,¹ ALICE PASETTO,¹ AND DEBORAH DULTZIN⁷

¹*Instituto de Radioastronomía y Astrofísica (IRyA-UNAM), 3-72 (Xangari), 8701, Morelia, Mexico*

²*Instituto de Astrofísica de Andalucía, CSIC, Glorieta de la Astronomía s/n E-18008, Granada, Spain*

³*Instituto de Física de Cantabria (CSIC-UC), Avenida de los Castros, 39005 Santander, Spain*

⁴*Instituto de Astrofísica de Canarias (IAC), C/Vía Láctea, s/n, E-38205 La Laguna, Spain*

⁵*Departamento de Astrofísica, Universidad de La Laguna (ULL), E-38205 La Laguna, Spain*

⁶*Korea Astronomy and Space Science Institute 776, Daedeokdae-ro, Yuseong-gu, Daejeon, Republic of Korea (34055)*

⁷*Instituto de Astronomía (IA-UNAM), Apartado Postal 70-264, 04510, Mexico DF, Mexico*

(Received January 1, 2019; Revised ?, 2019; Accepted September 2, 2019)

Submitted to ApJ

ABSTRACT

This is the second in a series of papers devoted to explore a set of six dusty models of active galactic nuclei (AGN) with available spectral energy distributions (SEDs). These models are the smooth torus by Fritz et al. (2006), the clumpy torus by Nenkova et al. (2008B), the clumpy torus by Hönig & Kishimoto (2010), the two phase torus by Siebenmorgen et al. (2015), the two phase torus by Stalevski et al. (2016), and the wind model by Hönig & Kishimoto (2017). The first paper explores discrimination among models and the parameter restriction using synthetic spectra (González-Martín et al. 2019A). Here we perform spectral fitting of a sample of 110 AGN drawn from the Swift/BAT survey with *Spitzer*/IRS spectroscopic data. The aim is to explore which is the model that describes better the data and the resulting parameters. The clumpy wind-disk model by Hönig & Kishimoto (2017) provides good fits for $\sim 50\%$ of the sample, and the clumpy torus model by Nenkova et al. (2008B) is good at describing $\sim 30\%$ of the objects. The wind-disk model by Hönig & Kishimoto (2017) is better for reproducing the mid-infrared spectra of Type-1 Seyferts (with 60% of the Type-1 Seyferts well reproduced by this model compared to the 10% well represented by the clumpy torus model by Nenkova et al. 2008B) while Type-2 Seyferts are equally fitted by both models (roughly 40% of the Type-2 Seyferts). Large residuals are found irrespective of the model used, indicating that the AGN dust continuum emission is more complex than predicted by the models or that the parameter space is not well sampled. We found that all the resulting parameters for our AGN sample are roughly constrained to 10-20% of the parameter space. Contrary to what is generally assumed, the derived outer radius of the torus is smaller (reaching up to a factor of ~ 5 times smaller for 10 pc tori) for the smooth torus by Fritz et al. (2006) and the two phase torus by Stalevski et al. (2016) than the one derived from the clumpy torus by (Nenkova et al. 2008B). Covering factors and line-of-sight viewing angles strongly depend on the model used. The total dust mass is the most robust derived quantity, giving equivalent results for four of these models.

Keywords: active — galaxies — mid-infrared — torus

1. INTRODUCTION

Corresponding author: Omaira González-Martín, faculty
o.gonzalez@irya.unam.mx

The nuclear obscurer of active galactic nuclei (AGN), dubbed the torus (Antonucci, & Miller 1985), produces a broad infrared spectral energy distribution (SED), whose power and shape depend on the fraction of the source absorbed, and the geometry of the absorber, re-

spectively (see Netzer 2015; Ramos Almeida & Ricci 2017, for a review on the topic). This emitting region is expected to be concentrated within the inner ~ 5 pc of the AGN (e.g. Ramos Almeida et al. 2009; Alonso-Herrero et al. 2011; Burtscher et al. 2013; López-Gonzaga et al. 2016) which makes almost impossible to image it with current single mirror telescopes due to a combination of insufficient spatial resolution and foreground contamination (Pasetto et al. 2019). Therefore, trying to reproduce the infrared SED of nearby AGN with torus models is one of the methods to constrain the properties of the nuclear obscurer.

We can divide torus models into three generic types according to the distribution of dust: continuous or smooth (e.g. Pier, & Krolik 1992; van Bemmel, & Dullemond 2003; Fritz et al. 2006), clumpy, (e.g. Dullemond, & van Bemmel 2005; Nenkova et al. 2008A,B; Höning et al. 2010; Höning & Kishimoto 2010, 2017), and composite (a combination of clumpy and continuous) (Stalevski et al. 2012, 2016; Siebenmorgen et al. 2015). However, this is not the only way to classify them. For instance, this can be done by looking at the morphological distribution of dust: torus-like (e.g. Fritz et al. 2006; Nenkova et al. 2008A,B; Höning et al. 2010; Höning & Kishimoto 2010; Stalevski et al. 2012; Siebenmorgen et al. 2015; Stalevski et al. 2016) or wind-like (e.g. Siebenmorgen et al. 2015; Höning & Kishimoto 2017) morphologies. Another way to classify torus models is according to the chemical composition and size of dust in: graphite grains (e.g. Fritz et al. 2006), standard ISM composition (e.g. Nenkova et al. 2008A,B; Höning et al. 2010; Höning & Kishimoto 2010; Stalevski et al. 2012, 2016; Höning & Kishimoto 2017), large-grains ISM composition (e.g. van Bemmel, & Dullemond 2003; Höning et al. 2010; Höning & Kishimoto 2010, 2017), or silicates and amorphous carbon (e.g. Siebenmorgen et al. 2015).

We study in a series of two papers six of these radiative transfer codes with available SEDs. Each code uses a different set of dust chemical composition, global morphology, and/or internal distribution:

1. **Smooth toroidal model by Fritz et al. (2006)** (see also Feltre et al. 2012). Radiative transfer code used to produce the SED of a simple torus geometry consisting in a flared disc that can be represented as two concentric spheres having the polar cones removed.
2. **Clumpy toroidal model by Nenkova et al. (2008B)** (see also Nenkova et al. 2008A). They developed a formalism that properly accounts for the concentration of dust in clumps or clouds, re-

ferred to as clumpy, to describe the nature of the AGN torus.

3. **Clumpy toroidal model by Höning & Kishimoto (2010)** (see also Höning et al. 2006, 2010). Radiative transfer model of 3D clumpy dust tori using optically thick dust clouds and a low torus volume filling factor.
4. **Two phase (clumpy + smooth) toroidal model by Siebenmorgen et al. (2015)**. They assumed that the dust near the AGN is distributed in a torus-like geometry with the inclusion of polar dust. The dust is distributed as a clumpy medium or an homogeneous disk, or a combination of the two.
5. **Two phase (clumpy + smooth) toroidal model by Stalevski et al. (2016)** (see also Stalevski et al. 2012). They model the dust with a torus geometry and a two-phase medium, consisting in a large number of high-density clumps embedded in a smooth dusty component of low density.
6. **Clumpy disk and outflowing model by Höning & Kishimoto (2017)**. This model consists in clumpy disk-like models (following that described by Höning & Kishimoto 2010) plus a polar, clumpy outflow.

For consistency with Paper I, these models are referred hereafter as [Fritz06], [Nenkova08], [Hoenig10], [Sieben15], [Stalev16], and [Hoenig17], respectively. Note that the main differences between [Nenkova08] versus [Hoenig10] and [Sieben15] versus [Stalev16] are the chemical composition of the dust and the radiative transfer equation solution. It is also worth to remark that the viewing angle is measured in all the cases from the pole to the equator of the system except for [Fritz06], which is measured in the opposite direction. See González-Martín et al. 2019A (hereinafter Paper I) for a complete description of these SED libraries.

The model that has been more extensively compared with the data is the clumpy model described by Nenkova et al. (2008B) (e.g. Ramos Almeida et al. 2009; Mor, & Netzer 2012; Alonso-Herrero et al. 2011; González-Martín et al. 2015; Martínez-Paredes et al. 2015; Fuller et al. 2016; González-Martín et al. 2017; Martínez-Paredes et al. 2017; García-Bernete et al. 2019). A systematic confrontation of these models against infrared SEDs is still lacking, but in those cases where it has been done, the resulting torus or cloud properties differ significantly (Höning et al. 2006; Schartmann et al. 2008).

Obj. Name	Dist. (Mpc)	Scale (kpc)	AGN class	log(L _X)	Obj. Name	Dist. (Mpc)	Scale (kpc)	AGN class	log(L _X)
(1)	(2)	(3)	(4)	(5)	(1)	(2)	(3)	(4)	(5)
1 NGC235A	95.2	1.7	Sy1.9	43.77	56 NGC4151	9.9	0.2	Sy1.5	43.17
2 Mrk348	21.5	0.4	B. AGN	43.86	57 NGC4235	24.2	0.4	Sy1.2	42.74
3 Mrk352	63.7	1.1	Sy1.2	43.19	58 M106	7.3	0.1	Sy1.9	41.06
4 NGC454E	51.9	0.9	Sy2	42.79	59 Mrk50	100.4	1.8	Sy1	43.43
5 NGC526A	81.8	1.4	Sy2	43.78	60 NGC4388	19.3	0.3	Sy2	43.64
6 ESO297-018	108.0	1.9	Sy2	43.99	61 NGC4395	4.2	0.1	Sy2	40.86
7 NGC788	58.3	1.0	Sy2	43.51	62 NGC4507	50.5	0.9	Sy1.9	43.76
8 Mrk590	91.2	1.6	Sy1.5	43.23	63 ESO506-G027	107.2	1.9	Sy2	44.11
9 IC1816	72.6	1.3	Sy1.8	43.14	64 NGC4686	71.7	1.3	Sy2	43.20
10 NGC973	60.0	1.0	Sy2	43.46	65 NGC4941	14.2	0.2	Sy2	41.78
11 NGC1052	20.6	0.4	B. AGN	42.24	66 NGC4939	36.1	0.6	Sy2	42.81
12 ESO417-G006	69.8	1.2	Sy2	43.27	67 ESO323-077	64.3	1.1	Sy1.5	43.19
13 NGC1275	69.0	1.2	B. AGN	43.76	68 NGC4992	107.7	1.9	Sy2	43.89
14 ESO548-G081	62.0	1.1	Sy1.9	43.29	69 IIZS010	146.8	2.6	Sy1.5	43.52
15 2MASXJ0350-5018	156.3	2.7	Sy2	43.83	70 MCG-03-34-064	85.6	1.5	Sy1.9	43.28
16 ESO549-G049	112.6	2.0	Sy1.9	43.52	71 CenA	3.8	0.1	B. AGN	42.98
17 3C120	141.4	2.5	. AGN	44.38	72 MCG-06-30-015	33.2	0.6	Sy1.9	42.89
18 MCG-02-12-050	155.7	2.7	Sy1.2	43.74	73 NGC5252	83.6	1.5	Sy2	44.09
19 MCG-01-13-025	68.1	1.2	Sy1.5	43.29	74 IC4329A	68.8	1.2	Sy1.5	44.18
20 CGCG420-015	125.9	2.2	Sy2	43.72	75 UM614	140.0	2.4	Sy1.5	43.60
21 2MASXJ0505-2351	150.1	2.6	Sy2	44.22	76 Mrk279	130.4	2.3	Sy1.5	43.87
22 CGCG468-002NED01	75.0	1.3	Sy1.9	43.26	77 CircinusGalaxy	4.2	0.1	Sy2	42.07
23 Ark120	138.2	2.4	Sy1	44.25	78 NGC5506	23.8	0.4	Sy1.9	43.31
24 PICTORA	150.1	2.6	Sy2	44.03	79 NGC5548	107.6	1.9	Sy1.5	43.76
25 NGC2110	35.6	0.6	Sy2	43.65	80 ESO511-G030	64.1	1.1	Sy1	43.65
26 2MASXJ0558-3820	145.1	2.5	Sy1.2	43.86	81 Mrk477	161.6	2.8	Sy1.9	43.66
27 Mrk3	61.4	1.1	Sy1.9	43.79	82 IC4518A	69.6	1.2	Sy2	43.19
28 ESO426-G002	96.1	1.7	Sy2	43.44	83 Mrk841	156.0	2.7	Sy1.2	44.01
29 UGC03478	45.9	0.8	Sy1.2	42.49	84 Mrk1392	154.8	2.7	Sy1.5	43.75
30 UGC03601	73.3	1.3	Sy1.9	43.08	85 Mrk290	126.7	2.2	Sy1.5	43.68
31 Mrk78	159.1	2.8	Sy2	43.50	86 ESO138-G001	39.1	0.7	Sy2	42.55
32 Mrk10	83.7	1.5	Sy1.5	43.47	87 Mrk501	119.0	2.1	B. AGN	44.27
33 IC0486	116.3	2.0	Sy1.9	43.75	88 NGC6300	12.3	0.2	Sy2	42.46
34 Mrk1210	57.8	1.0	Sy1.9	43.37	89 Fairall49	85.7	1.5	Sy1.9	43.11
35 Mrk622	99.5	1.7	Sy2	43.10	90 ESO103-035	56.9	1.0	Sy1.9	43.63
36 Mrk18	47.5	0.8	Sy1.9	42.61	91 Fairall51	45.9	0.8	Sy1.5	43.22
37 MCG-01-24-012	84.1	1.5	Sy2	43.61	92 ESO141-G055	158.9	2.8	Sy1.2	44.25
38 MCG+04-22-042	138.5	2.4	Sy1.2	43.93	93 NGC6814	11.8	0.2	Sy1.5	42.59
39 Mrk110	141.0	2.5	Sy1.5	44.25	94 Mrk509	147.3	2.6	Sy1.2	44.44
40 Mrk705	124.8	2.2	Sy1.2	43.54	95 IC5063	37.9	0.7	Sy2	43.29
41 MCG+10-14-025	168.6	2.9	Sy1.9	43.41	96 NGC7130	69.2	1.2	Sy1.9	43.01
42 MCG-05-23-016	36.3	0.6	Sy1.9	43.53	97 Mrk520	108.0	1.9	Sy2	43.71
43 NGC3081	25.3	0.4	Sy2	43.07	98 NGC7172	33.9	0.6	Sy2	43.43
44 ESO374-G044	121.9	2.1	Sy2	43.64	99 NGC7212NED02	114.2	2.0	Sy2	43.30
45 NGC3227	18.8	0.3	Sy1.5	42.58	100 NGC7213	22.0	0.4	B. AGN	42.46
46 NGC3281	45.7	0.8	Sy2	43.32	101 NGC7314	16.7	0.3	Sy1.9	42.47
47 NGC3393	53.6	0.9	Sy2	42.98	102 Mrk915	103.3	1.8	Sy1.9	43.63
48 Mrk417	140.3	2.4	Sy2	43.91	103 MCG+01-57-016	107.0	1.9	Sy1.5	43.42
49 Mrk421	85.2	1.5	B. AGN	44.46	104 UGC12282	71.2	1.2	Sy2	43.15
50 NGC3783	47.8	0.8	Sy1.2	43.56	105 NGC7603	126.4	2.2	Sy1	44.02
51 NGC3786	50.9	0.9	Sy1.9	42.41	106 UGC00488	143.5	2.5	Sy1	43.61
52 UGC06728	27.9	0.5	Sy1.2	42.40	107 Mrk1066	51.7	0.9	Sy2	42.51
53 2MASXJ1145-1827	141.1	2.5	Sy1.2	44.08	108 NGC3147	39.6	0.7	Sy2	42.20
54 Ark347	96.1	1.7	Sy2	43.52	109 ESO439-G009	105.8	1.8	Sy2	43.27
55 UGC07064	107.1	1.9	Sy1.9	43.28	110 Mrk273	161.8	2.8	Sy2	43.24

Table 1. Observational details of the AGN sample. Col. 1 gives the object name, Col. 2 the distance in Mpc, Col. 3 the spatial scale obtained with the short-low *Spitzer*/IRS spectral module (note that the long-low IRS/*Spitzer* module gives roughly 3 times lower resolution), Col. 4 the optical class reported by Oh et al. (2018), and Col. 5 the 2-10 keV intrinsic X-ray luminosity reported by Oh et al. (2018). “B. AGN” refers to beamed AGN (jet closely oriented toward the line of sight to the observer), according to the nomenclature reported by Oh et al. (2018).

In paper I we produced a set of synthetic spectra from current instruments GTC/CanariCam and *Spitzer*/IRS and future *JWST*/MIRI and *JWST*/ NIRSpec instruments using this set of six SED libraries. We found that, for a reasonable source brightness ($F_{12\mu\text{m}} > 100\text{mJy}$), we can actually distinguish among models except for parent models. We also found that the torus parameters can be constrained within 15% error, irrespective of the instrument used, for all but [Hoenig17]. The questions we try to answer in this second paper are: (1) are the models good enough to describe the mid-infrared SED of AGN? (2) which is the preferred model by the data? and (3) what can we say about the parameters involved and derived quantities, as the outer radius of the torus,

covering factor, and total dust mass, depending on the model used?

With these aims we confronted this set of SED libraries against a set of mid-infrared *Spitzer*/IRS spectra of 110 AGN selected from the *Swift*/BAT survey. The paper is organized as follows. Section 2 gives a brief summary of the AGN sample used along this paper. Section 3 describes the spectral fitting procedure. The main results on the spectral fitting are included in Section 4 and discussed in Section 5. The paper is summarized in Section 6.

2. THE SAMPLE AND THE DATA

We built an AGN sample with available low spectral resolution mid-infrared IRS/*Spitzer* spectra to confront

with models. As shown in Paper I, low spectral resolution IRS/*Spitzer* spectra provide enough coverage and sensitivity to constrain most of the parameters of the models at least for sources with intermediate brightness (i.e. $F_{12\mu\text{m}} \sim 100$ mJy), although host galaxy dilution should be taken into account.

To avoid biases against obscured objects (i.e. highly obscured AGN undetected by, e.g., optical wavelengths) we based our sample in the 105-months *Swift*/BAT survey (Oh et al. 2018). Out of the 1632 sources detected by the survey, 447 are identified as AGN with a redshift lower than 0.04 (i.e. distance below 170 Mpc, using $H_0 = 70\text{km/s/Mpc}$). We restricted the sample to the nearby Universe to ensure relatively high spatial resolution using IRS/*Spitzer* spectra (see spatial scales computed for the short-low IRS/*Spitzer* module¹ in Table 1, Col. 3). We then used CASSIS(Lebouteiller et al. 2011) to look for the data and downloaded the optical extraction provided. We avoided HR (high resolution) *Spitzer* data because they show poorer cosmetic continuum emission in the form of jumps when putting together each small wavelength module that conforms these spectra. LR (low resolution) *Spitzer* spectra are better joined because they are made up only by four of these wavelength modules. Among the 447 AGN, we found observations for 110 AGN. Table 1 includes the observational details of our sample.

According to their AGN classification, the sample contains 60 type-1 Seyferts (five Sy1, 13 Sy1.2, 17 Sy1.5, one Sy1.8, and 24 Sy1.9), 41 type-2 Seyferts, and eight beamed AGN. Beamed AGN are those with a jet pointing close to the line of sight to the observer. They cover a wide range of distances (4–168 Mpc) and therefore, a spatial scale for the unresolved IRS/*Spitzer* spectra of ~ 70 pc up to ~ 3 kpc. This spatial resolution reinforces the need for the spectral decomposition performed in this paper to decontaminate AGN dust from circumnuclear contributors. We also excluded all the observations extracted as extended within CASSIS because they are clearly dominated by off-nuclear processes (that have a major impact on the determination of the torus parameters, see Paper I). Our sample expands almost four orders of magnitude in X-ray luminosities ($\log(L_X) = 40.9 - 44.5$), with $12\mu\text{m}$ fluxes from ~ 10 mJy up to ~ 30 Jy. Note that this selection includes intermediate luminosity (ILAGN, $\log(L_{\text{bol}}) = 42 - 45$) and low-luminosity AGN (LLAGN, $\log(L_{\text{bol}}) < 42$). However, it excludes high luminosity AGN (HLAGN or

¹ The short-low IRS/*Spitzer* module gives 3.6 arcsec spatial resolution. The long-low IRS/*Spitzer* module gives roughly 3 times lower resolution.

QSOs, $\log(L_{\text{bol}} > 45)$ due to the cut in distance. The AGN with strong silicate emission features, including a set of QSOs, will be the subject of a subsequent investigation (Martínez-Paredes in prep.).

We converted the spectra into XSPEC (Arnaud 1996) format using FLX2XSP task within HEASOFT. These files are easily read by XSPEC to perform statistical tests when fitting to models².

3. SPECTRAL FITTING PROCEDURE

3.1. Model independent fit

In Paper I we compare the spectral shape of the different models by quantifying some features in our *Spitzer*/IRS synthetic spectra. These features are:

- Spectral slopes: We computed three spectral slopes of the form $\alpha = -\log(F_{\nu}(\lambda_2)/F_{\nu}(\lambda_1))/\log(\lambda_2/\lambda_1)$, with $\lambda_2 > \lambda_1$. Note that, under this nomenclature, negative (positive) values mean that the flux increases (decreases) with wavelength. We called α_{NIR} , α_{MIR} , and α_{FIR} to the slopes evaluated at $[\lambda_1, \lambda_2]$ equal to $[5.5, 7.5]$, $[7.5, 14]$, and $[25, 30]\mu\text{m}$, respectively³. These wavelengths were motivated from the residual analyses of the synthetic spectra and to compare with previous analysis (Hernán-Caballero et al. 2015; García-González et al. 2017; Höning & Kishimoto 2017).
- Silicate features strength: We also computed the silicate feature strength using the formula $\text{Si}_{\lambda} = -\ln(F_{\nu}(\lambda)/F_{\nu}(\text{continuum}))$, for the two silicate features located at $\sim 9.7\mu\text{m}$ and $\sim 18\mu\text{m}$. Silicate features in emission (absorption) show negative (positive) Si_{λ} .

We computed the same quantities for the 110 objects analyzed in this paper. Errors are computed as one standard deviation from 100 realizations with random variations of the spectral bins fluxes within the flux error. The resulting values for the $9.7\mu\text{m}$ silicate feature and α_{MIR} are fully consistent with those derived by García-González et al. (2017).

3.2. Dusty models

We fitted the *Spitzer*/IRS spectra of our sample of 110 AGN using the six models discussed throughout this paper. We excluded the narrow wavelength ranges where

² Note that models were also converted into XSPEC format, see Paper I.

³ Note that we called NIR, MIR and FIR slopes to those closer to the near-infrared, in the middle of the mid-infrared, and close to the far-infrared, respectively, although the three are in the mid-infrared wavelength range.

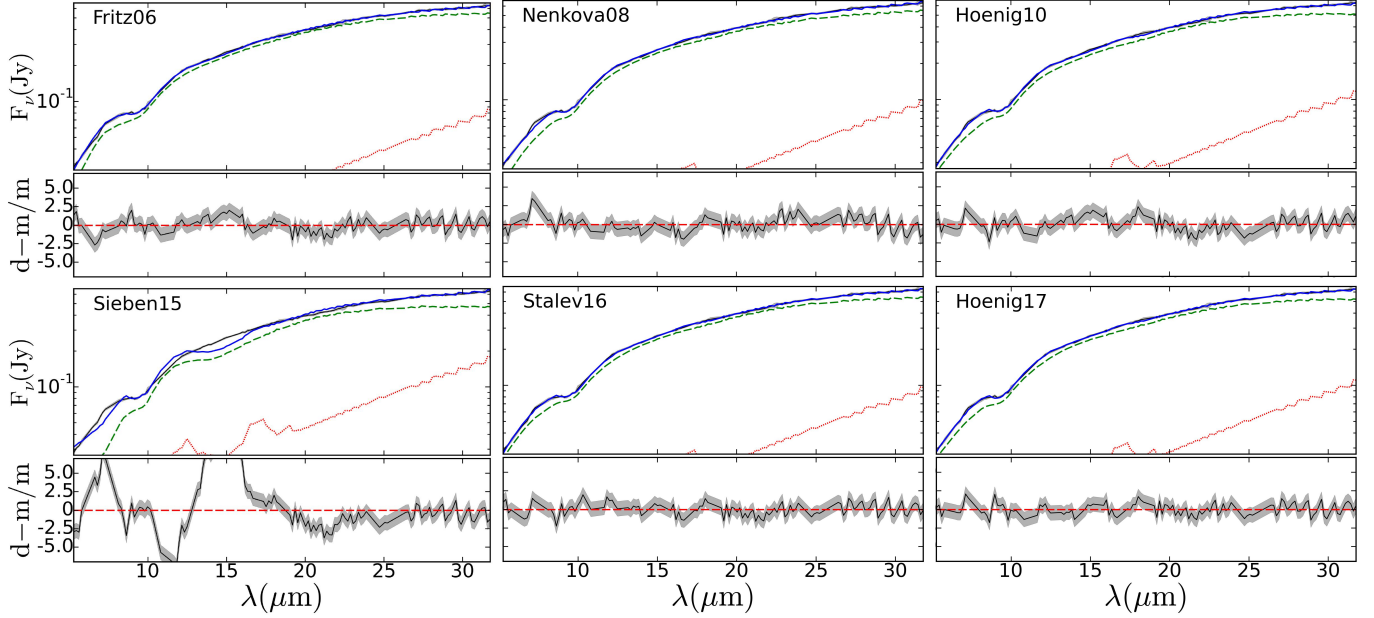


Figure 1. Best fit (top panel) and residuals (bottom panel) per parameter resulting when fitting the type-2 Seyfert galaxy IC 5063 with each model. Green dashed, red dotted, and blue continuous lines show AGN dust, the ISM components, and the sum of all the components, respectively. Note that, although not seen in the plot due to its low contribution, stellar component is included to explain wavelengths below $< 7\mu\text{m}$ for [Fritz06], [Nenkova08], and [Sieben15] (see Table 4).

the brightest emission lines are expected in order to isolate the continuum emission. We also added foreground extinction by dust grains to the dusty models using the ZDUST component (Pei 1992), already included as a multiplicative component within XSPEC. This component is suitable to describe foreground extinction in the infrared, optical, and UV wavebands. We used the Milky Way extinction curve and let free to vary the color excess $E_{(B-V)}$. We remark that extinction does not have a strong impact on the results; i.e. without foreground extinction we found identical results.

We added the stellar and/or ISM components to the best fitting AGN dust model for each source to account for circumnuclear components. The ISM component is taken from Smith et al. (2007), which are averaged Starburst templates in the $\sim 5\text{-}160\mu\text{m}$ wavelength range for different 6.2, 7.7, 11.3, and $17\mu\text{m}$ PAH feature strengths (see their Fig. 13). The stellar component corresponds to a stellar population of 10^{10} years and solar metallicity from the stellar libraries provided by Bruzual & Charlot (2003) (see Paper I for more details). Overall, the baseline models used to fit the data are:

$$M1 = zdust \times \{\text{Dust model}\} \quad (1)$$

$$M2 = zdust \times \{\text{Dust model}\} + \text{Stellar} \quad (2)$$

$$M3 = zdust \times \{\text{Dust model}\} + \text{ISM} \quad (3)$$

$$M4 = zdust \times \{\text{Dust model}\} + \text{ISM} + \text{Stellar} \quad (4)$$

	F06	N08	H10	S15	S16	H17
α_{NIR}	77.3	48.2	92.3	43.6	51.8	96.4
α_{MIR}	73.6	41.8	97.3	18.2	44.5	98.2
α_{FIR}	96.4	88.2	65.5	73.6	82.7	64.5
$\text{Si}_{9.7\mu\text{m}}$	97.3	84.5	64.5	98.2	96.4	72.7
$\text{Si}_{18\mu\text{m}}$	96.4	93.6	85.5	88.2	85.5	83.6
$\alpha_{\text{NIR}} \text{ vs } \alpha_{\text{MIR}}$	42.7	11.8	27.3	6.4	21.8	51.8
$\alpha_{\text{MIR}} \text{ vs } \alpha_{\text{FIR}}$	41.8	14.5	4.5	6.4	30.0	9.1
$\text{Si}_{9.7\mu\text{m}} \text{ vs } \text{Si}_{18\mu\text{m}}$	17.3	27.3	28.2	24.5	30.9	35.5

Table 2. Percentage of objects with the spectral parameters recovered by the synthetic SEDs. F06: [Fritz06]; N08: [Nenkova08]; H10: [Hoenig10]; S15: [Sieben15]; S16: [Stalev16]; and H17: [Hoenig17].

For all of them the initial parameters are set to the mean value. We compute the χ^2 statistics throughout to guarantee that we found an absolute minimum. We then used f-statistics to test whether the inclusion of the stellar, ISM, or the stellar+ISM components significantly improves the simpler model when f-test probability is below 10^{-4} . We also obtained the χ^2 statistics for the parameter space in 50 equally spaced bins with the SPEC command STEPPAR, which yields to the probability distribution function (PDF).

4. RESULTS

Table 4 (Appendix A) shows the best-fit model results per object (F06: [Fritz06]; N08: [Nenkova08]; H10: [Hoenig10]; S15: [Sieben15]; S16: [Stalev16]; and H17: [Hoenig17]), including the percentage contribution to

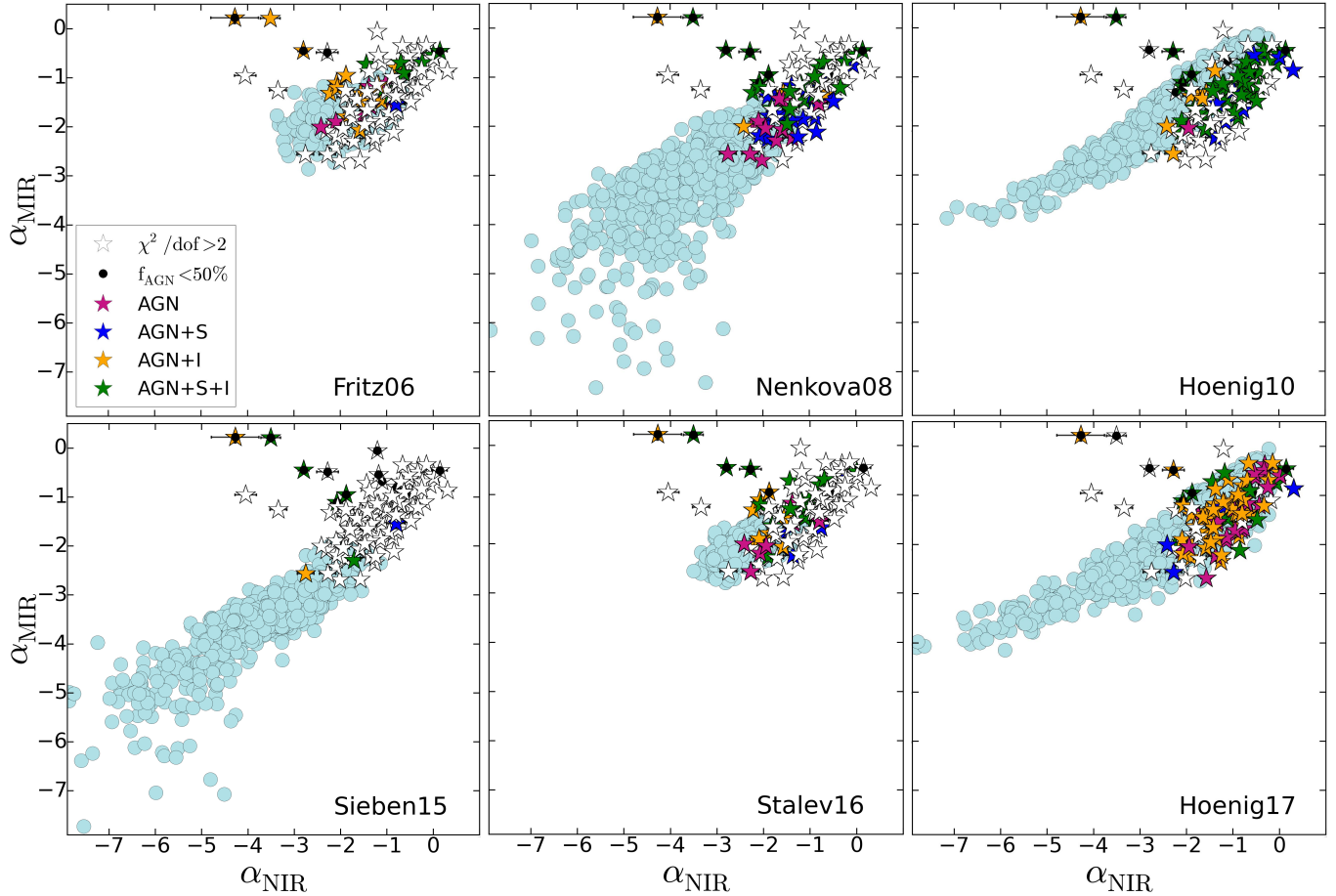


Figure 2. Spectral slope computed as the flux ratio between 14 and $7.5\mu\text{m}$ (α_{MIR}) versus the spectral slope computed as the flux ratio between the 7.5 and $5.5\mu\text{m}$ (α_{NIR}). Synthetic spectral results (Paper I) are shown with cyan circles and objects with stars. Objects where we were able to fit the spectrum (i.e. $\chi^2/\text{dof} < 2$) to pure AGN dust model, AGN+stellar, AGN+ISM, and AGN+stellar+ISM are shown with purple, blue, orange, and green stars. Objects not well fitted to any of the combinations are shown with white stars. Objects with low contribution of AGN dust are marked with a black dot.

the $5\text{-}30\mu\text{m}$ waveband per component (A: AGN; S: Stellar; and I: ISM), the reduced χ^2 (χ^2/dof , where dof is the degree of freedom), color excess for the foreground extinction, and the final parameters per model. Fig. 1 shows the results on the spectral fitting to the six dusty models for IC 5063 as an example.

Following our analysis on the synthetic spectra (Paper I), we selected objects showing high percentage of AGN (AGN-dominated hereinafter) as those with less than 50% of stellar component compared to the torus component at $5\mu\text{m}$ and less than 50% of ISM component compared to the torus component at $30\mu\text{m}$. They are marked with empty circles next to the model name in Table 4. We then considered as the best fit that showing the minimum χ^2/dof , and comparably good fits those with $\chi^2/\text{dof} < \min(\chi^2/\text{dof}) + 0.5$. They are marked with filled circles next to the model name in Table 4.

4.1. Adequacy of the models

We investigate the goodness of the fits to the data by comparing spectral slopes and silicate feature strengths for data and models. Figs. 2, 3, and 4 show the results for α_{NIR} versus α_{MIR} , α_{MIR} versus α_{FIR} , and $\text{Si}_{18\mu\text{m}}$ versus $\text{Si}_{9.7\mu\text{m}}$. These plots allow us to compare the spectral shape from models (circles) with our sample results (stars). The percentage of objects that are reproduced by the models are recovered in Table 2.

Objects requiring only the AGN dust model to fit its spectrum nicely fall in the same area compared to the synthetic spectra. However, many objects are in this area but they still require additional contributors or they cannot be fitted to the model at all. The reason is that they cannot predict at the same time all these features.

[Hoenig17] is the best at describing the near-infrared and mid-infrared spectral slopes, with $\sim 52\%$ of the objects within the grid of models (see Fig. 2). [Fritz06] is

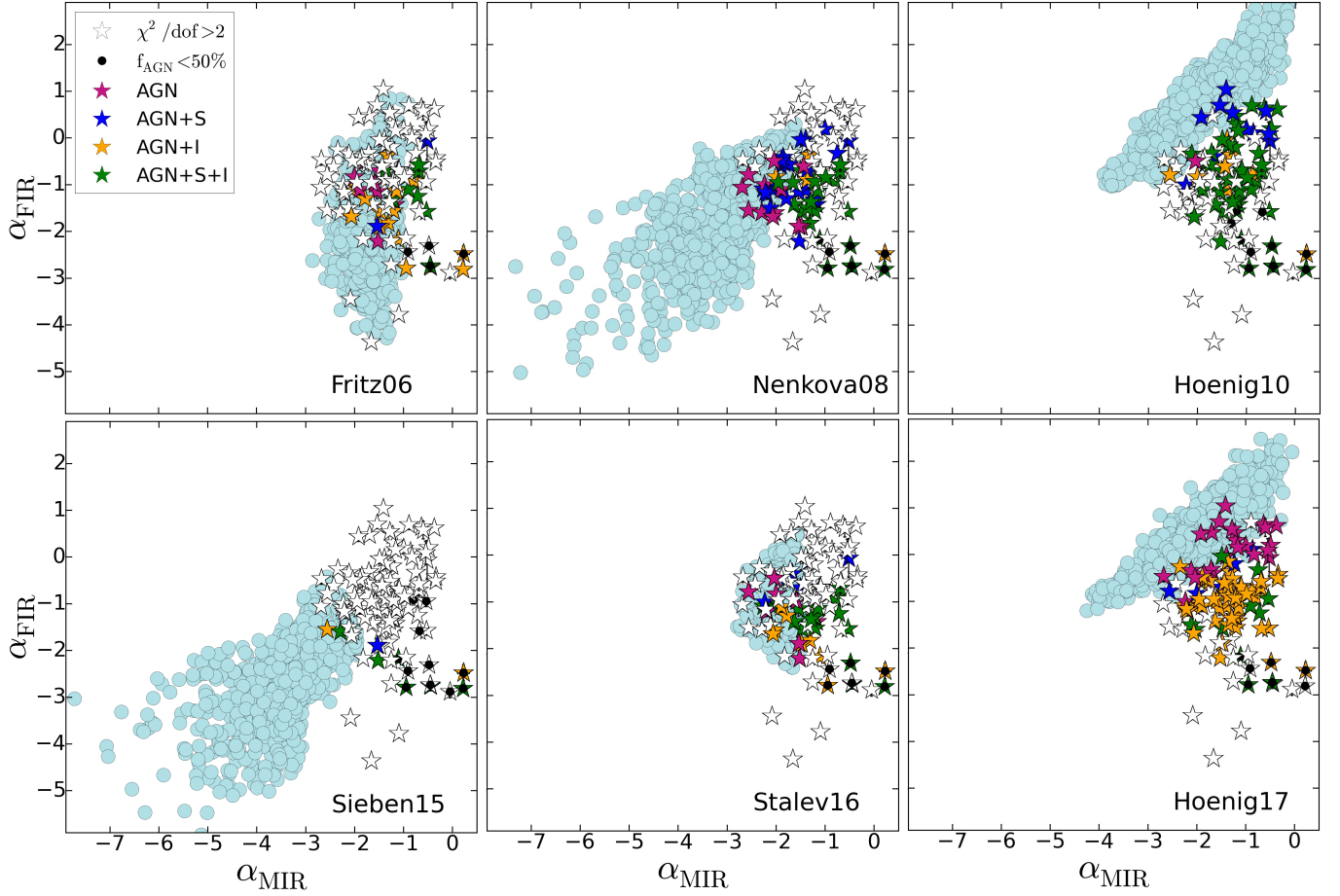


Figure 3. Spectral slope computed as the flux ratio between 30 and 25 μm (α_{FIR}) versus the spectral slope computed as the flux ratio between the 14 and 7.5 μm (α_{MIR}). Symbols as in Fig. 2.

also good at describing these slopes with $\sim 43\%$ of the sample within the grid of models. The other models are only able to describe $\sim 6 - 27\%$ of the objects, failing at describing at the same time flat near- and mid-infrared slopes. The best models at describing at the same time mid- and far-infrared slopes are [Fritz06] and [Stalev16] (see Fig. 3), with 30-40% of the AGN spectra with compatible slopes by these models compared to the $\sim 5-15\%$ of the sample with the rest of models.

These discrepancies between the observations and models are compensated by the inclusion of ISM and/or stellar components. For instance, [Hoenig17] manages to find a good fit including an ISM component to make the far-infrared slopes steeper (clearly seen by the large number of AGN+ISM best fits in Fig. 3). Furthermore, the lack of steepness of the near- and far-infrared slopes in [Hoenig10] is compensated by adding a stellar and ISM component in many objects (Figs. 2 and 3).

Interestingly, all the models produce a large fraction of SEDs that are not describing any observed spectrum,

suggesting that the parameter space is not realistic. The best models on that aspect are [Fritz06] and [Stalev16], although they also miss a significant proportion of the parameter space that we observe for our targets. We further explore this result by tracking different ranges of the model parameters to evaluate if a single parameter can produce this unrealistic parameter space. We found that the flat spectral index for the distribution of dust ($a > -1$) explains most of the SEDs producing simultaneously the steep near- and mid-infrared slopes for [Hoenig10] and [Hoenig17]. Small viewing angles with respect to the disk/torus equator also produce SEDs with steep near- and mid-infrared slopes. However, small viewing angles can also produce realistic values for these SED slopes and not all the unrealistic SED slopes are produced by SEDs with small viewing angles. Therefore, it seems that a single parameter cannot explain this effect.

In general, all the models fail at describing the strength of both silicate features at the same time,

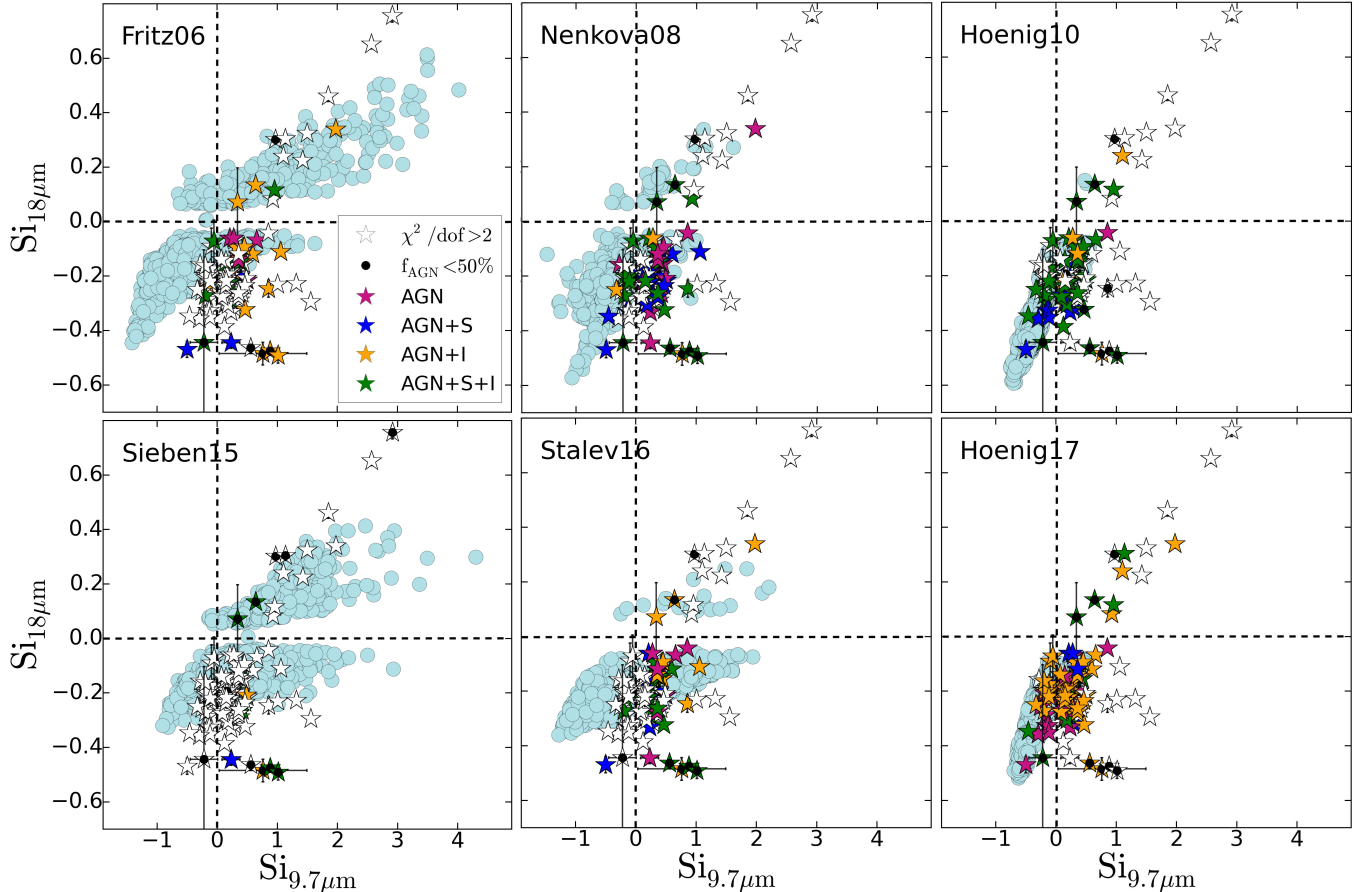


Figure 4. $18\mu\text{m}$ Silicate feature strength versus $9.7\mu\text{m}$ Silicate feature strength. Symbols as in Fig. 2.

with 17–35% of the sample well described by the models (see Table 2). Large silicate absorption features are not described by any of the models (see Fig. 4). These features might be associated with deeply dust-enshrouded objects like ULIRGs. However, some of them were not well fitted including the ISM component. This might indicate that our ISM templates need to be further extended in order to find good fits for these objects. Most objects reproduce the $9.7\mu\text{m}$ but fail to predict the $18\mu\text{m}$ silicate emission feature strength when the $9.7\mu\text{m}$ silicate feature is in absorption (also discussed in Martinez-Paredes et al. in prep.). Extremely large $18\mu\text{m}$ silicate emission features ($\text{Si}_{18\mu\text{m}} < -0.4$) are associated to low AGN dust contribution. In those cases the silicate feature is associated to dust heated by strong star-forming processes rather than the AGN. Again, the range of strengths of the silicate features of the models is larger compared to the data for all of them except [Hoenig10] and [Hoenig17]. In particular, all of them include SEDs with strong silicate emission features ($\text{Si}_{9.7\mu\text{m}} < -0.5$) which are not observed in the data. This is a well reported issue for smooth models and in

fact it is one of the reasons why clumpy models gained certain credibility against smooth models (Dullemond, & van Bemmel 2005; Feltre et al. 2012). However, the clumpy torus model by [Nenkova08] also predicts extreme silicate emission features which are not observed in our AGN sample. We do not expect any kind of bias against AGN with strong silicate emission features in our sample (that might be the case for absorption features contaminated by circumnuclear contributors). The clumpy torus model by [Hoenig10], although similar to [Nenkova08], better reproduces the range of silicate feature strengths. This yield to the conclusion that the differences might arise from parameter spaces or details on the radiative transfer solution. Indeed [Hoenig10] shows narrower parameter ranges than [Nenkova08] for the opacity of the clouds and the number of clouds along the equatorial plane (see Table 1 in Paper I). Moreover, in contrast to [Nenkova08], [Hoenig10] does not consider a limit on the outer radius of the torus (fixed to $Y = 150$). We also attempted here to find if a single model parameter could explain the unrealistic strengths of the silicate emission features. Although, in general,

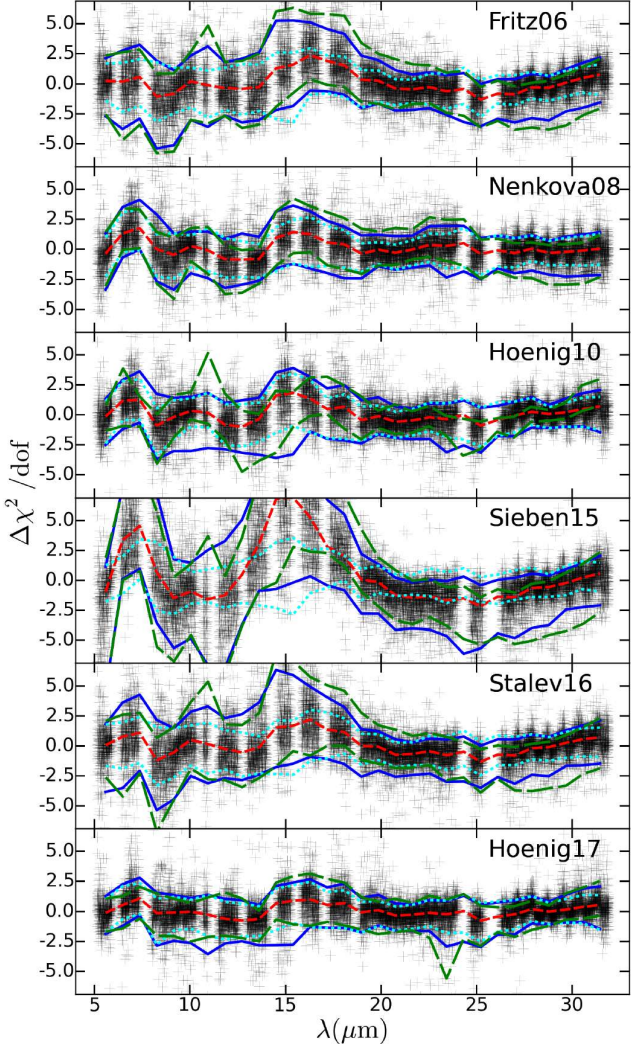


Figure 5. Residuals (expressed in terms of $\Delta\chi^2/\text{dof}$) on the spectral fit for the AGN sample with *Spitzer*/IRS data versus wavelength. The red short-dashed line shows the median value versus wavelength. The blue continuous, green long-dashed, and cyan dotted lines represent the 5 and 95% percentiles of the distribution for the entire sample, AGN-dominated (less than 50% of stellar component compared to the torus component at 5 μm and less than 50% of ISM component compared to the torus component at 30 μm), and spectral fits with $\chi^2/\text{dof} < 2$, respectively.

we could not find a single parameter for each model, it is interesting to notice that a small angular width of the torus ($\sigma < 30^\circ$) produces many of these SEDs with unrealistic strengths of the silicate emission feature for [Stalev16].

The goodness of the fit per model can also be evaluated in Fig. 5, which shows the residuals for all the spectra. The largest discrepancies between data and models are found for [Sieben15]. Even for objects with $\chi^2/\text{dof} < 2$ (cyan dotted line), the residuals are sig-

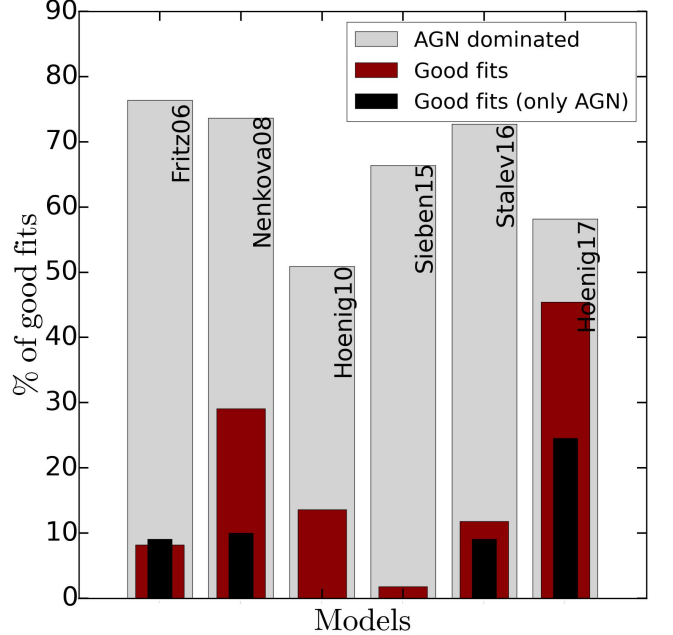


Figure 6. Percentage of objects with the mid-infrared flux dominated by the AGN component (AGN-dominated, gray filled bars), the percentage of those objects that are well fitted ($\chi^2/\text{dof} < 2$) with the AGN models plus circumnuclear contributors (brown filled bars), and those objects that are well fitted with only AGN models (black filled bars).

nificantly larger than those obtained when fitting the synthetic spectra to the same model used to produce them (see Paper I). This might indicate that the complexity of the spectra is not recovered by any of the models discussed here. AGN-dominated spectra (green long-dashed lines in Fig. 5) show discrepancies near the 9.7 and 18 μm silicate features (with residuals peaking at 11 and 15–17 μm), in the slopes below $\sim 7 \mu\text{m}$, and in the slopes above 25 μm . Among them, apart from [Sieben15], slightly larger residuals are shown when fitting to [Fritz06] and [Stalev16]. Indeed, both models show quite similar residuals, most probably because they come from the same radiative transfer code (SKIRT) with the same dust geometry. Objects showing a large contribution of stellar or ISM components (blue continuous) tend to show deep silicate absorption features compared to AGN-dominated spectra (green long-dashed lines).

Fig. 6 shows the percentage of AGN-dominated spectra (grey filled bars). 60% of objects where the nucleus is isolated at a resolution better than 500 pc are AGN-dominated. The AGN-dominated spectra are not directly linked to the spatial scales achieved by *Spitzer*/IRS because it is also dependent on the AGN bolometric luminosity and the particular environment of the source. The AGN isolation needs to be examined ob-

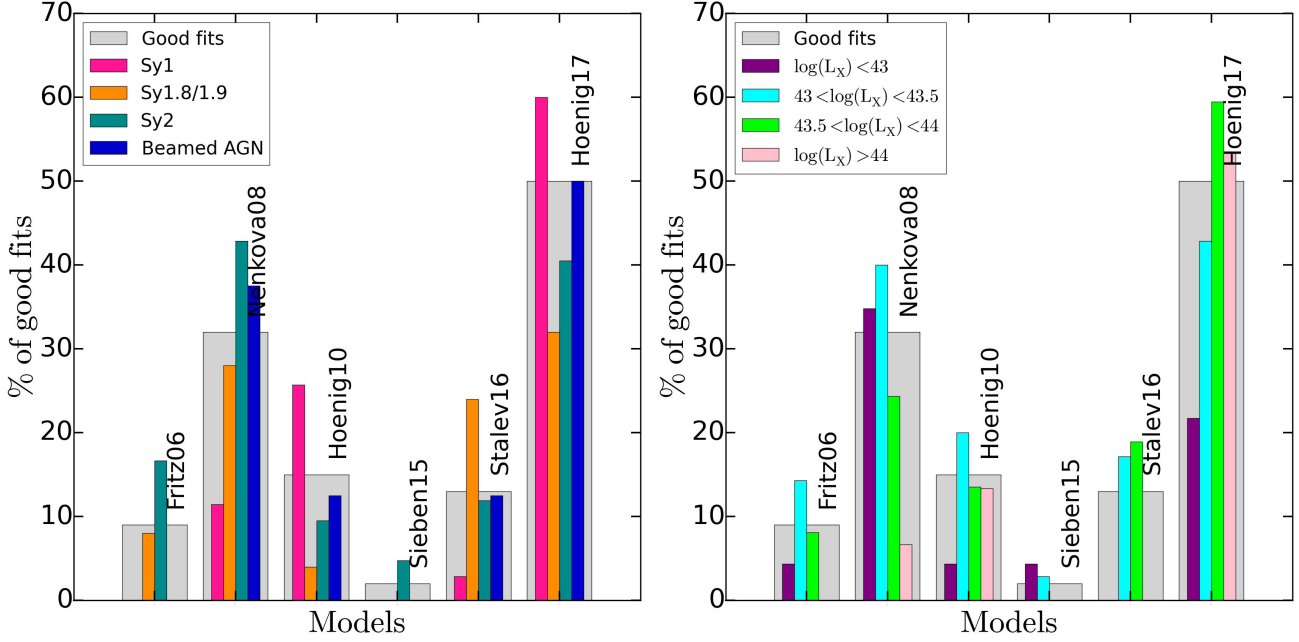


Figure 7. Broad gray bars show the total the percentage of objects with good fits. Narrow bars show percentage of objects with good fits per optical type (left panel) and luminosity range (right panel).

ject by object. Moreover, even this result depends on the model used; the largest number of objects that are AGN-dominated is found for [Fritz06] ($\sim 75\%$) and the lowest if found for [Hoenig10] ($\sim 50\%$). This is probably due to the fact that two of the main differences between models are the slopes at short and long wavelengths, which is compensated by the inclusion of different fractions of ISM and stellar components when fitting the data. Fig. 6 also shows the percentage of (AGN-dominated) objects that can be well fitted to each model (brown filled bars) and the same results but only using AGN dust model (i.e. without including circumnuclear components, see black filled bars in Fig. 6). The largest number of objects well fitted to a model is recovered when using [Hoenig17] ($\sim 45\%$) and the lowest number is found for [Sieben15] ($< 5\%$). [Nenkova08] also represents well the spectra for almost $\sim 30\%$ of the spectra. The number of objects well fitted to [Fritz06], [Hoenig10], and [Stalev16] drops to $\sim 10\%$. Note that these results change if we fit the spectra using only AGN dust models (black filled bars in Fig. 6). In this case, the percentage of objects with good fits decreases to 25% for [Hoenig17], and [Fritz06], [Nenkova08], and [Stalev16] show 10% of good fits.

We also investigate if the goodness of the fit depends on the optical type (Fig. 7, left panel) and the X-ray luminosity (Fig. 7, right panel). We split the sample into 31 Sy1s (including Sy1, Sy1.2, and Sy1.5), 25 Sy1.8/Sy1.9, 41 Sy2, and 8 beamed AGN (Oh et al. 2018). Moreover, we divided the sample into four segments of X-ray luminosities ($\Delta \log(L_X) = 0.5$) that

contain 23, 35, 37, and 15 objects from the lowest ($42.5 < \log(L_X) < 43$) to the highest ($44 < \log(L_X) < 44.5$) luminosity bin. Around 60% of the Sy1 and 4 out of the 8 beamed AGN are well fitted to [Hoenig17]. [Nenkova08] failed to reproduce Sy1, obtaining 10% of good fits. Note that this might be improved by a proper account of the AGN disk component. Furthermore, roughly 40% of the Sy2 and beamed AGN are well fitted to [Nenkova08] or [Hoenig17]. A lower percentage is obtained for Sy1.8/1.9 spectra (roughly 30% using [Nenkova08] or [Hoenig17]). Not far from these numbers and despite the low percentage of good fits, [Stalev16] seems to work for some Sy1.8/1.9 (20% of them). An important result is that, among the two models showing the largest number of good fits (i.e. [Nenkova08] and [Hoenig17]), [Hoenig17] is better suited for high-luminous AGN and [Nenkova08] for low-luminosity AGN. [Stalev16] seems to work only for intermediate luminosities.

4.2. Goodness of the parameter determination

We also investigate how well we constrain the parameters of the fit for those spectra that are AGN-dominated with $\chi^2/\text{dof} < 2$. Following the procedure used for the synthetic spectra (see Paper I), we consider that a parameter is restricted when its error bar is less than 15% of the parameter space. Irrespective of the model, roughly 80% of the parameters are restricted when a good fit is found. No particular differences are found for groups of either optical type or X-ray luminosity. Note,

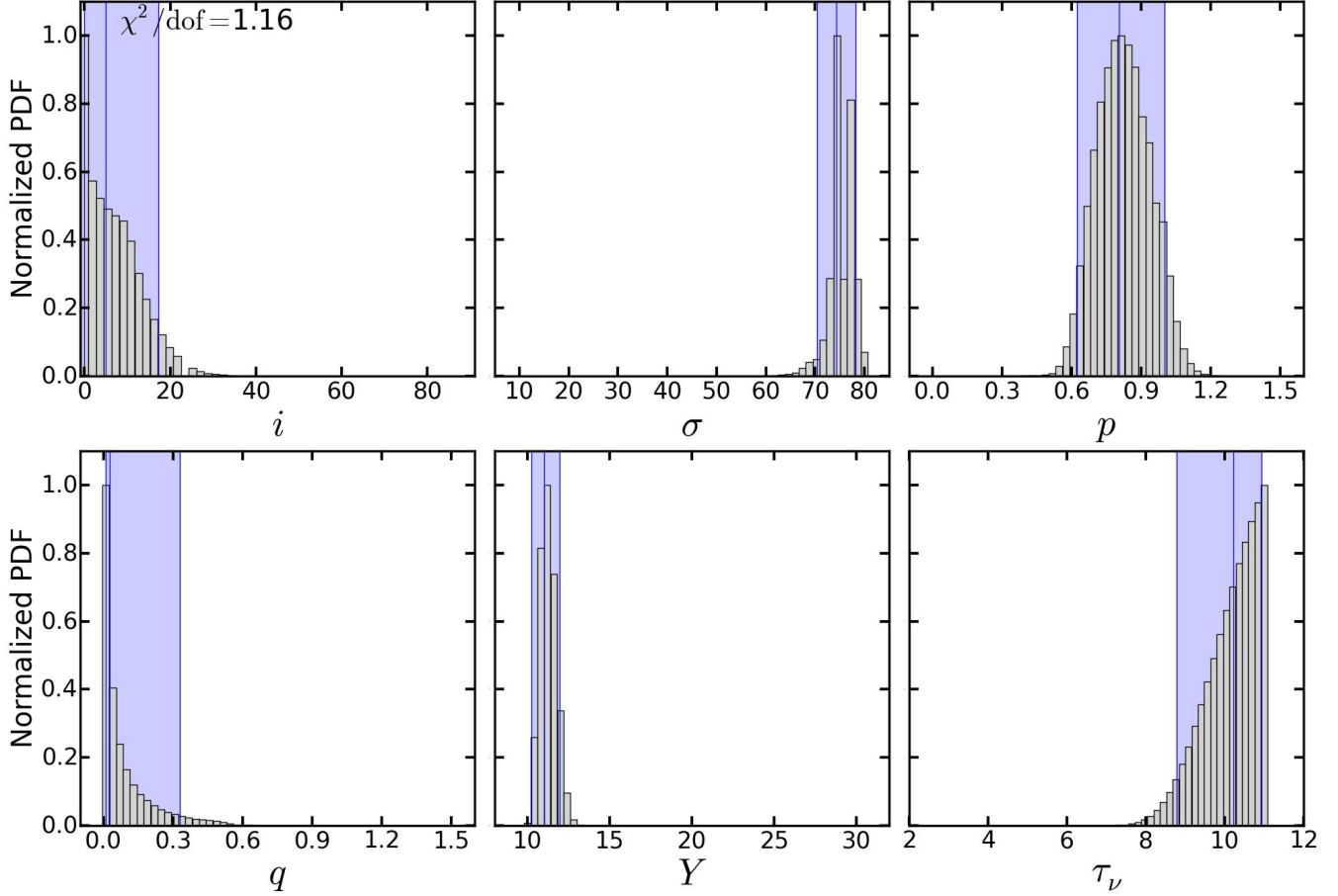


Figure 8. Probability distribution function (PDF, gray filled histogram) per parameter resulting when fitting IC5063 to [Stalev16]. Blue vertical line and blue shadowed area show the weighted median and 10-90% percentiles of the distribution per parameter.

however, that many parameters are clustered to the high or low limits. This might indicate that better results could be achieved if some parameters cover a broader parameter space (we further illustrate this below).

The analysis above assumes that the errors show a Poisson distribution so the standard deviation is a good representation of its error. However, this is not the case in general, with asymmetric parameter posterior distributions (see Fig. 8 for an example of the resulting PDF for IC 5063 using [Stalev16] model). From now on we use the PDFs to study the goodness of the parameters. Note that we also operate with the PDFs to compute derived quantities (e.g. dust mass, see below).

We use individual PDFs to build a parameter versus parameter plot by adding the normalized PDFs for all the objects in the sample. Fig. 9 shows the parameter versus parameter plots for [Nenkova08] (all the models included in Appendix B). This plot is computed as the addition of all the PDFs of the individual objects. Any horizontal or vertical cut shows the PDF found for a par-

ticular parameter value. The dispersion of the plot accounts for the accuracy on the determination of the parameter because it reflects the broadening of the PDFs for the full sample. A good parameter estimate will bring a good correlation along with the diagonal axis of the plot. Broad PDFs will yield to a non-linear relation in this parameter versus parameter plot. How the broadening of the distribution changes along the parameter space also gives information on the accuracy of the parameter determination. Finally, we can also explore with this plot which range of parameters is preferred by the sample (studying the distribution per parameter overlaid as blue-filled histograms) and if the parameter space is not enough to cover the spectral shapes shown by the data, i.e. when objects show parameters that tend to be clustered to the limits of the parameter space.

Fig. 9 confirms some of our results on the constraints of the parameters for [Nenkova08] model using synthetic spectra (Paper I): Parameters Y , q , and τ_ν are much better constrained than i , N_H , and σ . However, these plots

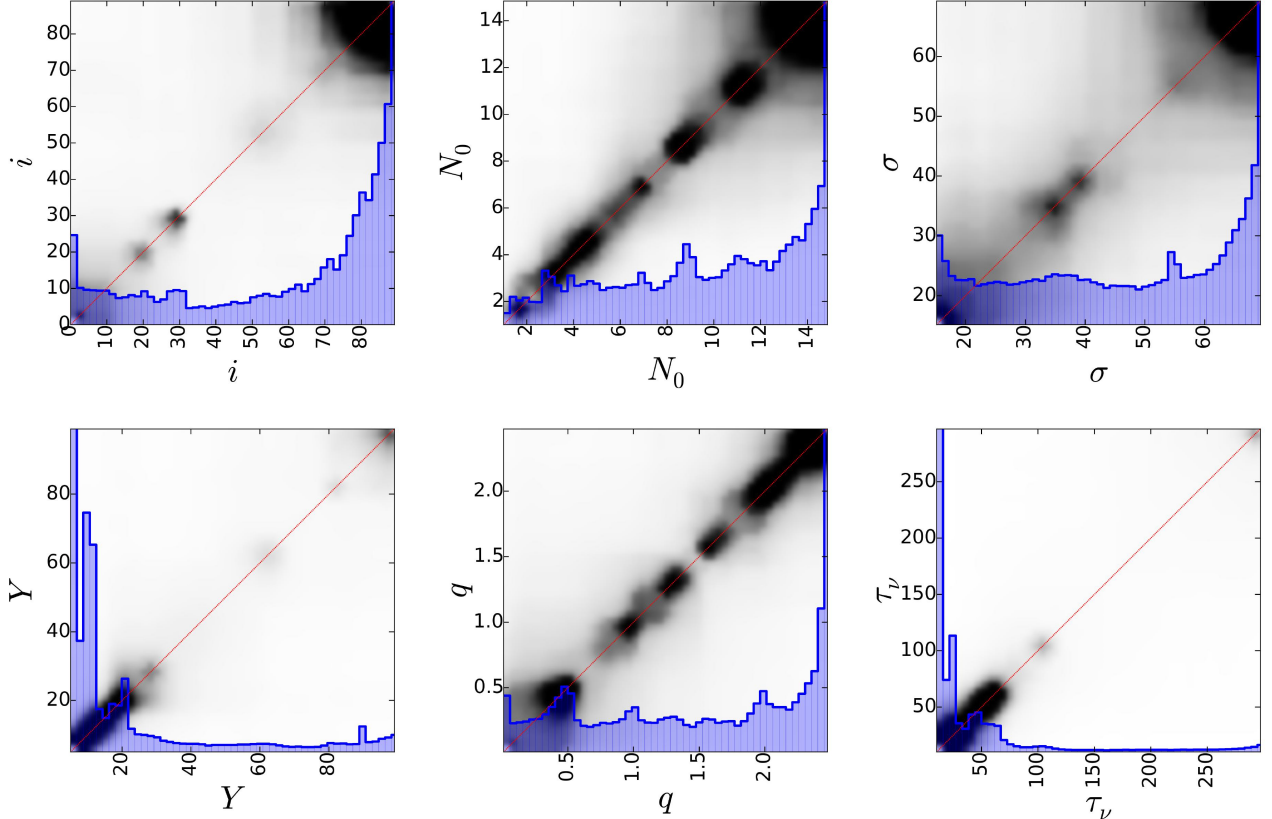


Figure 9. Parameter versus parameter estimated from the sample drawn from the probability distribution function (PDF, see text) for the model [Nenkova08]. The blue filled histogram shows the total AGN sample distribution per parameter. The minimum color level shows probabilities of 1%. The red line shows the one-to-one relation.

show further information. Firstly, some parameters are less constrained toward the lower and/or upper limits of the parameter range (e.g. i). Furthermore, objects tend to cluster toward the lower and upper boundaries for some parameters. For instance, above 30% of objects reaches the upper limit for N_0 . Finally, our sample prefers a narrow range of values compared to the parameter range (e.g. $\tau_\nu < 100$ and $Y < 40$). Different results might come from a sub-set of objects well fitted with a particular model. In order to investigate that, we repeated the analysis using only results with $\chi^2/\text{dof} < 2$ and AGN-dominated spectra. We recover similar results when using only good fits except for the clustering of some parameters at the lower and upper boundaries. For instance the density distribution slope γ in [Fritz06] reaches the high limit only when using all the results. Moreover, further restriction of the parameters are found. For instance, Y in [Stalev16] is restricted to values $Y < 15$ when using good fits. No differences are found when using the sub-set of AGN-dominated spectra.

Table 3 shows a summary of the results found using these parameter versus parameter plots for all the mod-

els. Note that all the parameters show a correlation coefficient $r > 0.8$, indicating that they are constrained. In general, the parameters are restricted to the 10-20% of its parameter space (consistent with our synthetic spectral analysis, see Paper I). We detect clear broadening of this percentage to the low and/or high limit for most of the parameters and many of them tend to be clustered at the low and high limit. This might further suggest that a strong revision of the SED libraries could result on a better match of the mid-infrared spectra. Table 3 summarizes some information that modelers may use to produce SED libraries adequate for the diversity of AGN dust.

An extension of these plots, in which we confront different parameters for a particular model, is useful to investigate if any parameter of the model is linked to another, therefore studying internal degeneracies among parameters. In practice, we repeat the analysis for each parameter with all the other parameters of the model looking for linear relations among them. This resulted in 10, 15, and 21 plots ($N(N - 1)/2$, with N the number of parameters) for models with five (i.e. [Hoenig10] and [Sieben15]), six (i.e. [Fritz06], [Nenkova08], and

Model	Par	Error	Comments	
			(%)	Error dependency
(1)	(2)	(3)	(4)	(5)
[F06]	i	9	low limit	pegged at $i = 20$
	σ	8	low limit	pegged at $\sigma = 20$
	γ	11		pegged at $\gamma = 0$
	β	15	high limit	pegged at $\beta = -1$
	Y	4		pegged at $Y = 0$
	τ_ν	10		pegged at $Y = 10$
[N08]	i	17	low and high limit	pegged at $i = 90$
	N_0	15	high limit	pegged at $N_0 = 15$
	σ	19	low and high limit	pegged at $\sigma = 70$
	Y	13		only $Y < 50$
	q	15	high limit	pegged at $Y = 10$
	τ_ν	10		pegged at $q = 2.5$
[H10]	i	15	low limit	pegged at $i = 0$
	N_0	13	high limit	pegged at $i = 90^*$
	θ	17	high limit	pegged at $N_0 = 10$
	a	6		pegged at $\theta = 60$
	τ_ν	12	low and high limit	only $\theta > 40^{**}$
	i	10		pegged at $a = 0$
[S15]	R_{in}	5		pegged at $\tau_\nu = 80$
	η	6		pegged at $R_{in} = 3$
	τ_{cl}	9	high limit	pegged at $\eta = 0^*$
	τ_{disk}	11		pegged at $\tau_{cl} = 100$
	i	12		pegged at $i = 90$
	σ	7		pegged at $\sigma = 10$
[S16]	p	10		pegged at $\sigma = 80$
	q	18		pegged at $p = 0$
	Y	7		pegged at $p = 1.5$
	τ_ν	11		pegged at $q = 0$
	i	12		pegged at $q = 1.5$
	σ	7		pegged at $Y = 10$
[H17]	N_0	20	high limit	only $Y < 15^{**}$
	a	11	low limit	pegged at $Y = 3$
	σ_θ	21	high limit	pegged at $a = -3$
	θ	20	high limit	pegged at $\sigma_\theta = 7.5$
	a_w	15	high limit	pegged at $\theta = 15$
	h	18	low and high limit	pegged at $a_w = -0.5$
	f_{wd}	18		pegged at $h = 0.1$
	i	16		pegged at $f_{wd} = 0.75$
	N_0	20		pegged at $i = 0$
	a	11		pegged at $i = 90$
	σ_θ	21		pegged at $N_0 = 10$
	θ	20		pegged at $a = -3$

Table 3. Summary of parameter results (F06: [Fritz06]; N08: [Nenkova08]; H10: [Hoenig10]; S15: [Sieben15]; S16: [Stalev16]; and H17: [Hoenig17]). (Col. 1): model name; (Col. 2): parameter name; (Col. 3): average percentage of error according to the standard deviation of the distributions compared to the parameter range; (Col. 4): comments on the dependency of the error on the parameter range; and (Col. 5): comments on the adequacy of the parameter range to the sample. We refer to the parameter results that are clustered toward the low and/or high limit as “pegged” following XSPEC syntax. In Col. 5 we mark with single asterisks the parameters that do not longer cluster to limits of parameter space when using only good fit results and with double asterisks those restrictions on the parameter that appear only when using only good fits (i.e. $\chi^2/\text{dof} < 2$).

[Stalev16]), and eight (i.e. [Hoenig17]) parameters, respectively. We did not find any linear relation among parameters of the same model, at least for the present sample. Note, however, that this relationship might be coupling several parameters at the same time or could not be linear. The study of such a complex coupling of parameters is out of the scope of this research.

We attempted a final extension of these plots, looking for linear relations between a particular parameter and all the parameters of the other models, could be used to find equivalencies between parameters of different models. This resulted in 537 parameter versus parameter plots. However, we did not find any linear relation between parameters. This implies that even external parameters as the viewing angle toward the observer, depend on the model assumption. Therefore, we confirmed the result from synthetic spectra (Paper I); the parameter results strongly depend on the chosen model.

We also investigated if different optical types or luminosity ranges lie in different parameter ranges by plotting the histograms of these sub-sets of objects. However, we did not find any significant relation among the parameters.

4.3. Derived quantities: outer radius, covering factor, and total dust mass

Although the values obtained for the individual parameters might not be well constrained (and, as shown above, the results depend on the model), some derived quantities could still be robust (e.g. the covering factor as suggested by [Ramos Almeida et al. 2011](#)). We explore here three derived quantities with strong physical significance: (1) outer radius of the torus; (2) total AGN dust mass; and (3) covering factor. We produced the PDF for each quantity, model, and object deriving it from the PDFs of the individual parameters involved.

We provide below the results for these derived quantities. As a general note, the following analysis was performed using the entire sample but we found the same using only good spectral-fit results (i.e. $\chi^2/\text{dof} < 2$) or using AGN-dominated objects only. Furthermore, no significant differences were found on the distribution of the derived quantities by splitting the sample into AGN types⁴. Finally, we have found awkward distributions for [Sieben15]. In particular, it shows a narrow range of covering factors and unrealistic dust masses ($\log(M_{\text{dust}}) > 6$) for a large fraction of sources.

4.3.1. Outer radius of the torus R_{out}

The Y parameter is fixed to a large value for all the SEDs in [Hoenig10], [Sieben15], and [Hoenig17]. Therefore, deriving R_{out} makes no sense for these three models. We derived R_{out} using the Y parameter PDF for [Fritz06], [Nenkova08], and [Stalev16]. Fig. 10 shows the parameter versus parameter plots for the R_{out} PDFs of the full sample. The correlation coefficient is $r > 0.8$ in all cases, except for [Fritz06] versus [Nenkova08]

⁴ We did not split the sample into bolometric luminosity bins because all these quantities depend on the luminosity itself.

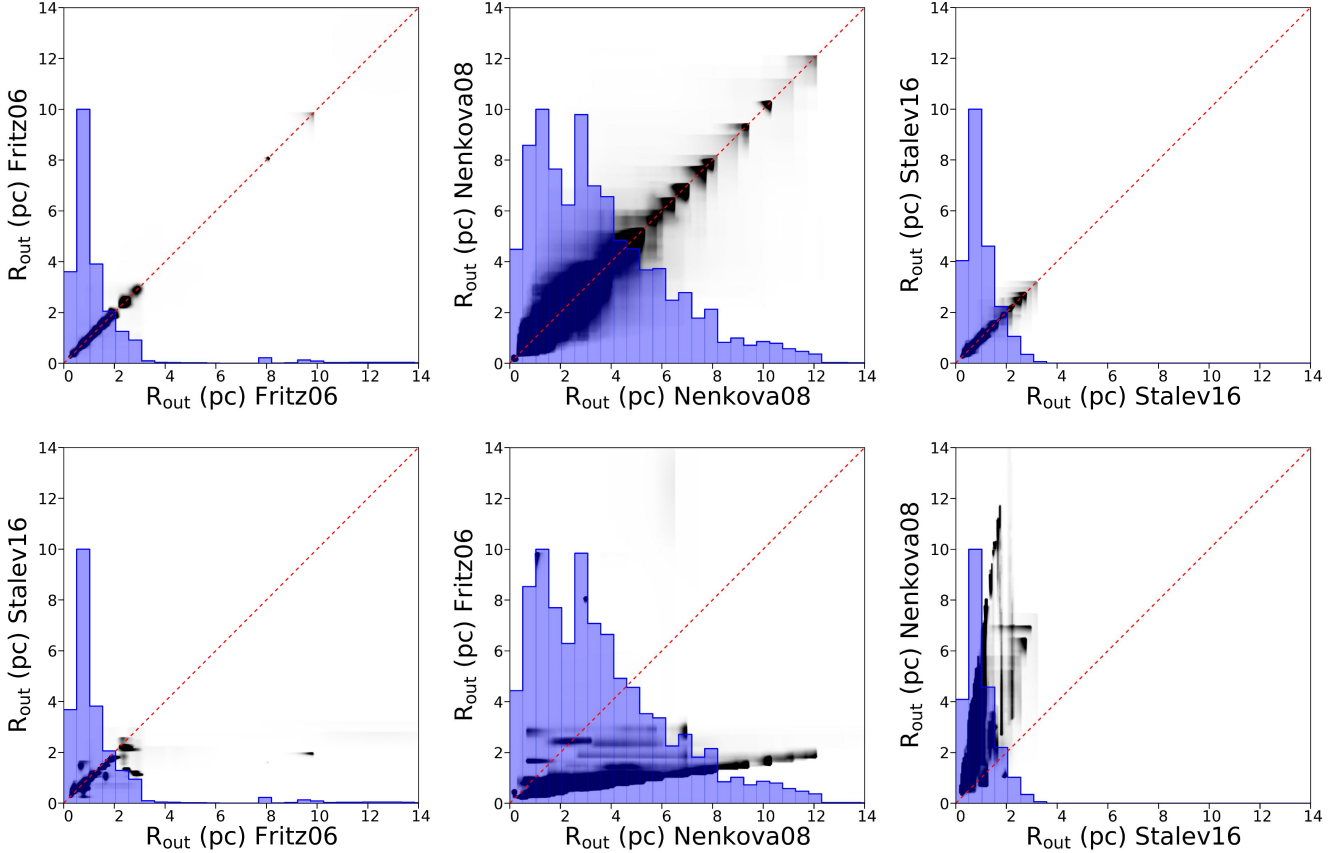


Figure 10. (top): Sum of the probability distribution function (PDF) for the outer radius of the dusty structure for our sample using [Fritz06] (left), [Nenkova08] (middle), and [Stalev16] (right). (bottom): Outer radius of the torus obtained for [Stalev16] versus [Fritz06] (left), [Fritz06] versus [Nenkova08] (middle), and [Nenkova08] versus [Stalev16] (right). The blue-filled histograms show the outer radius of the torus distribution per model (maximum of the distributions arbitrarily scaled to $R_{\text{out}} = 10\text{pc}$). The dotted line shows the one-to-one relationship expected for the best accuracy determination between parameters.

($r=0.5$). The three models rely on the assumption that their inner radius is linked to the dust sublimation radius, and therefore linked to the AGN bolometric luminosity⁵. Therefore, the linear relation might be the result of the bolometric luminosity being used in all the models to compute R_{out} . More interestingly, [Nenkova08] shows a large range of values $R_{\text{out}} < 12\text{ pc}$, while [Fritz06] (except for a small fraction of the sample with $8\text{ pc} < R_{\text{out}} < 10\text{ pc}$) and [Stalev16] show a small range of values $R_{\text{out}} < 3\text{ pc}$. In general, R_{out} is consistent among the three models for small values (i.e. when $R_{\text{out}} < 1\text{ pc}$).

4.3.2. Covering factor F_{cov}

We computed F_{cov} as the unity minus the escape probability, i.e. $\int e^{-\tau_{\nu}(\text{los})} \cos(\theta) d\theta$ where θ is the azimuthal

angle and $\tau_{\nu}(\text{los})$ is the line of sight opacity. The latter is computed from the equatorial opacity and the density distribution for smooth models, and from the distribution of clouds for clumpy models. The integration was made with the QUAD function within SCIPY (python 2.7). Fig. 11 shows the full sample F_{cov} distributions (through the parameter versus parameter plot) for each model, respectively. F_{cov} is poorly constrained for all the models (a non-negligible probability above 1% of F_{cov} is shown at any value) except for [Hoenig10] and [Hoenig17] (see Fig. 11). Indeed, only [Hoenig10] and [Hoenig17] show a marginal correlation ($r \sim 0.6$), suggesting that the parameter is constrained. Furthermore, most models show a maximum of F_{cov} distribution at large values with a tail reaching $F_{\text{cov}} \sim 0.1$. The exceptions are [Sieben15] ($0.1 < F_{\text{cov}} < 0.2$) and [Hoenig17] ($0.1 < F_{\text{cov}} < 0.6$).

4.3.3. Total dust mass M_{dust}

We computed M_{dust} integrating the density distribution function for each model within the dusty structure

⁵ Note that the bolometric luminosity is derived from the 2-10 keV X-ray luminosity, using the relation proposed by Marconi et al. (2004).

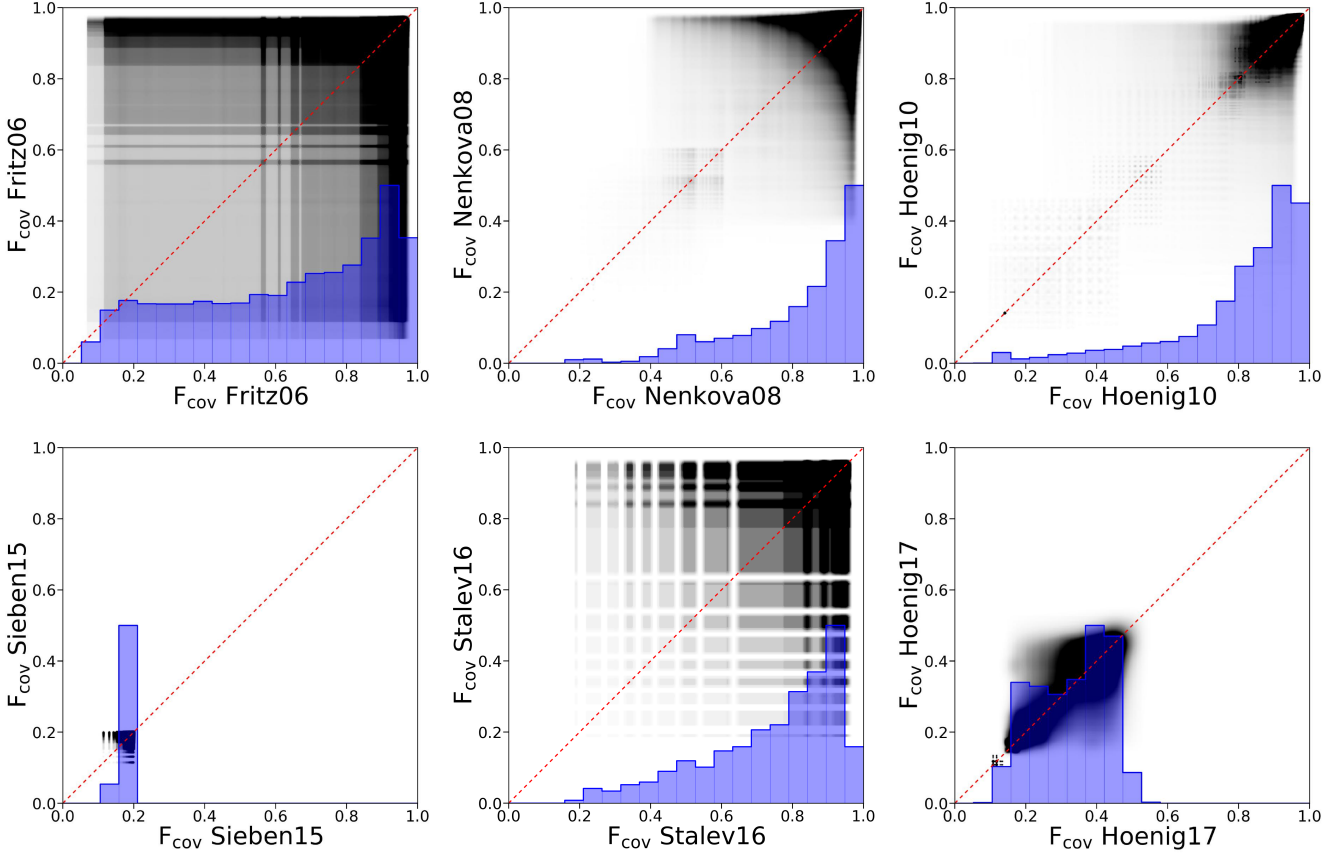


Figure 11. Total PDF distribution of the covering factor for the full sample. The blue-filled histograms show the covering factor distribution per model (maximum of the distribution scaled to the half of the y axis of the plot). The dotted line shows the one-to-one relationship expected for the best accuracy determination between parameters.

volume. We compute the parameter versus parameter plot for M_{dust} to evaluate if the mass is restricted (Fig. 12) and if there is a linear relation among M_{dust} derived from different models (Fig. 13). [Hoenig10], [Stalev16], and [Hoenig17] show a total mass that is roughly twice better restricted than the other three models. In general, [Fritz06], [Hoenig10], [Stalev16], and [Hoenig17] overlap in their estimates of M_{dust} with a range $0 < \log(M_{\text{dust}}) < 4$. [Nenkova08] tends to show larger M_{dust} ($2 < \log(M_{\text{dust}}) < 8$) compared to other models. When using [Sieben15], we recover a bimodal distribution of M_{dust} with two ranges, one overlapping with other models ($1 < \log(M_{\text{dust}}) < 4$) and another one showing large M_{dust} ($6 < \log(M_{\text{dust}}) < 9$). M_{dust} correlates among models ($r > 0.8$) for [Fritz06], [Hoenig10], [Stalev16], and [Hoenig17]. These estimates show a shift (within a factor of 10) with the lowest values for [Stalev16], and increasing for [Fritz06], [Hoenig17], and [Hoenig10].

5. DISCUSSION

5.1. Best model

The model that better reproduces the *Spitzer* spectra among the six models analysed is [Hoenig17]. This model is built on the idea that the dust around the AGN is distributed in an inflowing disk and an outflowing wind. This model is claimed to better reproduce the $3-5 \mu\text{m}$ bump observed in many Sy1, which clumpy models do not (García-González et al. 2017). Indeed, the disk-wind model [Hoenig17] is particularly good at describing Sy1 in our sample, while Sy2 (and, despite their low number, beamed AGN) are equally fitted to the clumpy torus model [Nenkova08] (see Fig. 7). As shown in Figs. 2 and 3, [Hoenig17] is good at describing near- and mid-infrared slopes although fails to describe the far-infrared slopes in our sample. Far-infrared slopes are better reproduced by [Fritz06], [Nenkova08], and [Stalev16].

The disk-wind model is consistent with an old interpretation of the dusty region in which the torus might be the dusty portion of an outflowing wind coming off the accretion disk (Efstathiou, & Rowan-Robinson 1995; Elitzur, & Shlosman 2006; Suganuma et al. 2006; Nenkova et al. 2008B; Netzer 2015; Ramos Almeida &

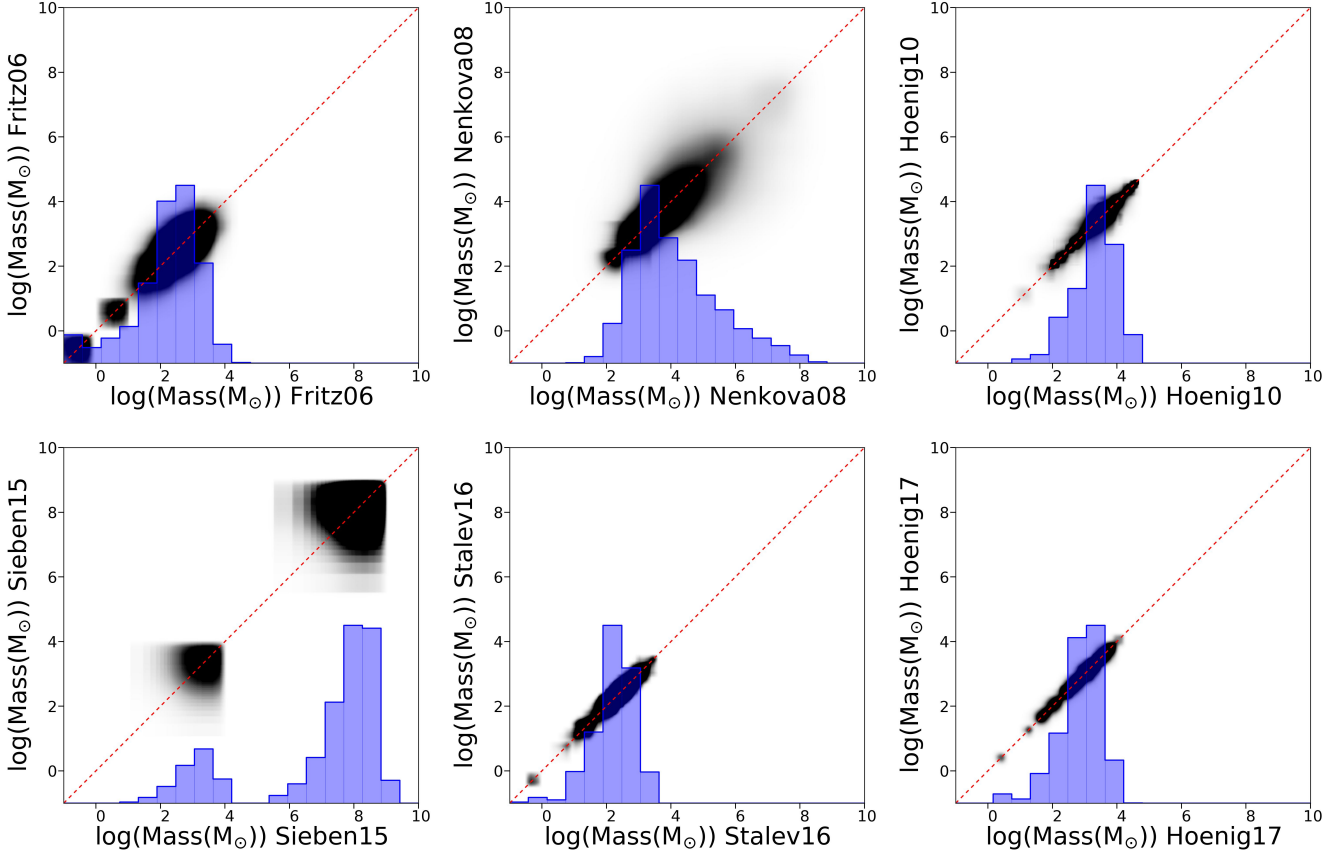


Figure 12. Parameter versus parameter plot using the sample PDF distributions for the total dust mass. The blue-filled histograms show the total dust mass distribution per model (maximum of the distribution arbitrarily scaled to $\log(M_{\text{dust}}) = 4.5$ for clarity of the plot). The dotted line shows the one-to-one relationship expected for the best accuracy determination between parameters.

Ricci 2017; Lyu, & Rieke 2018), which naturally extends the clumpy behavior of the BLR to further distances (Risaliti et al. 2002). Indeed, a significant part of the mid-infrared emission appears to come from the ionization cones (Braatz et al. 1993; Cameron et al. 1993; Höning et al. 2013; Asmus et al. 2016).

We also found that the best fitting model could be different for high and low luminosity AGN, with a larger percentage of best fits for [Hoenig17] for high luminous objects, while a larger number of low luminous AGN are better fitted to the clumpy torus model [Nenkova08] (see Fig. 6), also consistent with our findings when comparing best models describing Sy1 and Sy2. This result is expected if outflows dominate the high-luminosity end of AGN, while inefficient accretion flows are not able to produce these outflows at the low-luminosity end (also predicted by Elitzur, & Shlosman 2006). This is also consistent with outflows producing the short-term time variations associated to changes on the obscuration measured at X-rays in Sy1 (González-Martín 2018) and with the dependence on the covering factor on the Eddington

rate shown by Ricci et al. (2017). Unfortunately, we were not able to explore the dependence on our results on the Eddington rate because we found Eddington rates (or BH masses) only for $\sim 50\%$ of the sample (and they are biased toward the high accreting sources). Interestingly, our small sample of beamed AGN are reproduced equally well by [Nenkova08] and [Hoenig17] as it is the case for Sy2, indicating that some face-on AGN lack of the dusty wind signatures.

5.2. Are the models good enough?

Although able to statistically describe a good fraction of the spectra (up to 50% for [Hoenig17]) all the spectral fits show relatively large residuals (see Fig. 5), indicating that the scenario is more complex than shown by current models. Interestingly, the two models better describing a large portion of the sample (the clumpy torus model [Nenkova08] and clumpy disk-wind model [Hoenig17]) are the ones with the largest produced SED libraries, (1,250,000 and 132,000 SEDs, respectively). Another extreme case is [Sieben15] which manages to provide good fits for less than 5% of the spectra. This might be due

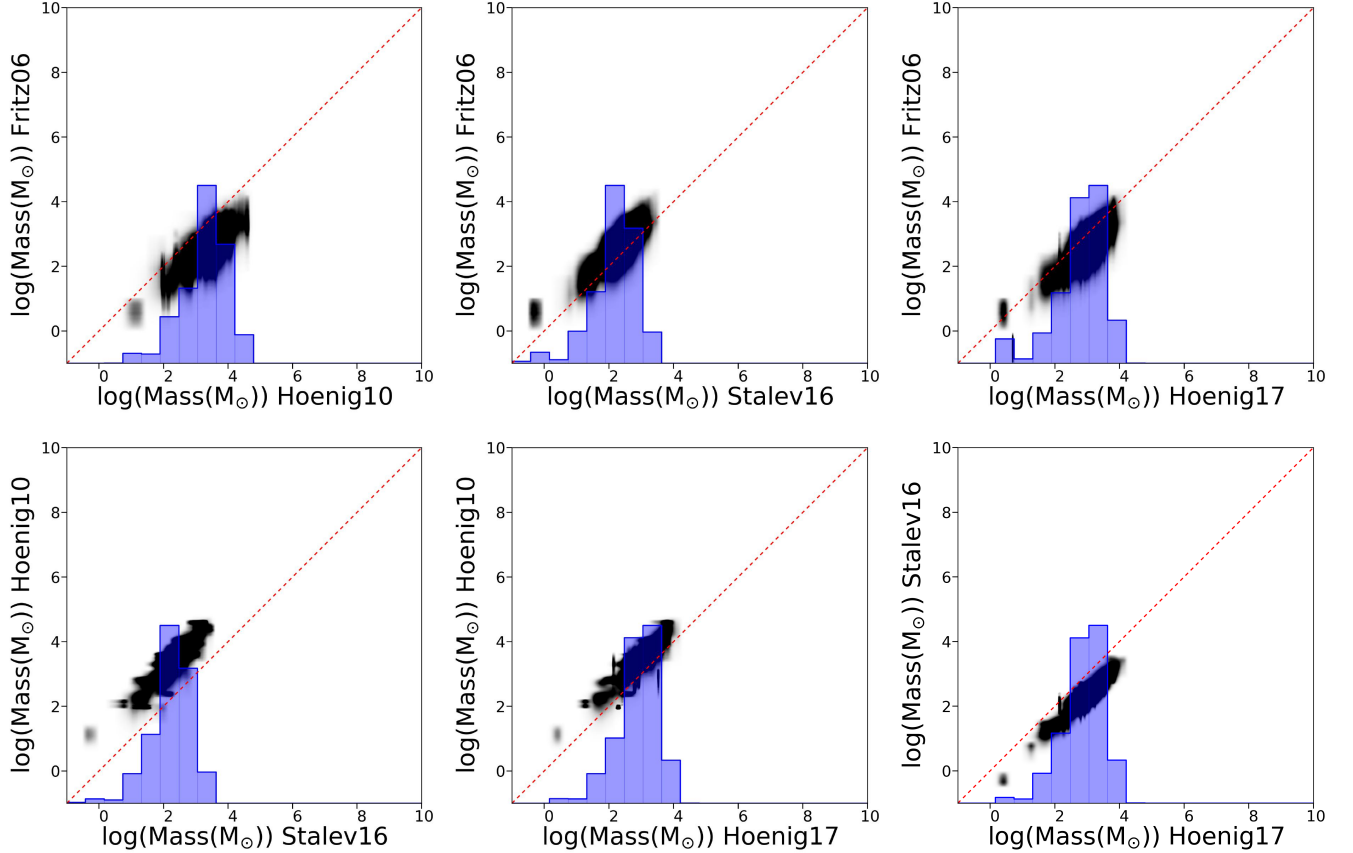


Figure 13. Correlations found among models PDF distribution for the sample total dust mass. The blue-filled histograms show the total dust mass distribution per model (maximum of the distribution arbitrarily scaled to $\log(M_{\text{dust}}) = 4.5$ for clarity of the plot). The dotted line shows the one-to-one relationship expected for the best accuracy determination between parameters.

to the small number of SEDs provided (3,600) and a fixed density distribution used for this model (which is also visible in the unrealistic large dust masses and narrow covering factor obtained using this model). Indeed, synthetic spectra showed that the model [Hoenig17] cannot be distinguished (using current or future facilities) from the clumpy model [Hoenig10] based solely on SED fitting (see Paper I). However, data do seem to prefer the latest wind version of the model [Hoenig17]. This might be due to a better coverage of the parameter space, including over 132,000 SEDs compared to 1,700 for [Hoenig10]. This embosses another important aspect when comparing models: modelers might want to provide well-sampled SED libraries to better compare them with data. It is also worth to mention that [Hoenig17] is better describing at the same time the near- and mid-infrared slopes (see Fig. 2), which might explain partially why this model is preferred against its partner model [Hoenig10].

The number of SEDs is not the only variable to be revisited when providing new SED libraries. Another important aspect is the parameter space, which in most

cases is not appropriate for reproducing the SED diversity (see Figs. 2–4). We show that many parameters tend to cluster towards their upper or lower limits provided by the SED library (see Table 3). For instance, the parameter governing the dust radial distribution (either in clumps or smooth) could be expanded to find a better match to the data. Moreover, other parameters seem to be over sampled; e.g. the Y parameter in the clumpy torus model [Nenkova08B] does not seem to require values larger than $Y = 50$. This can be easily spotted in Figs. 2–4, where many SEDs do not describe any AGN spectrum. Perhaps our conclusions are partially biased to the models with better sampled SED libraries.

5.3. Goodness of parameter determination

To decide which is the best model solution, attention should be paid to the actual parameters found and to the meaningful picture they should provide in terms of plausible physical description (see below). Furthermore, we have found misconceptions about the models. For example, the clumpy torus model [Nenkova08] is claimed to reproduce the spectra with smaller torus radii, consis-

tent with the interferometric data that have constrained the radial extent of the dusty structure to 10 pc (e.g. for Circinus galaxy, and Centaurus A, Tristram et al. 2007; Meisenheimer et al. 2007, respectively). However, this claim is actually inconsistent with our results. The smooth model [Fritz06] and the two phase model [Stalev16] provide twice smaller R_{out} compared to the clumpy model [Nenkova08] for the very same data analyzed here. This is in fact the expected behavior because smooth distributions are able to stock larger amount of dust than clumpy distributions of dust in the same volume. The historical reason behind the large tori found for smooth torus is that pioneer works try to fit at the same time mid- and far-infrared AGN SEDs (e.g. Pier, & Krolik 1992), being the latter dominated by dust heated by star-formation rather than the AGN. This resulted in unrealistic large tori.

Many attempts have been made to estimate the torus parameters using SED fitting, with photometric data (e.g. Ramos Almeida et al. 2009, 2011) or adding them to ground-based spectra (e.g. Alonso-Herrero et al. 2011). We demonstrate in Paper I that full-coverage 5–30 μm spectra are able to constrain all the parameters for most of the models studied here, with the exception of the wind model [Hoenig17]. Consistent with that, we found that the spectral coverage of the low resolution *Spitzer*/IRS spectra can restrict $\sim 80\%$ of the parameters within $\sim 10 - 20\%$ of the space parameter.

Ramos Almeida et al. (2014) used Bayesian techniques to constrain the parameters of the clumpy dusty model [Nenkova08]. They concluded that the torus width, viewing angle, and distribution of the clouds could be constrained with near- and mid-infrared photometry only, but mid-infrared spectroscopy is necessary to restrict the posterior distributions of the number of clouds and their optical depth. Furthermore, they show that 8–13 μm ground-based spectra alone reliably restrict some of these parameters (see also Alonso-Herrero et al. 2011). Using the full coverage of the low-resolution IRS/*Spitzer* spectra, we show that all the parameters of [Nenkova08] can be restricted, being q , Y , and τ_{ν} the best constrained. The range R_{out} found here when using the clumpy [Nenkova08] is fully consistent with that derived using Bayesian techniques for low-luminous AGN (González-Martín et al. 2017), Seyferts (Ramos Almeida et al. 2009; Alonso-Herrero et al. 2011), and QSOs (Martínez-Paredes et al. 2017).

Fritz et al. (2006) also studied the parameter restriction using infrared data by considering all the solutions with $\chi^2/\text{dof} < \chi^2/\text{dof}(\text{best}) + 3$ (being $\chi^2/\text{dof}(\text{best})$ the minimum χ^2 statistics). They found that R_{out} differs up to a factor of 3 while the parameters associated

to the dust density distribution are better constrained. This is consistent with our finding where R_{out} and the covering factor strongly depend on the selection of the model while M_{dust} is better constrained irrespective of the model. We further explore the degeneracy of the parameters within a model, finding no indication of linear relationships among them.

Note, however, that the resulting parameters are themselves dependent on the model assumed. In fact, we did not find any equivalence between parameters of different models, although expected in some cases (e.g. the viewing angle toward the dusty structure, see also Paper I). Therefore, we strongly suggest to evaluate the goodness of the model using a set of models before drawing conclusions from the resulting parameters.

However, there are two major concerns to derive the model parameters using *Spitzer*/IRS spectra: suitability of the models at describing the data and host galaxy dilution due to low spatial resolution data. The *Spitzer*/IRS data (with a spatial resolution of ~ 3 arcsec at 10 μm) are prone to contamination from the host galaxy or dust heated by circumnuclear star-formation (Fritz et al. 2006; Netzer et al. 2007; Siebenmorgen et al. 2015). Indeed, this is the result presented in this paper, where 30–50% of the sample (depending on the model used) is contaminated by more than 50% continuum emission not associated with the AGN (see Fig. 6). These results are consistent with previous results (Rodríguez Espinosa et al. 1987; Dultzin-Hacyan et al. 1988; Dultzin-Hacyan, & Benítez 1994; Dultzin-Hacyan, & Ruano 1996). Decomposition methods as those used in this paper, and previously in Netzer et al. (2007) (see also Hao et al. 2007; Hernán-Caballero et al. 2015) are then needed to decontaminate the torus component from circumnuclear contributors. However, as shown in this paper, when this contribution is large (stellar component contributing at least 50% compared to the torus component at 5 μm , or dust heated by star-formation contributing at least 50% compared to the torus component at 30 μm) dilution strongly influences the parameter determination. High spatial resolution observations are needed for the best isolation of the dust associated the AGN from other contributors, as those provided with ground-based facilities (Ramos Almeida et al. 2009; Alonso-Herrero et al. 2011; Fuller et al. 2016; Martínez-Paredes et al. 2017; García-Bernete et al. 2019), the novel combination of VLTI+GRAVITY and the future *JWST*. Note however that both N- and Q-bands ground-based spectra are available only for NGC 1068. Interestingly, both bands are not easily fitted with a single model (Victoria-Ceballos in prep.).

One way to solve the parameter space determination is the use of interferometric observations together with SED fitting (Höning et al. 2006; Höning & Kishimoto 2010). While interferometry provides the most direct access to the dust AGN structure, observations are limited to the brightest AGN with current facilities. Indeed, ALMA is providing for the first time the kinematics of the cold dust, finding large dust structures kinematically decoupled from the host galaxy (García-Burillo et al. 2016; Gallimore et al. 2016; Alonso-Herrero et al. 2018; Combes et al. 2019). Alternatively, we propose the use of X-ray reflected component (associated to the AGN dust structure) together with the mid-infrared spectrum to infer the torus properties (Esparza-Arredondo et al. in prep.).

6. SUMMARY

The main results from the fitting of *Spitzer*/IRS spectra of a sample of 110 AGN using six dust models:

1. When mid-infrared AGN-dominated spectra are selected, all but [Sieben15] show satisfactory residuals. However, residuals are larger than expected if we select the right model (i.e. self-fitting synthetic spectra to the same model). The main discrepancies are the same than those reported by our synthetic spectra (Paper I); i.e. slopes below $\sim 7 \mu\text{m}$ and above $\sim 25 \mu\text{m}$ and around the 10 and $18 \mu\text{m}$ silicate features.
2. The fraction of objects requiring a prominent circumnuclear component is small (20%) when using [Fritz06]; although up to 30-50% of the spectra require large circumnuclear components contribution for the other models.
3. The largest percentage of good fits (40%) is obtained when using [Hoenig17]; [Nenkova08] is the next one showing the largest percentage (30%); roughly 10% can be fitted with either [Fritz06] or [Hoenig10]; and less than 5% can be fitted with [Sieben15]. [Hoenig17] seems to be particularly good for Sy1 and [Nenkova08] for Sy2. [Hoenig17] is better suited for high and [Nenkova08] for low AGN luminosities.
4. When the model is good enough (i.e. $\chi^2/\text{dof} < 2$) to reproduce the data, we manage to constrain 80% of the parameters, irrespective of the optical class or the X-ray luminosity. The parameters are restricted to 10-20% of its parameter space and this percentage increases to the low and/or high limit for most of the parameters. Many of them tend to be clustered at the low and/or high limit.

This might further suggest that a strong revision of the SED libraries could result on a better match of the mid-infrared spectra of AGN.

5. We did not find equivalencies between parameters of different models. Therefore, the parameter results strongly depend on the chosen model. We also computed derived quantities and we compared the results using different models:

- The derived dust masses are equivalent for most of the models.
- The outer radius of the dusty structure in physical units is roughly twice larger for [Nenkova08] compared to [Fritz06] and [Stalev16].
- The covering factor strongly depends on the model used, showing a wide range of values for [Fritz06], [Nenkova08], [Hoenig10], and [Stalev16] and a narrow distribution for [Sieben15] and [Hoenig17].

van Bemmel, & Dullemond (2003) said more than 15 years ago that any “improvement of the models is only relevant when better observations are available to constrain the models, and when we have a better understanding of the contribution of star-formation to the infrared SED”. New data that *JWST* will provide soon are ideal for those purposes. Therefore, observers and modelers need to work together to obtain a better sample of well isolated mid-infrared spectra and on new SED libraries with a careful selection of the parameter space to be confronted against data.

We thank to the anonymous referee for his/her comments and suggestions which have improved significantly the results of this research. This research is mainly funded by the UNAM PAPIIT project IA103118 (PI OG-M). MM-P acknowledges support by KASI post-doctoral fellowships. IM and JM acknowledge financial support from the research project AYA2016-76682-C3-1-P (AEI/FEDER, UE). JMR-E acknowledge support from the Spanish Ministry of Science under grant AYA2015-70498-C2-1, and AYA2017-84061-P. IG-B acknowledges financial support from the Spanish Ministry of Science and Innovation (MICINN) through projects PN AYA2015-64346-C2-1-P and AYA2016-76682-C3-2-P. I.M. and J.M. acknowledge financial support from the State Agency for Research of the Spanish MCIU through the “Center of Excellence Severo Ochoa” award for the Instituto de Astrofísica de Andalucía (SEV-2017-0709). D. E.-A. acknowledges support from a CONACYT scholarship. D-D acknowledges PAPIIT UNAM

support from grant IN113719. This research has made use of dedicated servers maintained by Jaime Perea (HyperCat at IAA-CSIC), Alfonso Ginori González,

Gilberto Zavala, and Miguel Espejel (Galaxias, Posgrado04, and Arambolas at IRyA-UNAM) and Daniel Díaz-González (IRyAGN1 and IRyAGN2). All of them are gratefully acknowledged.

REFERENCES

- Antonucci, R. R. J., & Miller, J. S. 1985, *ApJ*, 297, 621.
- Alonso-Herrero, A., Ramos Almeida, C., Mason, R., et al. 2011, *ApJ*, 736, 82.
- Alonso-Herrero, A., Pereira-Santaella, M., García-Burillo, S., et al. 2018, *ApJ*, 859, 144.
- Arnaud, K. A. 1996, Astronomical Data Analysis Software and Systems V, 101, 17.
- Asmus, D., Höning, S. F., & Gandhi, P. 2016, *ApJ*, 822, 109
- Braatz, J. A., Wilson, A. S., Gezari, D. Y., et al. 1993, *ApJ*, 409, L5.
- Bruzual, G., & Charlot, S. 2003, *MNRAS*, 344, 1000.
- Burtscher, L., Meisenheimer, K., Tristram, K. R. W., et al. 2013, *A&A*, 558, A149.
- Cameron, M., Storey, J. W. V., Rotaciuc, V., et al. 1993, *ApJ*, 419, 136.
- Combes, F., García-Burillo, S., Audibert, A., et al. 2019, *A&A*, 623, A79.
- Dullemond, C. P., & van Bemmel, I. M. 2005, *A&A*, 436, 47.
- Efstathiou, A., & Rowan-Robinson, M. 1995, *MNRAS*, 273, 649.
- Dultzin-Hacyan, D., Moles, M., & Masegosa, J. 1988, *A&A*, 206, 95.
- Dultzin-Hacyan, D., & Benitez, E. 1994, *A&A*, 291, 720.
- Dultzin-Hacyan, D., & Ruano, C. 1996, *A&A*, 305, 719.
- Elitzur, M., & Shlosman, I. 2006, *ApJ*, 648, L101.
- Feltre, A., Hatziminaoglou, E., Fritz, J., & Franceschini, A. 2012, *MNRAS*, 426, 120.
- Fritz, J., Franceschini, A., & Hatziminaoglou, E. 2006, *MNRAS*, 366, 767 [Fritz06].
- Fuller, L., Lopez-Rodriguez, E., Packham, C., et al. 2016, *MNRAS*, 462, 2618.
- Gallimore, J. F., Elitzur, M., Maiolino, R., et al. 2016, *ApJL*, 829, L7
- García-Bernete, I., Ramos Almeida, C., Alonso-Herrero, A., et al. 2019, *MNRAS*, 486, 4917
- García-Burillo, S., Combes, F., Ramos Almeida, C., et al. 2016, *ApJL*, 823, L12.
- García-González, J., Alonso-Herrero, A., Höning, S. F., et al. 2017, *MNRAS*, 470, 2578.
- González-Martín, O., Masegosa, J., García-Bernete, I., et al. 2019, submitted (Paper I).
- González-Martín, O. 2018, *ApJ*, 858, 2.
- González-Martín, O., Masegosa, J., Hernán-Caballero, A., et al. 2017, *ApJ*, 841, 37.
- González-Martín, O., Masegosa, J., Márquez, I., et al. 2015, *A&A*, 578, A74.
- González-Martín, O., Rodríguez-Espinosa, J. M., Díaz-Santos, T., et al. 2013, *A&A*, 553, A35.
- Granato, G. L., Danese, L., & Franceschini, A. 1997, *ApJ*, 486, 147.
- Hao, L., Weedman, D. W., Spoon, H. W. W., et al. 2007, *ApJL*, 655, L77
- Hernán-Caballero, A., Alonso-Herrero, A., Hatziminaoglou, E., et al. 2015, *ApJ*, 803, 109
- Höning, S. F., Beckert, T., Ohnaka, K., & Weigelt, G. 2006, *A&A*, 452, 459
- Höning, S. F., Kishimoto, M., Gandhi, P., et al. 2010, *A&A*, 515, A23
- Höning, S. F., & Kishimoto, M. 2010, *A&A*, 523, A27 [Hoenig10].
- Höning, S. F., Kishimoto, M., Tristram, K. R. W., et al. 2013, *ApJ*, 771, 87.
- Höning, S. F., & Kishimoto, M. 2017, *ApJL*, 838, L20 [Hoenig17].
- Lebouteiller, V., Barry, D. J., Spoon, H. W. W., et al. 2011, *ApJS*, 196, 8
- Lyu, J., & Rieke, G. H. 2018, *ApJ*, 866, 92.
- López-Gonzaga, N., Burtscher, L., Tristram, K. R. W., Meisenheimer, K., & Schartmann, M. 2016, *A&A*, 591, A47.
- Marconi, A., Risaliti, G., Gilli, R., et al. 2004, *MNRAS*, 351, 169.
- Martínez-Paredes, M., Alonso-Herrero, A., Aretxaga, I., et al. 2015, *MNRAS*, 454, 3577.
- Martínez-Paredes, M., Aretxaga, I., Alonso-Herrero, A., et al. 2017, *MNRAS*, 468, 2.
- Meisenheimer, K., Tristram, K. R. W., Jaffe, W., et al. 2007, *A&A*, 471, 453
- Mor, R., & Netzer, H. 2012, *MNRAS*, 420, 526.
- Nenkova, M., Sirocky, M. M., Ivezić, Ž., et al. 2008, *ApJ*, 685, 147.
- Nenkova, M., Sirocky, M. M., Nikutta, R., Ivezić, Ž., & Elitzur, M. 2008, *ApJ*, 685, 160-180 [Nenkova08].
- Netzer, H., Lutz, D., Schweitzer, M., et al. 2007, *ApJ*, 666, 806

- Netzer, H. 2015, Annual Review of Astronomy and Astrophysics, 53, 365.
- Pier, E. A., & Krolik, J. H. 1992, ApJ, 401, 99.
- Ramos Almeida, C., Levenson, N. A., Rodríguez Espinosa, J. M., et al. 2009, ApJ, 702, 1127
- Ramos Almeida, C., Levenson, N. A., Alonso-Herrero, A., et al. 2011, ApJ, 731, 92
- Ramos Almeida, C., Alonso-Herrero, A., Levenson, N. A., et al. 2014, MNRAS, 439, 3847
- Ramos Almeida, C., & Ricci, C. 2017, Nature Astronomy, 1, 679
- Ricci, C., Trakhtenbrot, B., Koss, M. J., et al. 2017, Nature, 549, 488
- Risaliti, G., Elvis, M., & Nicastro, F. 2002, ApJ, 571, 234.
- Rodriguez Espinosa, J. M., Rudy, R. J., & Jones, B. 1987, ApJ, 312, 555.
- Siebenmorgen, R., Heymann, F., & Efstathiou, A. 2015, A&A, 583, A120 [Sieben15].
- Smith, J. D. T., Draine, B. T., Dale, D. A., et al. 2007, ApJ, 656, 770.
- Stalevski, M., Fritz, J., Baes, M., et al. 2012, MNRAS, 420, 2756.
- Stalevski, M., Ricci, C., Ueda, Y., et al. 2016, MNRAS, 458, 2288 [Stalev16].
- Oh, K., Koss, M., Markwardt, C. B., et al. 2018, ApJS, 235, 4
- Pasetto, A., González-Martín, O., Esparza-Arredondo, D., et al. 2019, ApJ, 872, 69.
- Pei, Y. C. 1992, ApJ, 395, 130
- Schartmann, M., Meisenheimer, K., Camenzind, M., et al. 2008, A&A, 482, 67
- Suganuma, M., Yoshii, Y., Kobayashi, Y., et al. 2006, ApJ, 639, 46.
- Tristram, K. R. W., Meisenheimer, K., Jaffe, W., et al. 2007, A&A, 474, 837
- van Bemmel, I. M., & Dullemond, C. P. 2003, A&A, 404, 1

APPENDIX

A. SPECTRAL FITS FOR THE AGN SAMPLE

Table 4 shows the results on the model fitting of 110 AGN selected from the *Swift*/BAT sample with available *Spitzer* spectra.

Obj.	Mod	A / S / I %	χ^2/dof	$E_{(B-V)}$	Parameters						
	F06				i	σ	Γ	β	Y	$\tau_{9.7\mu\text{m}}$	
	N08				i	N_0	σ	Y	q	τ_v	
	H10				i	N_0	θ	a	τ_{cl}		
	S15				i	R_{in}	η	τ_{cl}	τ_{disk}		
	S16				i	σ	p	q	Y	$\tau_{9.7\mu\text{m}}$	
	H17				i	N_0	a	σ	θ	a_w	h
NGC235A	F06o	49.8 / 0.0 / 50.2	1.83	0.9 ^{1.0} _{-0.8}	<15.3	<23.9	<0.1	>-0.1	27.4 ^{29.1} _{-32.4}	2.0 ^{2.3} _{-2.0}	
	N08o	36.1 / 6.7 / 57.2	1.98	1.5 ^{1.4} _{-0.8}	52.4 ^{55.9} _{-49.1}	>14.8	>69.2	19.9 ^{20.1} _{-19.6}	1.0 ^{1.0} _{-0.98}	20.0 ^{21.1} _{-19.9}	
	H10o	23.9 / 8.0 / 68.1	2.35	2.0 ^{2.4} _{-1.9}	>83.7	3.1 ^{3.5} _{-2.8}	>5.0	>-0.1	>78.4		
	S15o	27.8 / 6.8 / 65.4	2.43	2.2 ^{2.3} _{-1.9}	<21.3	<3.0	>77.3	<0.1	13.5 ^{13.5} _{-13.5}		
	S16o•	56.1 / 0.0 / 43.9	1.79	0.8 ^{1.0} _{-0.7}	86.1 ^{89.1} _{-78.8}	24.6 ^{31.5} _{-21.1}	1.3 ^{1.4} _{-1.2}	>0.0	>21.5	<4.1	
	H17o	30.5 / 0.0 / 69.5	2.07	2.1 ^{2.1} _{-1.9}	21.3 ^{21.1} _{-21.1}	>9.9	<-3.0	>14.7	>44.5	>-0.5	<0.1
Mrk348	F06o	94.9 / 5.1 / 0.0	1.79	<0.5	<11.0	<20.3	3.4 ^{3.6} _{-3.3}	>0.0	<10.0	6.0 ^{6.1} _{-5.8}	>0.7
	N08o	90.4 / 9.6 / 0.0	1.59	0.4 ^{0.4} _{-0.3}	>87.5	>14.9	>68.6	14.8 ^{17.7} _{-10.95}	1.9 ^{2.0} _{-1.8}	<10.3	
	H10o•	79.9 / 9.3 / 10.8	1.44	0.2 ^{0.1} _{-0.1}	75.0 ^{78.7} _{-72.9}	7.1 ^{7.8} _{-6.1}	<8.8	-1.05 ^{-1.05} _{-1.09}	44.8 ^{47.6} _{-41.5}		
	S15o	81.9 / 11.1 / 7.0	12.06	1.2 ^{1.2} _{-1.1}	>85.9	<3.0	7.7 ^{7.71} _{-7.45}	<0.0	13.5 ^{13.5} _{-13.5}		
	S16o•	91.2 / 5.7 / 3.2	1.53	<0.5	79.8 ^{83.1} _{-66.0}	73.4 ^{78.6} _{-66.0}	>1.5	>1.1	<10.2	7.0 ^{7.7} _{-6.6}	
	H17o•	86.3 / 6.9 / 6.9	1.09	0.3 ^{0.4} _{-0.3}	59.9 ^{59.3} _{-60.6}	>9.8	-2.5 ^{-2.48} _{-2.52}	<7.1	>44.6	>-0.5	>0.5
Mrk352	F06o	92.4 / 7.6 / 0.0	1.68	<0.5	62.3 ^{65.5} _{-59.4}	<20.3	>6.0	<-1.0	<10.0	>9.0	
	N08o•	94.2 / 5.8 / 0.0	1.14	<0.5	>72.4	<3.4	>15.0	<7.7	>2.2	33.1 ^{61.1} _{-23.3}	
	H10o•	93.5 / 4.0 / 2.5	1.14	<0.5	<59.6	<4.5	>44.5	-1.32 ^{-1.27} _{-1.37}	>71.5		
	S15o	85.2 / 14.8 / 0.0	5.42	<0.5	33.1 ^{33.5} _{-32.0}	<3.0	<1.5	<0.0	13.5 ^{13.5} _{-13.5}		
	S16o	93.3 / 6.7 / 0.0	1.87	<0.5	30.9 ^{22.3} _{-22.3}	>78.8	>1.5	>1.5	<10.0	<3.0	
	H17o•	100.0 / 0.0 / 0.0	1.20	<0.5	<15.0	>5.2	-2.81 ^{-2.76} _{-2.86}	>7.0	34.2 ^{35.5} _{-31.7}	>-0.9	<0.4
NGC454E	F06o•	74.4 / 5.0 / 20.6	1.26	<0.5	48.0 ^{54.0} _{-45.2}	34.2 ^{36.9} _{-31.9}	<0.0	-0.5 ^{-0.2} _{-0.8}	<10.9	3.9 ^{4.2} _{-3.6}	
	N08o•	66.7 / 10.5 / 22.8	1.08	<0.5	>75.3	10.8 ^{13.9} _{-10.1}	25.2 ^{58.0} _{-15.7}	19.8 ^{21.3} _{-15.5}	1.5 ^{1.7} _{-1.6}	22.8 ^{27.2} _{-19.9}	
	H10	56.5 / 11.6 / 31.9	1.09	<0.5	>77.5	3.6 ^{2.9} _{-2.9}	>45.7	>0.1	70.7 ^{79.6} _{-67.7}		
	S15	65.2 / 7.8 / 27.0	2.39	<0.5	>85.9	<3.0	7.7 ^{7.9} _{-7.5}	30.0 ^{30.9} _{-28.1}	13.6 ^{14.2} _{-13.0}		
	S16	66.4 / 9.0 / 24.6	1.08	<0.5	17.2 ^{32.2} _{-14.8}	>73.6	<0.0	<0.1	13.0 ^{12.8} _{-12.8}	4.9 ^{5.3} _{-4.1}	
	H17	58.7 / 9.4 / 31.9	0.96	<0.5	61.5 ^{65.0} _{-53.0}	>8.4	-2.3 ^{-2.2} _{-2.4}	>13.3	>42.7	>-0.9	>0.2
NGC526A	F06o	94.8 / 5.2 / 0.0	12.76	<0.5	20.0 ^{20.2} _{-19.9}	<20.0	>6.0	>0.0	<10.0	>10.0	
	N08o	94.6 / 5.4 / 0.0	8.70	<0.5	>86.5	9.0 ^{9.1} _{-8.8}	>66.8	<5.0	0.3 ^{0.5} _{-0.1}	<10.0	
	H10o	93.9 / 6.1 / 0.0	1.29	<0.5	78.1 ^{88.9} _{-73.7}	>8.7	>33.2	-1.43 ^{-1.38} _{-1.49}	53.9 ^{61.0} _{-50.7}		
	S15o	91.8 / 8.2 / 0.0	34.65	0.4 ^{0.4} _{-0.4}	>86.0	<3.0	1.62 ^{1.63} _{-1.61}	<0.0	13.5 ^{13.5} _{-13.5}		
	S16o	96.7 / 3.3 / 0.0	10.43	<0.5	>79.5	>79.9	>1.5	0.67 ^{0.68} _{-0.64}	<10.0	<3.0	
	H17o•	96.8 / 3.2 / 0.0	0.75	0.3 ^{0.3} _{-0.2}	60.0 ^{60.5} _{-58.3}	>7.3	-2.66 ^{-2.59} _{-2.69}	>14.8	>44.5	-0.82 ^{-0.77} _{-1.45}	0.41 ^{0.44} _{-0.39}
E297-018	F06o	93.6 / 0.0 / 6.4	1.70	0.6 ^{0.7} _{-0.8}	<0.0	<20.2	2.15 ^{2.18} _{-2.13}	<1.0	<10.0	3.0 ^{4.03} _{-2.99}	
	N08o•	87.6 / 4.0 / 8.4	0.93	0.5 ^{0.5} _{-0.5}	>74.3	>14.7	>66.9	<5.0	1.13 ^{1.24} _{-1.06}	<10.4	
	H10	82.7 / 2.6 / 14.6	0.99	0.6 ^{0.6} _{-0.6}	60.0 ^{67.5} _{-29.7}	>9.6	<23.7	-1.91 ^{-1.88} _{-1.93}	>78.4		
	S15o	84.3 / 7.9 / 7.8	15.11	0.8 ^{0.8} _{-0.9}	>85.9	<3.0	<1.5	<0.0	17.0 ^{17.3} _{-16.7}		
	S16o	90.7 / 1.2 / 8.1	2.32	0.7 ^{0.7} _{-0.6}	>88.8	70.5 ^{71.6} _{-69.8}	>1.5	>1.5	<10.0	5.0 ^{5.04} _{-4.98}	
	H17	88.7 / 0.0 / 11.3	0.87	0.6 ^{0.7} _{-0.6}	>80.1	>7.7	<2.9	<11.4	36.1 ^{41.7} _{-34.0}	-1.2 ^{-1.1} _{-1.4}	0.25 ^{0.33} _{-0.17}
NGC788	F06o	100.0 / 0.0 / 0.0	3.34	<0.5	0.3 ^{0.7} _{-0.1}	<20.3	4.81 ^{4.83} _{-4.78}	>0.0	<10.0	>9.8	
	N08o•	94.2 / 4.0 / 1.8	1.30	<0.5	>77.3	11.3 ^{13.5} _{-10.4}	>47.2	10.0 ^{11.8} _{-9.6}	2.1 ^{2.3} _{-2.0}	20.0 ^{21.0} _{-17.9}	
	H10o	83.8 / 3.3 / 12.9	2.16	<0.5	84.0 ^{88.7} _{-80.0}	>9.8	>56.8	-0.9 ^{-0.8} _{-1.0}	37.0 ^{40.6} _{-34.2}		
	S15o	91.7 / 3.9 / 4.4	20.71	0.8 ^{0.8} _{-0.8}	>86.0	<3.0	7.4 ^{7.7} _{-7.1}	<0.0	13.5 ^{13.5} _{-13.5}		
	S16o	97.0 / 0.0 / 3.0	2.54	<0.5	19.9 ^{21.0} _{-16.5}	>79.0	>1.5	0.65 ^{0.7} _{-0.58}	<10.0	8.9 ^{9.3} _{-8.4}	
	H17o•	91.1 / 0.0 / 8.9	1.25	0.2 ^{0.3} _{-0.2}	50.5 ^{51.7} _{-49.1}	7.0 ^{7.2} _{-6.8}	<3.0	13.7 ^{14.8} _{-11.8}	>44.8	-1.5 ^{-1.51} _{-1.51}	>0.5
Mrk590	F06o	99.4 / 6.0 / 0.0	8.91	<0.5	<0.0	<20.0	>6.0	-0.25 ^{-0.22} _{-0.25}	10.44 ^{10.53} _{-10.39}	9.3 ^{9.6} _{-9.1}	
	N08o	96.0 / 4.0 / 0.0	2.96	<0.5	>83.2	5.7 ^{6.0} _{-5.3}	>62.6	7.2 ^{7.9} _{-6.8}	>2.5	103.6 ^{106.5} _{-99.3}	
	H10o	91.6 / 2.8 / 5.6	4.04	<0.5	51.7 ^{52.3} _{-49.9}	9.2 ^{9.3} _{-8.6}	>57.9	>0.0	40.7 ^{42.1} _{-38.3}		
	S15o	96.3 / 3.7 / 0.0	24.09	0.4 ^{0.4} _{-0.4}	>86.0	<3.0	<1.5	<0.0	42.0 ^{41.7} _{-41.7}		
	S16o	99.3 / 0.7 / 0.0	6.64	<0.5	60.3 ^{61.3} _{-59.3}	>79.8	<0.0	>1.5	<10.0	6.5 ^{6.6} _{-6.4}	
	H17o•	95.4 / 0.0 / 4.6	1.15	0.1 ^{0.1} _{-0.1}	30.0 ^{32.3} _{-28.3}	>9.5	<-3.0	11.4 ^{11.6} _{-11.2}	36.1 ^{37.3} _{-33.3}	>-0.5	<0.1
IC1816	F06o	78.9 / 0.0 / 21.1	2.23	<0.5	62.0 ^{63.1} _{-60.8}	<20.2	0.08 ^{0.1} _{-0.06}	>0.0	<10.0	>9.0	
	N08	66.5 / 5.0 / 28.5	1.18	0.6 ^{0.6} _{-0.5}	>72.0	>13.2	>60.6	7.2 ^{8.9} _{-6.2}	<2.1	58.2 ^{63.2} _{-52.5}	
	H10	68.9 / 2.5 / 28.6	2.56	0.4 ^{0.4} _{-0.2}	65.3 ^{67.7} _{-60.0}	>8.1	>58.9	>0.1	62.9 ^{66.2} _{-57.4}		
	S15o	73.8 / 2.3 / 24.0	5.08	0.8 ^{0.8} _{-0.8}	>85.8	<3.0	4.0 ^{4.1} _{-3.9}	<0.0	>44.6		
	S16	69.2 / 1.5 / 29.3	1.39	<0.0	29.6 ^{31.5} _{-27.9}	>77.9	<0.0	<0.0	10.3 ^{10.4} _{-10.2}	>10.7	
	H17	63.6 / 4.6 / 31.8	1.36	<0.0	>89.9	>9.8	>-0.5	>14.3	<30.1	>-0.6	<0.1
NGC973	F06	17.6 / 18.7 / 63.7	2.76	2.9 ^{3.2} _{-2.8}	<0.0	>59.7	0.09 ^{0.13} _{-0.07}	<-1.0	<10.1	3.0 ^{3.03} _{-2.98}	
	N08	17.2 / 20.2 / 62.6	2.01	3.8 ^{4.3} _{-3.6}	35.9 ^{31.0} _{-31.0}	>14.9	>69.5	9.3 ^{9.7} _{-9.0}	<0.0	20.0 ^{20.8} _{-19.8}	
	H10	5.8 / 16.5 / 77.7	2.59	5.5 ^{5.7} _{-5.3}	>80.8	>9.0	44.4 ^{49.7} _{-43.8}	<2.0	>75.5		
	S15	24.9 / 23.0 / 52.1	7.79	0.6 ^{0.7} _{-0.5}	<19.5	<3.0	7.7 ^{8.0} _{-7.5}	>956.2	>44.4		
	S16	13.4 / 19.8 / 66.8	3.03	3.6 ^{3.5} _{-3.5}	>79.0	>75.6	>1.5	>1.4	<10.1	5.0 ^{5.4} _{-4.62}	
	H17	8.8 / 16.6 / 74.5	2.09	4.7 ^{4.9} _{-4.6}	60.1 ^{63.3} _{-54.3}	<5.2	<-3.0	>13.4	>42.8	-1.7 ^{-1.74} _{-1.74}	<0.1
NGC1052	F06o	95.6 / 4.4 / 0.0	4.38	<0.5	<0.1	<20.1	>6.0	>0.0	13.7 ^{14.6} _{-13.6}	8.5 ^{8.6} _{-8.29}	
	N08o	92.6 / 5.1 / 2.4	1.79	<0.5	>87.8	3.8 ^{4.1} _{-3.8}	<16.1	10.0 ^{10.3} _{-9.9}	0.9 ^{0.8} _{-0.8}	57.8 ^{82.9} _{-52.9}	
	H10o	87.4 / 5.2 / 7.5	1.75	0.2 ^{0.2} _{-0.1}	49.7 ^{52.6} _{-44.3}	5.7 ^{5.8} _{-5.3}	>57.8	>0.0	72.7 ^{77.3} _{-67.9}		
	S15o	88.9 / 6.4 / 4.7	11.57	<0.5							

Obj.	Mod	A / S / I %	χ^2/dof	$E_{(B-V)}$	Parameters							
	F06				i	σ	Γ	β	Y	$\tau_{9.7\mu m}$		
	N08				i	N_0	σ	Y	q	τ_v		
	H10				i	N_0	θ	a	τ_{cl}			
	S15				i	R_{in}	η	τ_{cl}	τ_{disk}			
	S16				i	σ	p	q	Y	$\tau_{9.7\mu m}$		
	H17				i	N_0	a	σ	θ	a_w	h	f_w
E417-G006	F06 \bullet	85.1 / 0.0 / 14.9	1.44	<0.5	>76.7	36.1 _{35.1} ^{37.5}	<0.0	>-0.0	11.2 _{1.2} ^{11.6}	>9.8		
	N08	68.2 / 7.9 / 23.9	1.17	<0.5	<22.2	>12.4	35.2 _{39.6} ^{36.4}	13.3 _{11.8} ^{24.8}	0.8 _{0.1} ^{1.1}	121.2 _{105.5} ^{160.3}		
	H10	65.9 / 7.7 / 26.5	1.35	<0.5	51.9 _{45.3} ^{55.7}	>9.8	55.2 _{52.2} ^{59.6}	>0.0	>79.2			
	S15 \circ	74.1 / 7.7 / 18.2	1.86	<0.5	51.6 _{45.3} ^{52.5}	<3.0	<1.7	>958.6	>43.4			
	S16	64.6 / 7.2 / 28.2	1.44	<0.5	20.7 _{12.8} ^{32.8}	70.0 _{67.3} ^{71.4}	<0.0	<0.0	11.7 _{11.3} ^{12.0}	>10.8		
	H17	63.1 / 8.2 / 28.7	1.35	<0.5	40.1 _{12.8} ^{14.8}	>9.8	>-0.5	<8.4	>41.6	>-1.1	>0.5	<0.2
NGC1275	F06 \circ	99.2 / 0.8 / 0.0	7.22	<0.5	29.0 _{30.3} ^{30.3}	<21.2	>5.9	>0.0	30.9 _{30.7} ^{31.1}	>9.9		
	N08 \bullet	93.8 / 1.1 / 5.1	1.22	<0.5	41.2 _{39.9} ^{42.2}	3.0 _{2.6} ^{3.8}	>46.7	11.2 _{10.3} ^{13.1}	1.0 _{0.5} ^{1.4}	>257.3		
	H10 \circ	97.5 / 1.0 / 1.5	4.71	<0.5	54.1 _{53.5} ^{54.2}	>10.0	56.6 _{56.0} ^{57.2}	>0.0	>80.0			
	S15 \circ	93.5 / 1.6 / 5.0	7.42	<0.5	>85.5	3.12 _{2.68} ^{3.18}	2.7 _{2.6} ^{2.8}	<0.0	>44.5			
	S16 \circ	100.0 / 0.0 / 0.0	8.98	<0.5	40.0 _{39.4} ^{40.1}	53.5 _{53.3} ^{53.8}	<0.0	<0.0	11.26 _{11.21} ^{11.32}	>11.0		
	H17 \circ	97.8 / 0.4 / 1.8	2.74	<0.5	30.1 _{29.6} ^{30.4}	>9.7	>-0.5	7.55 _{7.26} ^{7.65}	>44.8	>-0.5	>0.5	>0.7
E548-G081	F06 \circ	90.2 / 9.8 / 0.0	6.97	<0.5	<0.0	<20.0	4.0 _{3.99} ^{4.01}	<-1.0	<10.0	2.44 _{2.42} ^{2.46}		
	N08 \circ	89.9 / 10.1 / 0.0	2.62	<0.5	>89.5	11.0 _{10.7} ^{11.3}	<28.7	<5.3	>2.5	<10.2		
	H10 \bullet	89.8 / 7.6 / 2.6	1.51	<0.5	44.4 _{45.3} ^{55.3}	>8.3	>48.2	-1.75 _{-1.81} ^{-1.72}	>75.2			
	S15 \circ	81.8 / 18.2 / 0.0	41.64	<0.5	33.0 _{33.06} ^{32.95}	<3.0	<1.5	<0.0	13.5 _{13.5} ^{13.5}			
	S16 \circ	89.2 / 10.8 / 0.0	9.09	<0.5	49.1 _{50.6} ^{50.6}	>79.8	>1.5	>1.5	<10.0	<3.0		
	H17 \bullet	100.0 / 0.0 / 0.0	1.67	0.3 _{0.3} ^{0.3}	14.9 _{13.3} ^{13.3}	7.0 _{6.9} ^{7.1}	<-3.0	<7.0	<30.0	>-0.5	<0.1	0.63 _{0.61} ^{0.64}
2M0350-50	F06	14.3 / 0.0 / 85.7	1.44	2.3 _{1.7} ^{2.7}	>42.8	<21.7	>5.9	>0.0	110.8 _{99.1} ^{139.5}	6.0 _{5.2} ^{6.7}		
	N08	5.8 / 6.2 / 88.0	1.27	<0.5	>54.1	>11.7	>57.0	22.3 _{20.4} ^{24.5}	<0.3	>222.8		
	H10	2.5 / 6.1 / 91.4	1.75	2.9 _{2.4} ^{3.4}	>79.5	>9.2	31.6 _{13.0} ^{35.9}	>0.0	>78.5			
	S15	3.9 / 6.0 / 90.0	1.25	<0.5	>85.1	10.0 _{9.0} ^{10.7}	<2.7	>939.2	>4.9			
	S16	7.6 / 5.6 / 86.8	1.44	1.0 _{0.5} ^{1.5}	60.7 _{65.7} ^{71.5}	49.7 _{48.2} ^{48.4}	<0.0	<0.2	>29.3	>9.6		
	H17	0.8 / 5.9 / 93.2	1.67	5.3 _{4.8} ^{6.8}	44.9 _{42.7} ^{46.4}	>9.6	-1.0 _{-1.2} ^{-0.6}	>14.3	>44.6	>-0.5	0.3 _{0.25} ^{0.36}	>0.7
E549-G049	F06	13.8 / 0.0 / 86.2	1.91	1.5 _{1.8} ^{1.8}	39.7 _{37.4} ^{41.3}	<44.2	<0.0	-0.7 _{-0.8} ^{-0.6}	36.5 _{29.9} ^{42.6}	3.0 _{2.8} ^{3.2}		
	N08	7.8 / 7.2 / 85.0	1.54	2.3 _{2.7} ^{2.9}	>41.1	9.0 _{8.4} ^{9.7}	>63.1	50.0 _{45.9} ^{45.9}	0.5 _{0.3} ^{1.0}	<10.3		
	H10	5.8 / 8.6 / 85.6	2.19	2.3 _{1.6} ^{2.8}	>89.2	>9.8	>56.8	>0.0	>79.3			
	S15	3.5 / 7.3 / 89.3	1.67	0.9 _{0.2} ^{1.2}	>73.3	4.7 _{4.2} ^{4.9}	>75.7	<1.2	13.6 _{13.5} ^{15.0}			
	S16	6.7 / 6.3 / 87.0	1.65	1.7 _{1.6} ^{2.0}	60.0 _{58.3} ^{65.7}	60.0 _{58.3} ^{66.2}	<0.6	<0.5	>29.3	6.1 _{5.2} ^{7.0}		
	H17	4.0 / 8.4 / 87.6	2.04	2.9 _{2.8} ^{3.1}	45.0 _{43.6} ^{46.6}	>9.8	>-0.6	>14.6	>44.7	>-0.5	>0.4	>0.7
3C120	F06 \circ	90.7 / 6.3 / 3.0	3.37	<0.5	<0.0	<20.2	>6.0	>0.1	11.5 _{11.7} ^{11.7}	6.0 _{6.5} ^{6.5}		
	N08 \circ	91.7 / 6.0 / 2.3	1.45	<0.5	>86.3	3.0 _{2.8} ^{3.2}	27.6 _{16.9} ^{43.5}	20.0 _{16.6} ^{21.5}	2.1 _{1.97} ^{2.15}	58.6 _{53.2} ^{61.7}		
	H10 \circ	86.1 / 5.6 / 8.3	1.53	<0.5	50.5 _{47.0} ^{55.2}	6.5 _{5.7} ¹¹	>57.6	-0.61 _{-0.65} ^{-0.65}	>73.6			
	S15 \circ	85.2 / 7.9 / 7.0	14.02	<0.5	>85.9	<3.0	2.58 _{2.54} ^{2.62}	<0.0	13.5 _{13.5} ^{13.5}			
	S16 \circ	88.2 / 5.9 / 5.8	3.72	<0.5	>87.0	>78.7	<0.0	>1.5	10.3 _{10.5} ^{10.5}	3.7 _{3.6} ^{4.0}		
	H17 \bullet	93.8 / 0.0 / 6.2	0.80	0.2 _{0.2} ^{0.2}	30.0 _{29.0} ^{30.2}	>9.4	-2.52 _{-2.53} ^{-2.49}	<7.1	38.0 _{37.2} ^{38.6}	>-0.5	<0.1	>0.7
M-02-12-050	F06	81.4 / 6.0 / 12.7	1.02	<0.5	<0.2	<23.5	>5.9	-0.8 _{-0.9} ^{-0.7}	10.9 _{10.5} ^{11.5}	2.8 _{2.3} ^{3.5}		
	N08	78.9 / 7.4 / 13.7	1.56	<0.5	>75.6	1.25 _{1.19} ^{1.48}	54.7 _{25.7} ^{61.3}	60.0 _{69.9} ^{95.9}	>2.4	78.6 _{66.2} ^{87.8}		
	H10	75.2 / 6.7 / 18.1	1.42	<0.5	29.7 _{26.6} ^{30.3}	>9.0	>59.5	-0.72 _{-0.75} ^{-0.75}	>78.8			
	S15	72.4 / 9.5 / 18.1	2.82	<0.5	>84.0	<3.0	<1.5	<0.0	13.5 _{13.5} ^{14.16}			
	S16	78.4 / 6.8 / 14.7	1.31	<0.5	<11.6	56.0 _{52.5} ^{58.6}	>1.3	>1.3	<10.5	>10.1		
	H17	86.9 / 0.0 / 13.1	0.83	0.2 _{0.2} ^{0.2}	<0.0	>9.2	<-3.0	10.9 _{9.0} ^{12.2}	39.5 _{37.7} ^{40.9}	>-0.5	0.23 _{0.2} ^{0.3}	>0.7
M-01-13-025	F06 \circ	88.8 / 11.2 / 0.0	4.44	<0.5	27.8 _{23.1} ^{29.0}	<20.1	>6.0	>0.0	<10.0	8.7		
	N08 \circ	90.3 / 9.7 / 0.0	2.05	0.6 _{0.6} ^{0.7}	<5.5	>14.4	>16.0	10.0 _{9.6} ^{10.1}	2.0 _{1.9} ^{2.1}	25.1 _{24.0} ^{26.2}		
	H10 \bullet	84.8 / 10.9 / 4.3	1.20	0.4 _{0.3} ^{0.4}	51.6 _{38.5} ^{74.2}	<2.6	50.0 _{43.6} ^{53.2}	-0.4 _{-0.5} ^{-0.5}	<30.7			
	S15 \circ	86.4 / 13.6 / 0.0	6.23	<0.5	>85.6	<3.0	<1.5	<0.0	13.5 _{13.5} ^{13.55}			
	S16 \circ	90.4 / 9.6 / 0.0	4.64	<0.5	70.0 _{69.2} ^{71.9}	>79.7	>1.5	>1.4	<10.0	4.0 _{3.9} ^{4.1}		
	H17 \bullet	91.2 / 8.8 / 0.0	1.52	0.3 _{0.2} ^{0.3}	44.9 _{43.0} ^{46.9}	<5.1	-2.42 _{-2.51} ^{-2.37}	<9.4	>41.4	-0.8 _{-1.0} ^{-0.7}	<0.1	0.32 _{0.28} ^{0.38}
C420-015	F06 \circ	94.7 / 3.9 / 1.4	2.69	<0.5	<0.0	<20.1	4.0 _{3.9} ^{4.13}	>0.0	<10.0	4.37 _{4.43} ^{4.43}		
	N08 \circ	92.9 / 5.4 / 1.7	2.90	<0.5	>87.9	4.5 _{4.4} ^{4.9}	44.7 _{41.4} ^{41.4}	9.2 _{9.6} ^{9.6}	>2.4	40.0 _{37.7} ^{37.7}		
	H10 \circ	90.3 / 3.7 / 6.0	1.77	<0.5	32.0 _{25.0} ^{37.5}	>9.5	39.1 _{37.5} ^{37.5}	-1.35 _{-1.38} ^{-1.32}	>78.2			
	S15 \circ	88.4 / 7.7 / 3.9	35.58	0.4 _{0.4} ^{0.4}	>86.0	<3.0	1.63 _{1.62} ^{1.65}	<0.0	13.5 _{13.5} ^{13.53}			
	S16 \circ	93.3 / 3.5 / 3.2	3.56	<0.5	65.5 _{63.4} ^{68.4}	>78.9	>1.5	>1.5	<10.0	5.25 _{5.16} ^{5.43}		
	H17 \bullet	96.0 / 0.5 / 3.4	0.86	0.2 _{0.1} ^{0.2}	75.1 _{74.0} ^{83.9}	5.6 _{5.2} ^{6.0}	<-3.0	>13.7	36.0 _{35.4} ^{37.2}	>-0.5	>0.5	>0.7
2M0505-23	F06 \circ	100.0 / 0.0 / 0.0	3.03	<0.5	10.0 _{7.5} ^{7.5}	<20.1	4.0 _{3.99} ^{3.99}	<-1.0	<10.0	5.61 _{5.59} ^{5.66}		
	N08 \circ	92.9 / 5.1 / 2.0	1.37	<0.5	>73.9	10.0 _{8.9} ^{10.7}	>60.6	6.5 _{6.0} ^{6.8}	>2.2	20.0 _{19.6} ^{20.3}		
	H10 \bullet	89.5 / 3.0 / 7.5	1.28	0.3 _{0.3} ^{0.3}	75.0 _{72.4} ^{80.5}	>9.9	<5.4	-1.53 _{-1.56} ^{-1.53}	50.4 _{49.6} ^{52.1}			
	S15 \circ	90.2 / 7.0 / 2.8	28.09	0.7 _{0.6} ^{0.7}	>86.0	<3.0	1.81 _{1.79} ^{1.82}	<0.0	13.5 _{13.5} ^{13.52}			
	S16 \circ	95.7 / 2.0 / 2.3	3.79	<0.5	>88.6	>78.8	>1.5	>1.5	<10.0	5.0 _{4.98} ^{5.03}		
	H17 \bullet	94.4 / 0.0 / 5.6	0.85	0.3 _{0.3} ^{0.3}	60.2 _{56.9} ^{62.7}	>7.7	<-3.0	9.9 _{7.5} ^{10.8}	>38.6	-1.5 _{-1.55} ^{-1.55}	0.4 _{0.36} ^{0.45}	>0.6
C468-002	F06	64.4 / 0.0 / 35.6	1.22									

Obj.	Mod	A / S / I %	χ^2/dof	$E_{(B-V)}$	Parameters							
					i	σ	Γ	β	Y	q	$\tau_{9.7\mu m}$	
	F06				i	N_0	σ	Y	q	τ_{cl}	τ_v	
	N08				i	N_0	θ	a			<td></td>	
	H10				i	R_{in}	η	τ_{cl}			<td></td>	
	S15				i	σ	p	Y_{disk}				
	S16				i	N_0	a	q	Y			
	H17				i		σ	θ	θ	$\tau_{9.7\mu m}$		
										a_w	h	f_w
Pictor A	F06o	97.2 / 2.8 / 0.0	10.41	<0.5	26.6 _{36.9} ^{27.2}	<20.0	>6.0	>-0.0	<10.0		>9.9	
	N08o	97.5 / 2.5 / 0.0	7.32	<0.5	52.6 _{50.3} ^{34.9}	9.0 _{8.9} ^{9.1}	>68.9	9.99 _{9.82} ^{10.02}	1.99 _{1.97} ^{2.0}		<10.0	
	H10o	94.8 / 3.2 / 1.9	2.36	<0.5	51.6 _{43.6} ^{33.8}	>8.7	>55.4	-0.61 _{-0.64} ^{-0.58}		<31.8		
	S15o	94.3 / 5.7 / 0.0	20.94	<0.5	>85.9	<3.0	<1.5	<0.0	13.5 _{13.5} ^{13.51}			
	S16o	99.1 / 0.9 / 0.0	10.13	<0.5	79.8 _{80.9} ^{80.9}	>79.9	>1.5	0.87 _{0.85} ^{0.9}	<10.0		<3.0	
NGC2110	H17o•	100.0 / 0.0 / 0.0	1.17	0.3 _{0.2} ^{0.3}	30.0 _{28.8} ^{28.8}	7.0 _{6.9} ^{7.2}	<3.0	<9.4	30.2 _{30.3} ^{30.3}	>-0.5	0.3 _{0.29} ^{0.31}	>0.7
	F06	80.6 / 6.8 / 12.6	3.31	<0.5	<0.0	<20.2	>6.0	>0.0	11.2 _{11.3} ^{11.3}	7.0 _{6.7} ^{7.4}		
	N08	80.7 / 7.4 / 11.9	1.54	<0.5	<40.4	7.0 _{8.6} ^{8.6}	<16.8	9.7 _{7.4} ^{11.6}	1.8 _{1.8} ^{2.0}	109.9 _{87.0} ^{131.8}		
	H10	76.6 / 6.5 / 16.9	1.94	<0.5	<33.7	6.2 _{5.7} ^{5.7}	>58.8	>-0.1	61.4 _{58.0} ^{67.5}			
	S15	77.8 / 8.2 / 14.0	6.71	<0.5	>85.8	<3.0	<1.5	<0.0	21.4 _{20.6} ^{21.6}			
	S16	78.6 / 6.4 / 15.0	3.59	<0.5	>86.4	>79.2	<0.0	>1.5	<10.0			
	H17	85.8 / 0.0 / 14.2	1.84	0.1 _{0.0} ^{0.1}	15.0 _{12.1} ^{15.3}	>9.6	<-2.9	>13.5	32.3 _{31.7} ^{32.6}	>-0.5	<0.1	0.61 _{0.58} ^{0.63}
2M0558-38	F06o	100.0 / 0.0 / 0.0	5.57	2.0 _{1.9} ^{5.5}	<0.1	<20.1	<0.0	<-1.0	<10.0	0.67 _{0.66} ^{0.68}		
	N08o	85.7 / 14.3 / 0.0	2.79	0.5 _{0.3} ^{6.9}	40.7 _{34.2} ^{46.5}	>14.7	>68.2	<5.0	>2.5		<10.0	
	H10o	86.7 / 9.2 / 4.1	1.26	0.9 _{0.8} ^{0.9}	68.5 _{53.9} ^{54.3}	6.0 _{5.6} ^{6.4}	45.0 _{43.7} ^{46.0}	<-2.0	>79.4			
	S15o	80.6 / 19.4 / 0.0	23.40	<0.5	33.0 _{32.7} ^{33.9}	<3.0	<1.5	<0.0	13.5 _{13.5} ^{13.51}			
	S16o	85.3 / 14.7 / 0.0	8.56	0.1 _{0.2} ^{0.2}	>88.3	>79.4	>1.5	>10.0		<3.1		
	H17o•	93.8 / 5.6 / 0.6	0.39	0.7 _{0.6} ^{0.7}	<0.1	6.9 _{5.7} ^{8.0}	<-3.0	9.4 _{7.9} ^{10.6}	>40.7	-1.89 _{-1.91} ^{-1.85}	<0.1	>0.7
Mrk3	F06o	100.0 / 0.0 / 0.0	21.03	0.3 _{0.3} ^{0.4}	<0.0	<20.0	5.3 _{5.31} ^{5.39}	-0.25 _{-0.25} ^{-0.25}	13.1 _{13.0} ^{13.3}	>10.0		
	N08o	97.0 / 3.0 / 0.0	6.33	<0.5	>88.9	14.0 _{13.0} ^{14.2}	55.1 _{54.5} ^{56.3}	10.01 _{9.99} ^{10.24}	<0.0	<10.3		
	H10o	82.5 / 4.6 / 12.9	5.49	<0.5	>89.7	7.2 _{6.9} ^{8.0}	>51.2	>-0.0	31.8 _{32.5} ^{32.5}			
	S15o	97.8 / 2.2 / 0.0	23.65	0.9 _{0.9} ^{1.0}	>86.0	<3.0	7.7 _{7.6} ^{7.7}	29.9 _{29.2} ^{30.0}	13.5 _{13.5} ^{13.51}			
	S16o	100.0 / 0.0 / 0.0	7.83	<0.5	60.0 _{51.5} ^{51.5}	>79.5	0.1 _{0.07} ^{0.07}	<0.0	10.3 _{10.26} ^{10.75}	5.5 _{5.4} ^{6.1}		
	H17o•	92.3 / 0.0 / 7.7	5.42	0.6 _{0.5} ^{0.6}	45.0 _{44.9} ^{44.9}	>9.9	-2.63 _{-2.64} ^{-2.62}	>14.9	>45.0	>-0.5	0.34 _{0.34} ^{0.36}	0.36 _{0.36} ^{0.37}
E426-G002	F06o•	100.0 / 0.0 / 0.0	1.27	<0.5	<0.0	53.7 _{52.8} ^{54.3}	>5.8	<-0.9	12.2 _{11.8} ^{12.7}	4.3 _{4.2} ^{4.7}		
	N08o	89.2 / 5.0 / 5.8	1.82	<0.5	<2.0	>13.6	38.5 _{37.9} ^{39.4}	7.4 _{7.4} ^{7.6}	<0.0	40.3 _{38.7} ^{45.0}		
	H10o•	89.2 / 2.8 / 8.0	1.07	0.2 _{0.2} ^{0.3}	15.0 _{11.3} ^{15.6}	>9.9	46.8 _{45.9} ^{47.7}	-0.3 _{-0.52} ^{-0.42}	>79.5			
	S15o	80.2 / 6.5 / 13.2	9.18	0.5 _{0.5} ^{0.5}	>85.9	<3.0	7.5 _{7.2} ^{7.7}	<0.0	13.5 _{13.5} ^{13.52}			
	S16o•	90.4 / 3.1 / 6.5	1.09	0.2 _{0.2} ^{0.2}	10.0 _{6.2} ^{11.6}	62.6 _{62.0} ^{63.0}	1.2 _{1.2} ^{1.3}	<0.0	<10.3	>10.9		
	H17o•	94.6 / 0.0 / 5.4	1.18	0.5 _{0.5} ^{0.5}	<0.0	>9.9	-1.36 _{-1.38} ^{-1.35}	<7.8	>43.6	>-0.6	>0.5	0.6 _{0.57} ^{0.65}
UGC3478	F06	73.3 / 8.6 / 18.1	1.90	<0.5	<0.1	<21.2	4.0 _{3.8} ^{4.3}	>-0.3	33.6 _{32.6} ^{34.9}	2.2 _{2.1} ^{2.3}		
	N08	74.7 / 8.5 / 16.9	2.59	<0.5	<14.5	2.3 _{2.1} ^{3.1}	>62.4	20.0 _{19.0} ^{20.9}	0.6 _{0.2} ^{0.2}	44.7 _{40.9} ^{52.6}		
	H10	70.0 / 8.7 / 21.3	2.65	<0.5	46.2 _{43.8} ^{46.7}	8.9 _{8.4} ^{8.6}	>59.5	>-0.0	>79.7			
	S15	67.6 / 9.2 / 23.1	2.08	<0.5	52.0 _{48.8} ^{52.2}	<3.0	12.3 _{10.3} ^{12.4}	<0.0	13.5 _{13.5} ^{13.68}			
	S16	72.7 / 7.8 / 19.6	1.79	<0.5	63.0 _{56.4} ^{60.8}	49.8 _{45.4} ^{62.8}	<0.0	>1.3	17.0 _{15.8} ^{18.8}	<3.7		
	H17	73.7 / 5.9 / 20.4	1.58	<0.5	<1.1	>9.8	-1.35 _{-1.43} ^{-1.29}	>14.6	>44.5	>-0.5	0.29 _{0.25} ^{0.32}	>0.7
UGC3601	F06o	89.4 / 2.4 / 8.1	2.20	<0.5	<0.0	<20.4	>5.9	-0.11 _{-0.26} ^{-0.06}	10.6 _{10.4} ^{11.2}	7.9 _{7.2} ^{8.4}		
	N08o•	86.8 / 3.5 / 9.7	1.36	<0.5	>79.8	>9.5	<20.3	10.1 _{9.7} ^{10.3}	0.4 _{0.1} ^{0.7}	<12.8		
	H10	77.7 / 4.2 / 18.2	1.32	<0.5	51.0 _{38.5} ^{62.0}	6.1 _{4.0} ^{6.9}	>48.7	>-0.0	<38.5			
	S15	83.2 / 5.0 / 11.8	5.07	<0.5	>85.8	<3.0	4.0 _{3.2} ^{4.2}	<0.0	13.5 _{13.5} ^{13.56}			
	S16o	89.0 / 2.1 / 8.9	2.10	<0.5	9.8 _{8.0} ^{10.7}	78.3 _{77.3} ^{78.7}	1.0 _{0.99} ^{1.02}	<0.0	<10.0	4.8 _{4.6} ^{5.0}		
	H17	84.5 / 0.0 / 15.5	1.10	<0.5	45.0 _{44.3} ^{45.6}	7.0 _{6.8} ^{7.5}	-2.52 _{-2.62} ^{-2.49}	12.6 _{11.9} ^{13.1}	>44.6	>-0.5	<0.2	0.3 _{0.29} ^{0.32}
Mrk78	F06o	84.1 / 0.0 / 15.9	1.89	<0.5	60.2 _{51.3} ^{53.2}	<20.2	<0.0	>-0.0	<10.0	4.3 _{4.2} ^{4.4}		
	N08o•	77.7 / 6.8 / 15.5	1.20	0.4 _{0.3} ^{0.4}	>82.1	12.4 _{10.8} ^{13.4}	>58.0	10.0 _{9.9} ^{10.5}	1.0 _{0.8} ^{1.1}	20.9 _{19.1} ^{19.6}		
	H10	59.8 / 6.9 / 33.3	2.15	0.2 _{0.2} ^{0.3}	>86.5	>9.2	>58.4	>-0.1	34.1 _{31.9} ^{36.6}			
	S15o	81.3 / 5.3 / 13.3	9.31	1.2 _{1.2} ^{1.2}	>86.0	<3.0	1.89 _{1.87} ^{1.92}	30.0 _{29.3} ^{30.2}	>44.9			
	S16o•	74.6 / 3.9 / 21.4	1.26	<0.0	80.0 _{74.8} ^{83.2}	>77.0	0.4 _{0.2} ^{0.3}	<0.2	10.3 _{10.1} ^{10.5}	9.0 _{8.5} ^{9.4}		
	H17o•	65.1 / 6.9 / 27.9	1.64	0.4 _{0.4} ^{0.5}	>89.7	<6.0	-1.4 _{-1.8} ^{-1.3}	>14.4	>44.1	>-0.5	<0.1	0.6 _{0.57} ^{0.66}
Mrk10	F06o	100.0 / 0.0 / 0.0	1.67	<0.5	>85.4	33.4 _{32.1} ^{33.8}	<0.0	>-0.0	10.4 _{10.2} ^{10.5}	>9.5		
	N08o•	84.8 / 8.2 / 7.1	0.96	<0.5	>46.4	>7.3	>15.0	>69.3	>2.2	45.5 _{34.5} ^{53.6}		
	H10o•	75.4 / 8.2 / 16.4	1.41	<0.5	55.8 _{52.3} ^{56.8}	>8.8	>55.9	>-0.0	66.1 _{63.2} ^{70.8}			
	S15o	76.8 / 8.5 / 14.7	3.63	<0.5	>85.9	<3.0	2.06 _{1.97} ^{2.1}	<0.0	>44.7			
	S16o•	80.7 / 7.2 / 12.1	1.11	<0.5	25.8 _{23.7} ^{31.3}	64.1 _{61.8} ^{68.8}	<0.0	<0.1	<10.2	>10.5		
	H17	72.3 / 8.3 / 19.4	1.25	<0.5	75.0 _{74.2} ^{74.2}	>9.7	>-0.5	10.0 _{8.4} ^{10.4}	>41.0	-1.0 _{-1.1} ^{-0.9}	<0.3	0.57 _{0.51} ^{0.64}
IC0486	F06o•	87.3 / 0.0 / 12.7	1.48	<0.5	>85.8	34.3 _{33.6} ^{35.1}	<0.0	>-0.0	11.0 _{10.6} ^{11.1}	>9.8		
	N08	66.2 / 8.0 / 25.8	1.03	<0.5	32.3 _{31.7} ^{34.7}	>9.6	41.0 _{37.8} ^{43.8}	7.5 _{7.0} ^{8.4}	<0.6	120.0 _{98.8} ^{136.8}		
	H10	65.8 / 7.8 / 26.4	1.49	<0.5	57.1 _{54.2} ^{58.3}	>9.8	>56.0	>-0.0	74.8 _{71.9} ^{76.7}			
	S15	64.7 / 8.0 / 27.4	3.46	<0.5	>85.8	<3.0	2.7 _{2.61} ^{2.75}	<0.0	>44.6			
	S16	67.5 / 6.9 / 25.6	1.34	<0.5	29.8 _{22.0} ^{31.0}	64.1 _{62.8} ^{65.3}	<0.0	<0.0	10.8 _{10.0} ^{11.0}	>10.9		
	H17	64.1 / 8.4 / 27.5	1.21	<0.5	86.4 _{86.2} ^{86.6}	>9.8	>-0.5	<9.5	<31.6	-1.5 _{-1.6} ^{-1.2}	<0.1	<0.2
Mrk1210	F06o	99.2 / 0.8 / 0.0	11.59	<0.5	10.0 _{9.5} ^{10.1}	<20.0	>6.0	>-0.0	17.1 _{15.0} ^{17.2}	>10.0		
	N08o	97.6 / 2.4 / 0.0	3.39	<0.5	>77.6	10.9 _{10.7} ^{11.3}	>67.4	19.9 _{19.6} ^{20.0}	1.2 _{1.18} ^{1.22}	<10.0		
	H10o	86.5 / 4.3 / 9.2	1.97	0.2 _{0.2} ^{0.3}	>88.3	<2.5	>59.0	>-0.0	66.5 _{65.4} ^{67.2}			
	S15o	97.2 / 2.8 / 0.0	9.30	0.7 _{0.7} ^{0.8}	>86.0	<3.0	7.69 _{7.61} ^{7.71}	5.9 _{5.3} ^{6.5}	13.5 _{13.2} ^{13.52}			
	S16o	100.0 / 0.0										

Table 4. Spectral fit results (continuation).

Obj.	Mod	A / S / I %	χ^2/dof	$E_{(B-V)}$	Parameters								
					i	σ	Γ	β	Y	$\tau_{9.7\mu m}$	τ_v	τ_{cl}	τ_{disk}
	F06												
	N08				i	N_0	σ	Y	q				
	H10				i	N_0	θ	a					
	S15				i	R_{in}	η	τ_{cl}					
	S16				i	σ	p	q	Y				
	H17				i	N_0	a	σ	θ	$\tau_{9.7\mu m}$			
Mrk18	F06	6.7/ 8.7/ 84.6	1.51	1.2 _{1.0} ^{1.3}	40.0 _{37.4} ^{41.5}	49.0 _{47.8} ^{49.9}	<0.0	-0.75 _{-0.76} ^{-0.66}	39.7 _{30.3} ^{55.4}	4.6 _{3.9} ^{5.3}			
	N08	7.5/ 10.2/ 82.3	1.19	0.5 _{0.9} ^{1.1}	>48.9	>9.9	>55.7	20.0 _{17.8} ^{21.5}	<1.2	>198.5			
	H10	9.2/ 11.8/ 79.0	1.99	1.2 _{1.0} ^{1.4}	>76.5	>9.9	<7.6	>-0.0	>79.6				
	S15	5.3/ 10.1/ 84.5	1.19	<0.5	>79.6	4.1 _{4.4} ^{4.4}	39.0 _{27.1} ^{60.1}	>787.9	14.4 _{10.8} ^{22.6}				
	S16	10.0/ 9.9/ 80.2	1.33	<0.5	>84.4	46.5 _{44.1} ^{44.1}	<0.2	<0.4	>28.7	>9.9			
	H17	3.7/ 11.7/ 84.6	2.02	3.5 _{3.8} ^{3.7}	45.1 _{44.8} ^{48.0}	>9.9	>-0.6	>14.7	>44.8	>-0.5	>0.4	>0.7	
M-01-24-012	F06o●	100.0/ 0.0/ 0.0	0.66	0.7 _{0.8} ^{0.9}	69.2 _{61.3} ^{61.3}	<24.7	2.1 _{1.5} ^{2.5}	<-0.6	20.2 _{16.3} ^{22.9}	>9.2			
	N08o	80.6/ 8.2/ 11.3	2.39	0.9 _{0.8} ^{0.9}	<31.7	9.0 _{8.4} ^{14.4}	>64.4	13.2 _{12.8} ^{14.6}	<0.7	25.9 _{22.4} ^{29.1}			
	H10o	66.7/ 10.0/ 23.4	1.90	0.9 _{0.8} ^{0.9}	45.1 _{49.6} ^{49.6}	5.6 _{4.7} ^{4.7}	42.4 _{39.7} ^{46.7}	>-0.0	>79.6				
	S15o	65.0/ 10.2/ 24.8	3.41	1.3 _{1.2} ^{1.8}	59.1 _{58.3} ^{58.3}	<3.0	38.5 _{38.1} ^{38.6}	<0.0	13.5 _{13.5} ^{13.5}				
	S16o●	100.0/ 0.0/ 0.0	0.87	0.8 _{0.7} ^{0.9}	73.1 _{69.9} ^{26.0}	>24.8 _{24.0} ^{26.0}	>1.5	>1.3	20.9 _{19.7} ^{22.9}	6.1 _{5.7} ^{6.6}			
	H17o●	87.9/ 0.0/ 12.1	1.12	1.3 _{1.2} ^{1.2}	1.6 _{1.6} ^{1.6}	>9.9	-1.28 _{-1.31} ^{-1.24}	>14.9	>44.9	>-0.5	>0.5	>0.7	
M+04-22-042	F06o	94.9/ 5.1/ 0.0	7.05	<0.5	20.1 _{19.9} ^{20.3}	<20.0	>6.0	<-1.0	<10.0	>10.0			
	N08o	94.3/ 5.7/ 0.0	4.66	<0.5	>86.6	>14.6	34.4 _{30.8} ^{40.8}	9.0 _{8.3} ^{9.3}	>2.5	<10.1			
	H10o	93.1/ 4.8/ 2.1	1.71	<0.5	54.0 _{49.5} ^{58.2}	>9.4	37.3 _{34.7} ^{34.7}	-1.71 _{-1.77} ^{-1.77}	>79.1				
	S15o	91.6/ 8.4/ 0.0	49.23	<0.5	>85.9	<3.0	<1.5	<0.0	13.5 _{13.5} ^{13.5}				
	S16o	95.8/ 4.2/ 0.0	7.75	<0.5	>87.2	>79.9	>1.5	>1.5	<10.0	3.76 _{3.73} ^{3.78}			
	H17o●	98.5/ 1.5/ 0.0	0.97	0.0 _{0.0} ^{0.1}	60.1 _{59.3} ^{61.2}	>9.4	<3.0	9.4 _{8.8} ^{9.7}	43.2 _{40.8} ^{44.7}	>-0.5	>0.4	0.3 _{0.24} ^{0.32}	
Mrk110	F06o	94.3/ 5.7/ 0.0	14.39	<0.5	<0.0	<20.0	4.0 _{3.99} ^{4.01}	<-1.0	<10.0	2.342 _{2.31} ^{2.38}			
	N08o	94.2/ 5.8/ 0.0	7.22	<0.5	70.2 _{66.6} ^{77.7}	7.0 _{6.9} ^{7.1}	>68.7	<5.0	>2.5	<10.0			
	H10o●	91.9/ 6.9/ 1.2	1.95	<0.5	75.4 _{79.0} ^{79.0}	>9.8	45.1 _{43.6} ^{46.7}	-1.5 _{-1.51} ^{-1.5}	<30.2				
	S15o	86.5/ 13.5/ 0.0	33.11	<0.5	33.0 _{33.1} ^{33.1}	<3.0	<1.5	<0.0	13.5 _{13.5} ^{13.5}				
	S16o	93.0/ 7.0/ 0.0	15.28	<0.5	51.8 _{49.7} ^{49.7}	>79.8	>1.5	>1.5	<10.0	<3.0			
	H17o	94.3/ 5.7/ 0.0	2.52	<0.5	60.1 _{59.5} ^{60.9}	7.0 _{6.9} ^{7.2}	-2.5 _{-2.51} ^{-2.5}	10.0 _{9.8} ^{10.8}	>44.6	<-2.4	0.4 _{0.39} ^{0.41}	>0.7	
Mrk705	F06o	89.5/ 4.3/ 6.2	3.77	<0.5	10.5 _{10.1} ^{10.8}	<20.1	>6.0	>-0.0	>10.0	>9.9			
	N08o	89.2/ 4.6/ 6.3	2.09	<0.5	>89.2	10.9 _{10.4} ^{11.8}	<24.8	10.0 _{9.7} ^{10.4}	2.342 _{2.29} ^{2.43}	20.0 _{18.9} ^{20.9}			
	H10o	82.0/ 4.1/ 13.8	2.73	<0.5	57.9 _{56.0} ^{64.9}	>9.6	>52.6	-0.91 _{-0.95} ^{-0.87}	36.7 _{34.5} ^{37.9}				
	S15o	85.1/ 6.6/ 8.4	26.67	0.4 _{0.4} ^{0.4}	>86.0	<3.0	<1.5	<0.0	16.4 _{16.2} ^{16.6}				
	S16o	90.0/ 2.4/ 7.5	4.62	<0.5	70.1 _{68.7} ^{71.0}	>79.8	>1.5	>1.5	<10.0	5.5 _{5.4} ^{5.6}			
	H17	86.7/ 1.7/ 11.6	1.46	<0.5	45.7 _{45.0} ^{46.2}	7.01 _{6.95} ^{7.24}	<3.0	<7.2	>44.9	-1.5 _{-1.51} ^{-1.5}	>0.5	0.61 _{0.59} ^{0.63}	
M+10-14-025	F06o	53.4/ 14.5/ 32.1	6.21	3.7 _{4.0} ^{4.0}	<1.2	>59.6	2.0 _{1.2} ^{2.2}	>-0.0	>147.8	1.7 _{1.6} ^{1.8}			
	N08	9.8/ 22.7/ 67.5	8.21	6.5 _{6.7} ^{6.7}	59.9 _{50.6} ^{62.4}	3.3 _{2.8} ^{3.9}	<15.6	>98.1	1.32 _{1.26} ^{1.37}	>280.5			
	H10	3.9/ 24.0/ 72.2	10.49	6.2 _{6.4} ^{6.4}	<0.0	>9.9	19.2 _{15.4} ^{21.7}	>-0.0	>79.8				
	S15	19.1/ 21.5/ 59.4	7.49	5.3 _{5.4} ^{5.4}	51.9 _{51.3} ^{52.4}	>15.3	>75.6	>962.1	4.9 _{4.8} ^{5.0}				
	S16o	35.7/ 6.8/ 57.5	6.81	5.2 _{5.3} ^{5.3}	70.0 _{67.0} ^{70.0}	19.9 _{17.6} ^{20.0}	<0.1	<0.0	>29.7	>10.9			
	H17	1.7/ 24.2/ 74.1	11.32	8.2 _{8.1} ^{8.3}	88.4 _{88.1} ^{88.1}	>10.0	>0.5	10.1 _{9.3} ^{11.7}	>42.3	<-2.5	<0.1	0.3 _{0.29} ^{0.32}	
M-05-23-016	F06o	100.0/ 0.0/ 0.0	1.79	<0.5	59.9 _{57.8} ^{60.6}	<20.1	2.05 _{2.01} ^{2.09}	>-0.0	<10.0	8.5 _{8.9} ^{8.9}			
	N08o	94.4/ 5.6/ 0.0	1.61	0.4 _{0.3} ^{0.4}	<1.8	>14.6	>67.8	11.4 _{11.6} ^{11.6}	1.72 _{1.61} ^{1.74}	20.0 _{19.6} ^{20.14}			
	H10o	83.0/ 5.7/ 11.3	1.60	0.3 _{0.2} ^{0.3}	59.7 _{53.3} ^{68.0}	>9.5	<19.6	-1.27 _{-1.33} ^{-1.22}	64.4 _{62.0} ^{68.1}				
	S15o	86.7/ 6.3/ 7.0	29.63	1.3 _{1.3} ^{1.3}	>86.0	<3.0	<1.5	<0.0	>45.0				
	S16o●	92.5/ 3.0/ 4.5	0.95	<0.5	10.5 _{10.1} ^{15.4}	>78.5	>1.4	0.5 _{0.4} ^{0.6}	11.3 _{10.8} ^{11.4}	>10.6			
	H17o●	89.8/ 3.3/ 7.0	0.94	0.4 _{0.4} ^{0.5}	>77.3	>8.4	-2.65 _{-2.74} ^{-2.6}	>13.7	>43.2	-0.9 _{-1.0} ^{-0.8}	0.29 _{0.25} ^{0.33}	>0.6	
NGC3081	F06o	98.5/ 1.5/ 0.0	3.77	<0.5	9.96 _{8.06} ^{10.04}	<20.1	>5.8	>-0.0	18.0 _{17.8} ^{18.2}	>10.0			
	N08o●	92.0/ 3.5/ 4.5	1.26	<0.0	>71.3	5.5 _{5.7} ^{5.7}	>60.9	16.8 _{16.3} ^{18.5}	2.0 _{1.97} ^{2.03}	56.4 _{52.3} ^{59.1}			
	H10o	80.7/ 3.6/ 15.7	2.24	<0.5	77.8 _{74.9} ^{80.8}	3.6 _{3.4} ^{3.9}	>56.8	>0.0	67.4 _{66.2} ^{69.2}				
	S15o	91.6/ 3.0/ 5.4	10.71	0.5 _{0.5} ^{0.5}	>86.0	<3.0	<1.5	9.2 _{8.2} ^{10.3}	>44.9				
	S16o	93.0/ 1.1/ 5.8	1.97	<0.5	40.1 _{38.8} ^{40.8}	61.8 _{61.1} ^{62.4}	<0.0	<0.0	<10.0	7.0 _{6.8} ^{7.1}			
	H17o●	83.7/ 0.5/ 15.8	1.01	<0.5	52.5 _{50.7} ^{50.7}	>6.8	<3.0	>13.6	42.2 _{40.6} ^{43.4}	>-0.5	<0.3	>0.5	
E374-G044	F06o	100.0/ 0.0/ 0.0	8.14	<0.5	<0.0	<20.1	5.7 _{5.6} ^{5.8}	-0.25 _{-0.26} ^{-0.25}	11.8 _{11.7} ^{12.1}	>10.0			
	N08o	97.2/ 2.8/ 0.0	2.21	<0.5	>85.4	11.3 _{10.9} ^{12.5}	>63.5	10.0 _{9.9} ^{10.1}	>2.5	47.5 _{35.8} ^{49.7}			
	H10o	85.8/ 2.4/ 11.9	2.21	<0.5	>88.7	4.1 _{3.9} ^{3.9}	>88.7	48.2 _{44.4} ^{58.4}	>-0.0	38.1 _{36.7} ^{40.1}			
	S15o	100.0/ 0.0/ 0.0	10.39	0.6 _{0.6} ^{0.7}	>86.0	<3.0	7.68 _{7.61} ^{7.74}	1.0 _{0.9} ^{1.1}	13.5 _{13.5} ^{13.54}				
	S16o	100.0/ 0.0/ 0.0	2.97	<0.5	50.0 _{48.8} ^{50.9}	>79.8	<0.0	<0.0	<10.0	4.2 _{4.12} ^{4.24}			
	H17o●	92.1/ 0.0/ 7.9	1.17	0.2 _{0.1} ^{0.2}	45.0 _{44.6} ^{45.7}	7.0 _{6.8} ^{7.2}	-2.72 _{-2.74} ^{-2.7}	>14.8	>44.9	>-0.5	<0.1	0.36 _{0.36} ^{0.38}	
NGC3227	F06o	75.8/ 0.0/ 24.2	1.82	<0.5	60.0 _{57.3} ^{64.2}	<26.3	<0.0	-0.3 _{-0.3} ^{-0.2}	13.7 _{12.9} ^{14.7}	3.0 _{2.6} ^{3.2}			
	N08	62.5/ 6.7/ 30.9	1.36	<0.5	>82.8	11.1 _{10.4} ^{12.5}	>33.4	25.4 _{22.4} ^{31.1}	1.0 _{0.8} ^{1.6}	<10.5			
	H10	52.4/ 7.5/ 40.1	1.64	0.1 _{0.0} ^{0.1}	>87.9	<2.7	>58.7	>0.0	>78.9				
	S15	66.7											

Obj.	Mod	A / S / I %	χ^2/dof	$E_{(B-V)}$	Parameters						
	F06				i	σ	Γ	β	Y	$\tau_{9.7\mu m}$	
	N08				i	N_0	σ	Y	q		τ_v
	H10				i	N_0	θ	a			τ_{cl}
	S15				i	R_{in}	η	τ_{cl}			τ_{disk}
	S16				i	σ	p	q			Y
	H17				i	N_0	a	σ	θ		$\tau_{9.7\mu m}$
Mrk417	F06o	97.9/ 2.1/ 0.0	5.35	<0.5	9.9 _{6.8} ^{10.1}	<20.1	5.52 _{5.48} ^{5.58}	>-0.0	<10.0	>10.0	
	N08o	95.9/ 4.1/ 0.0	3.60	<0.5	>83.6	>14.6	>67.3	10.0 _{9.9} ^{10.1}	1.99 _{1.95} ^{2.01}	<10.1	
	H10o•	92.3/ 5.4/ 2.3	1.49	<0.5	76.6 _{74.2} ^{81.3}	>9.6	>58.0	-0.83 _{-0.86} ^{0.79}	<30.7		
	S15o	93.9/ 6.1/ 0.0	10.93	0.8 _{0.8} ^{0.8}	>85.9	<3.0	3.5 _{3.4} ^{3.6}	<0.0	13.5 _{13.5} ^{13.52}		
	S16o	100.0/ 0.0/ 0.0	3.80	<0.5	>75.9	>79.7	>1.5	<0.0	<10.0	<3.1	
	H17o•	95.9/ 4.1/ 0.0	1.47	0.2 _{0.1} ^{0.2}	59.7 _{57.8} ^{75.8}	>9.8	-2.5 _{-2.52} ^{-2.49}	>14.7	>44.8	-1.97 _{-1.99} ^{-1.95}	>0.5 >0.7
Mrk421	F06o	88.9/ 7.4/ 3.7	3.51	0.8 _{0.9} ^{0.9}	39.9 _{32.3} ^{46.0}	<20.2	<0.0	<-1.0	<10.0	0.55 _{0.54} ^{0.56}	
	N08	82.8/ 13.0/ 4.2	4.75	<0.5	>89.7	8.6 _{8.3} ^{8.8}	<17.4	<5.0	>2.5	<10.1	
	H10	83.9/ 8.6/ 7.6	2.28	<0.5	60.2 _{51.5} ^{61.5}	5.0 _{4.9} ^{4.9}	45.0 _{43.9} ^{45.5}	<-2.0	>79.5		
	S15o	76.7/ 21.4/ 1.9	23.57	<0.5	33.0 _{33.9} ^{33.3}	<3.0	<1.5	<0.0	13.5 _{13.5} ^{13.51}		
	S16o	83.2/ 13.4/ 3.3	7.19	<0.5	32.3 _{33.1} ^{33.9}	70.1 _{69.8} ^{70.7}	>1.5	>1.5	<10.0	<3.0	
	H17	85.5/ 7.8/ 6.8	1.49	<0.5	81.3 _{78.5} ^{78.5}	6.2 _{5.3} ^{5.3}	<-3.0	<7.8	>43.5	-2.23 _{-2.27} ^{-2.18}	<0.1 >0.6
NGC3783	F06o	100.0/ 0.0/ 0.0	4.37	<0.5	60.0 _{59.7} ^{60.4}	28.1 _{27.6} ^{28.4}	0.08 _{0.06} ^{0.1}	-0.5 _{-0.52} ^{-0.45}	<10.0	4.3 _{4.2} ^{4.5}	
	N08o	92.2/ 7.8/ 0.0	2.63	<0.5	84.3 _{82.2} ^{86.1}	5.0 _{4.7} ^{5.5}	<21.4	10.5 _{10.2} ^{10.6}	<0.0	40.6 _{38.7} ^{43.3}	
	H10o•	88.0/ 7.8/ 4.2	1.00	<0.5	47.2 _{40.2} ^{40.2}	5.0 _{4.2} ^{4.2}	48.6 _{46.1} ^{52.1}	>0.0	>79.3		
	S15o	91.4/ 8.3/ 0.3	7.80	<0.5	>86.0	<3.0	<1.5	0.18 _{0.17} ^{0.2}	>44.9		
	S16o	94.1/ 5.9/ 0.0	1.59	<0.5	40.0 _{38.2} ^{41.8}	59.8 _{58.1} ^{60.6}	<0.0	<0.1	11.1 _{10.8} ^{11.3}	4.0 _{3.7} ^{4.3}	
	H17o•	98.3/ 0.0/ 1.7	0.66	0.4 _{0.3} ^{0.4}	29.9 _{29.6} ^{29.6}	>10.0	-1.97 _{-1.99} ^{-1.94}	10.0 _{9.98} ^{10.07}	>44.9	-0.58 _{-0.6} ^{-0.56}	>0.5 >0.7
NGC3786	F06	34.4/ 5.5/ 60.1	1.66	<0.5	59.8 _{54.1} ^{62.2}	<22.7	<0.0	-0.7 _{-0.9} ^{-0.5}	<10.7	2.6 _{2.4} ^{3.1}	
	N08	34.9/ 9.2/ 55.9	1.67	<0.5	>40.0	>8.2	>45.6	<5.2	2.1 _{1.8} ^{2.3}	>200.6	
	H10	29.6/ 8.0/ 62.4	1.52	1.0 _{1.4} ^{1.4}	>76.5	<5.2	>55.7	>-0.0	60.6 _{59.6} ^{61.6}		
	S15	32.5/ 8.5/ 58.9	2.07	0.7 _{0.6} ^{0.8}	>85.5	<3.0	7.7 _{7.0} ^{7.9}	0.7 _{0.4} ^{1.1}	13.52 _{13.51} ^{14.06}		
	S16	30.9/ 7.1/ 61.9	1.63	<0.5	>55.2	>74.1	>1.2	>0.0	15.3 _{14.9} ^{15.9}	5.0 _{3.9} ^{9.3}	
	H17	42.4/ 0.0/ 57.6	1.79	1.2 _{1.0} ^{1.3}	<0.4	>9.5	-2.7 _{-2.9} ^{-2.6}	>13.4	35.8 _{35.1} ^{38.3}	>-0.5	<0.1 >0.7
UGC6728	F06o	93.4/ 6.6/ 0.0	3.17	<0.5	23.1 _{22.6} ^{23.7}	<20.1	>6.0	<-1.0	<10.0	>9.8	
	N08o	93.3/ 6.7/ 0.0	1.84	<0.5	>68.7	11.3 _{10.0} ^{13.0}	<52.5	10.0 _{9.2} ^{10.3}	2.3 _{2.1} ^{2.4}	<10.3	
	H10o•	90.5/ 6.5/ 3.0	1.28	<0.5	>86.3	3.1 _{2.7} ^{3.8}	<13.7	-1.52 _{-1.57} ^{-1.48}	>73.0		
	S15o	90.2/ 9.8/ 0.0	10.78	<0.5	>20.8	<3.0	<1.5	<0.0	13.5 _{13.5} ^{13.53}		
	S16o	94.3/ 5.7/ 0.0	3.25	<0.5	>77.8	>79.5	>1.5	1.18 _{1.15} ^{1.22}	<10.0	<3.2	
	H17o•	95.3/ 3.2/ 1.6	1.07	<0.5	54.2 _{53.4} ^{58.0}	<5.7	<-2.9	>14.2	>43.6	>-0.5	>0.5 0.18 _{0.16} ^{0.21}
2MX1145-18	F06o	93.6/ 6.4/ 0.0	4.53	<0.5	18.0 _{17.6} ^{17.6}	<20.0	>6.0	<-1.0	<10.0	>9.9	
	N08o	92.9/ 7.1/ 0.0	2.65	<0.5	45.4 _{45.8} ^{56.8}	7.1 _{8.1} ^{8.4}	>30.0	9.0 _{8.4} ^{10.9}	>2.4	19.9 _{15.6} ^{20.7}	
	H10o	91.3/ 6.1/ 2.6	1.91	<0.5	60.1 _{58.3} ^{64.1}	8.3 _{7.6} ^{8.2}	>43.6	-1.57 _{-1.61} ^{-1.52}	>78.5		
	S15o	90.1/ 9.8/ 0.1	26.67	<0.5	>85.9	<3.0	<1.5	<0.0	13.5 _{13.5} ^{13.51}		
	S16o	94.3/ 5.7/ 0.0	5.09	<0.5	79.8 _{77.6} ^{82.3}	>79.8	>1.5	>1.5	<10.0	4.0 _{3.9} ^{4.2}	
	H17o•	97.1/ 1.5/ 0.8	1.08	0.0 _{0.0} ^{0.1}	60.0 _{59.2} ^{59.2}	<5.1	<3.0	>14.4	>43.6	>-0.5	>0.4 0.28 _{0.26} ^{0.31}
Ark347	F06o	88.4/ 6.1/ 5.6	2.00	<0.5	<0.0	<21.0	>5.9	>-0.0	11.2 _{11.1} ^{11.4}	8.5 _{8.3} ^{9.0}	
	N08o	88.4/ 6.3/ 5.3	1.51	<0.5	>51.2	1.9 _{1.7} ^{4.2}	>50.8	6.9 _{7.3} ^{7.3}	<0.9	60.0 _{55.1} ^{65.9}	
	H10o	85.7/ 5.1/ 9.1	2.09	<0.5	45.0 _{36.9} ^{49.4}	>9.5	56.0 _{55.1} ^{59.1}	-0.7 _{-0.8} ^{-0.6}	73.1 _{69.8} ^{78.9}		
	S15o	84.1/ 7.7/ 8.2	12.36	0.3 _{0.2} ^{0.3}	>85.9	<3.0	<1.5	<0.0	27.0 _{26.3} ^{27.2}		
	S16o	88.5/ 5.1/ 6.4	2.13	<0.5	10.0 _{10.6} ^{10.6}	75.9 _{75.6} ^{75.6}	1.0 _{0.99} ^{1.01}	<0.0	<10.0	5.0 _{4.97} ^{5.03}	
	H17o•	90.9/ 0.0/ 9.1	1.01	<0.0	28.4 _{30.6} ^{30.6}	<6.2	<3.0	10.0 _{9.4} ^{10.2}	>44.2	>-0.6	<0.2 0.63 _{0.59} ^{0.75}
UGC7064	F06o	83.6/ 0.0/ 16.4	2.33	<0.5	66.0 _{53.7} ^{63.7}	<21.2	<0.1	>-0.1	11.8 _{11.6} ^{12.4}	5.6 _{5.0} ^{6.1}	
	N08o•	75.2/ 3.9/ 20.9	1.29	<0.5	>86.5	6.4 _{6.1} ^{6.8}	<42.3	19.9 _{18.4} ^{20.8}	1.5 _{1.3} ^{1.6}	42.2 _{33.2} ^{33.2}	
	H10o	65.4/ 4.7/ 29.9	1.59	<0.5	72.0 _{69.1} ^{73.6}	3.8 _{3.5} ^{4.2}	>52.2	>0.0	>79.3		
	S15	73.3/ 3.9/ 22.8	3.88	<0.5	>85.8	<3.0	<1.7	28.3 _{14.2} ^{31.0}	>44.6		
	S16	73.7/ 2.8/ 23.5	1.52	<0.5	49.4 _{45.1} ^{51.5}	50.4 _{48.9} ^{51.4}	<0.0	<0.0	<10.2	7.0 _{6.5} ^{7.3}	
	H17	70.8/ 0.0/ 29.2	1.09	0.1 _{0.0} ^{0.1}	21.3 _{20.4} ^{30.4}	>8.4	<-2.9	>13.9	>41.3	>-0.5	<0.1 >0.7
NGC4151	F06o	96.0/ 4.0/ 0.0	3.94	<0.5	10.2 _{7.1} ^{28.4}	<20.1	>6.0	>0.0	<10.0	>9.8	
	N08o	94.8/ 5.2/ 0.0	2.02	<0.5	>87.5	>14.1	28.7 _{25.1} ^{35.6}	10.1 _{9.7} ^{10.7}	1.64 _{1.58} ^{1.75}	<10.2	
	H10o	88.1/ 4.8/ 7.1	1.89	<0.5	69.6 _{64.8} ^{78.4}	8.3 _{6.0} ^{9.5}	>54.4	-0.77 _{-0.82} ^{-0.73}	36.3 _{33.8} ^{33.8}		
	S15o	89.9/ 7.0/ 3.1	22.13	0.6 _{0.6} ^{0.6}	>86.0	<3.0	2.38 _{2.34} ^{2.41}	<0.0	13.5 _{13.5} ^{13.51}		
	S16o	97.2/ 2.8/ 0.0	3.44	<0.5	>16.1	>79.6	>1.5	<0.0	<10.0	3.81 _{3.76} ^{4.0}	
	H17o•	92.7/ 2.7/ 4.5	1.23	<0.5	59.9 _{59.1} ^{60.8}	7.0 _{6.9} ^{7.1}	-2.5 _{-2.52} ^{-2.47}	>14.1	>44.8	-0.92 _{-0.96} ^{-0.90}	0.4 _{0.39} ^{0.41} 0.38 _{0.36} ^{0.41}
NGC4235	F06	78.5/ 11.7/ 9.9	1.51	<0.5	38.8 _{37.3} ^{41.3}	<20.4	>5.9	>0.0	<10.0	>8.4	
	N08	79.3/ 11.6/ 9.1	1.13	<0.5	<73.0	5.7 _{4.3} ^{9.4}	<40.0	<9.4	>1.1	79.6 _{40.3} ^{104.9}	
	H10	78.8/ 8.9/ 12.3	1.28	<0.5	44.6 _{40.9} ^{51.8}	6.4 _{5.4} ^{4.8}	>53.9	-1.1 _{-1.2} ^{-0.6}	>71.5		
	S15	76.3/ 14.1/ 9.6	2.91	<0.5	32.9 _{33.8} ^{33.8}	<3.0	<1.5	<0.0	13.5 _{13.5} ^{13.57}		
	S16	79.9/ 9.8/ 10.3	1.70	<0.5	69.6 _{64.8} ^{64.8}	>78.7	>1.4	>1.4	<10.2	3.4 _{3.2} ^{3.7}	
	H17	84.6/ 4.8/ 10.6	1.13	0.3 _{0.3} ^{0.4}	<3.6	>5.0	-2.51 _{-2.69} ^{-2.47}	<14.5	33.9 _{31.4} ^{34.3}	>-0.7	<0.1 >0.3
M106	F06	84.7/ 4.7/ 10.6	2.39	<0.5	<0.1	<20.2	>6.0	>0.0	<10.1	5.0 _{4.8} ^{5.6}	
	N08	85.3/ 4.6/ 10.1	1.25	<0.5	<75.4	4.0 _{3.3} ^{5.4}	<28.2	<5.6	<1.5	91.4 _{59.2} ^{118.8}	
	H10	83.3/ 3.1/ 13.6	1.91	<0.5	<31.7	6.8 _{6.0} ^{8.3}	>58.8	-0.66 _{-0.7} ^{-0.61}	70.1 _{62.3} ^{76.8}		
	S15	81.6/ 7.0/ 11.4	4.45	<0.5	80.4 _{68.4} ^{82.3}	<3.0	<1.5	<0.0	13.5 _{13.5} ^{13.54}		
	S16	85.1/ 4.2/ 10.7	3.10	<0.5	66.						

Obj.	Mod	A / S / I %	χ^2/dof	$E_{(B-V)}$	Parameters								
					i	σ	Γ	β	Y	$\tau_{9.7\mu m}$	τ_v	τ_{cl}	τ_{disk}
F06													
N08					i	N_0	σ	Y	q				
H10					i	N_0	θ	a					
S15					i	R_{in}	η	τ_{cl}					
S16					i	σ	p	q	Y				
H17					i	N_0	a	σ	θ	$\tau_{9.7\mu m}$			
NGC4388	F06o●	83.2 / 0.0 / 16.8	1.86	<0.5	<10.1	<20.2	0.09 ^{0.12} _{0.08}	>-0.0	27.9 ^{28.9} _{17.0}	3.0 ^{3.4} _{2.9}			
	N08o●	62.0 / 10.0 / 28.0	1.44	0.9 ^{1.0} _{0.9}	>86.9	>14.3	46.6 ^{41.7} _{41.7}	30.0 ^{32.9} _{29.2}	1.1 ^{1.2} _{1.0}	<10.3			
	H10o	50.8 / 12.2 / 37.0	3.94	1.3 ^{1.4} _{1.3}	>89.8	4.1 ^{4.3} _{4.0}	>59.0	>-0.0		>79.1			
	S15o	46.9 / 8.4 / 44.7	3.73	<0.5	<19.8	<3.0	76.5 ^{77.0} _{75.6}	<0.0		13.5 ^{13.51} _{13.5}			
	S16o●	78.9 / 0.0 / 21.1	1.65	0.3 ^{0.4} _{0.3}	70.2 ^{71.2} _{69.4}	50.0 ^{51.4} _{49.2}	1.23 ^{1.26} _{1.21}	<0.5	>28.9	6.2 ^{6.4} _{5.8}			
	H17o	42.7 / 9.9 / 47.4	2.29	1.6 ^{1.8} _{1.5}	51.0 ^{52.9} _{49.7}	>9.9	-1.99 ^{-1.97} _{-2.01}	>14.4		>44.7	>-0.5	0.3 ^{0.31} _{0.29}	>0.7
NGC4395	F06o	92.0 / 8.0 / 0.0	1.59	<0.5	20.1 ^{17.5} _{17.5}	<21.0	>5.9	>-0.1	68.9 ^{71.6} _{67.4}	6.0 ^{6.3} _{5.7}			
	N08o●	92.7 / 7.3 / 0.0	1.04	<0.5	27.7 ^{35.3} _{19.8}	11.0 ^{11.9} _{9.6}	>58.9	66.1 ^{69.3} _{63.6}	0.5 ^{0.52} _{0.36}	<10.2			
	H10o	58.3 / 12.7 / 29.0	3.45	<0.5	>89.7	>10.0	>59.6	>-0.0		>79.9			
	S15o●	71.6 / 10.1 / 18.3	1.34	<0.5	59.6 ^{62.3} _{58.3}	>15.3	2.2 ^{2.5} _{2.1}	<0.0		>43.2			
	S16o	94.0 / 6.0 / 0.0	1.57	<0.5	46.9 ^{48.3} _{45.3}	<0.0	<0.1	>29.3		5.3 ^{6.7} _{5.1}			
	H17o	53.0 / 11.5 / 35.5	3.22	0.1 ^{0.1} _{0.0}	51.1 ^{53.4} _{48.6}	>10.0	>-0.5	>14.9	>44.9	>-0.5	>0.5	>0.7	
NGC4507	F06o	87.1 / 2.6 / 10.3	1.98	<0.5	60.9 ^{57.7} _{57.7}	27.7 ^{28.1} _{27.2}	<0.1	>-0.5	<10.5	3.5 ^{3.8} _{3.5}			
	N08o●	82.1 / 7.6 / 10.4	1.28	<0.5	>88.0	7.5 ^{8.7} _{6.9}	<37.3	29.9 ^{49.0} _{23.8}	1.7 ^{1.9} _{1.6}	20.0 ^{23.3} _{16.1}			
	H10o	70.0 / 8.4 / 21.6	1.50	<0.5	73.1 ^{79.8} _{66.4}	<3.2	>53.5	-0.4 ^{-0.3} _{-0.6}	>76.6				
	S15o	77.2 / 8.9 / 13.9	4.34	<0.5	>85.9	<3.0	<1.5	<0.0	>30.0				
	S16o	78.0 / 6.9 / 15.0	1.69	<0.5	59.0 ^{64.8} _{55.8}	59.4 ^{62.2} _{55.8}	<0.0	0.7 ^{1.2} _{0.3}	<10.4	4.4 ^{5.6} _{3.5}			
	H17o●	86.9 / 0.0 / 13.1	1.29	0.1 ^{0.2} _{0.1}	15.1 ^{19.8} _{15.3}	>9.1	<-2.9	>14.7	>43.0	>-0.5	<0.2	0.54 ^{0.57} _{0.51}	
E506-G027	F06	75.8 / 0.0 / 24.2	3.65	2.6 ^{2.7} _{2.6}	<0.0	>59.9	<0.0	<-1.0	<10.0	1.45 ^{1.47} _{1.44}			
	N08o	76.5 / 12.6 / 10.9	2.78	1.9 ^{1.9} _{1.8}	<0.2	>14.9	>69.5	<5.0	0.5 ^{0.53} _{0.32}	20.0 ^{19.9} _{19.9}			
	H10o	71.6 / 0.0 / 28.4	1.74	2.4 ^{2.4} _{2.3}	45.8 ^{48.4} _{40.0}	5.0 ^{5.1} _{4.8}	29.9 ^{31.1} _{23.2}	<-2.0	>78.7				
	S15o	64.5 / 21.9 / 13.5	13.88	0.9 ^{0.9} _{0.8}	>85.9	<3.0	7.69 ^{7.27} _{7.27}	<0.0	13.5 ^{13.54} _{13.5}				
	S16o	81.2 / 10.5 / 8.3	5.62	2.4 ^{2.4} _{2.3}	<13.4	70.0 ^{71.0} _{69.8}	>1.5	>1.5	<10.0	<3.0			
	H17o	74.1 / 0.0 / 25.9	0.61	2.2 ^{2.3} _{2.2}	>88.9	8.4 ^{8.7} _{6.9}	<-2.9	>14.4	>44.2	<-2.4	<0.1	>0.7	
NGC4686	F06	81.0 / 9.3 / 9.7	1.44	0.4 ^{0.5} _{0.3}	9.9 ^{10.6} _{9.8}	<20.2	4.02 ^{4.1} _{3.98}	<-1.0	<10.0	5.6 ^{5.7} _{5.4}			
	N08o●	79.8 / 10.7 / 9.5	0.66	0.7 ^{0.8} _{0.6}	>69.9	>11.4	>37.2	<5.1	>2.3	17.8 ^{21.9} _{14.7}			
	H10o	72.1 / 10.3 / 17.5	1.10	0.5 ^{0.6} _{0.4}	>58.9	>9.6	<7.6	-1.6 ^{-1.56} _{-1.64}	49.6 ^{52.9} _{46.5}				
	S15o	72.5 / 16.3 / 11.2	4.28	0.8 ^{0.8} _{0.7}	>85.8	<3.0	1.74 ^{1.79} _{1.68}	<0.0	13.5 ^{13.67} _{13.5}				
	S16o	78.2 / 10.5 / 11.3	1.72	0.4 ^{0.5} _{0.4}	>85.3	>78.3	>1.5	>1.5	<10.0	4.9 ^{5.0} _{4.8}			
	H17o	85.7 / 0.0 / 14.3	0.69	0.8 ^{0.7} _{0.7}	<32.9	<6.4	<-3.0	>7.0	>41.4	-1.0 ^{-1.0} _{-1.1}	<0.1	0.3 ^{0.35} _{0.26}	
NGC4941	F06o	100.0 / 0.0 / 0.0	3.34	<0.5	70.0 ^{70.3} _{69.6}	<20.3	<0.1	<-0.9	<12.2	7.9 ^{8.5} _{5.5}			
	N08o●	78.1 / 6.2 / 15.7	1.21	<0.5	>0.0	6.0 ^{10.9} _{4.9}	>37.4	10.0 ^{11.8} _{9.1}	>1.0	199.2 ^{231.1} _{172.5}			
	H10o	75.4 / 5.7 / 18.8	2.46	<0.5	64.8 ^{67.0} _{62.9}	6.3 ^{6.0} _{6.0}	>59.2	>0.0	>79.4				
	S15o	89.7 / 4.1 / 6.2	4.25	<0.5	>85.9	<3.0	7.7 ^{7.8} _{7.5}	14.1 ^{17.1} _{13.7}	13.5 ^{13.5} _{13.5}				
	S16o	98.3 / 1.7 / 0.0	3.35	<0.5	>90.0	<10.0	<0.0	>1.4	11.8 ^{11.5} _{11.5}	<3.1			
	H17o	75.8 / 5.5 / 18.7	1.94	<0.5	37.4 ^{41.5} _{38.2}	>8.3	>-0.5	>13.9	>42.9	>-0.7	0.36 ^{0.39} _{0.33}	0.29 ^{0.31} _{0.19}	
NGC4939	F06o	97.2 / 2.8 / 0.0	2.73	<0.5	19.9 ^{20.2} _{19.3}	<20.1	>6.0	>0.0	28.5 ^{28.9} _{27.9}	>9.9			
	N08o●	97.1 / 2.9 / 0.0	1.27	<0.5	79.7 ^{82.3} _{79.3}	>14.8	22.0 ^{27.9} _{20.2}	20.0 ^{20.3} _{19.8}	0.49 ^{0.51} _{0.24}	<10.2			
	H10o	88.3 / 5.5 / 6.2	1.83	<0.5	84.4 ^{84.8} _{82.0}	3.2 ^{3.3} _{3.0}	>58.6	>0.0	>79.6				
	S15o	96.5 / 3.5 / 0.0	3.10	<0.5	>85.8	<3.0	8.8 ^{8.9} _{7.1}	30.0 ^{30.8} _{29.8}	13.5 ^{17.0} _{13.4}				
	S16o	98.4 / 1.6 / 0.0	1.99	<0.5	40.0 ^{44.5} _{33.9}	>78.4	<0.0	<0.0	17.0 ^{17.8} _{16.2}	<3.6			
	H17o●	94.0 / 0.0 / 6.0	1.16	2.4 ^{2.4} _{2.3}	24.3 ^{33.9} _{33.9}	>9.2	<-2.9	>14.5	>42.8	>-0.5	<0.2	>0.7	
E323-077	F06	76.3 / 4.0 / 19.6	2.09	<0.5	27.6 ^{30.4} _{24.3}	51.5 ^{56.1} _{49.6}	<0.0	<1.0	<10.1	1.4 ^{1.6} _{1.4}			
	N08	69.4 / 8.9 / 21.7	3.19	<0.5	>87.6	3.0 ^{2.9} _{2.9}	42.5 ^{43.3} _{40.0}	>82.8	>2.5	45.6 ^{44.7} _{44.7}			
	H10o	66.1 / 8.0 / 25.9	2.54	<0.5	14.9 ^{17.4} _{6.1}	>9.6	51.8 ^{53.1} _{50.7}	-0.85 ^{-0.8} _{-0.89}	>79.3				
	S15o	65.3 / 10.4 / 24.3	9.64	<0.5	>85.8	<3.0	1.59 ^{1.62} _{1.55}	<0.0	13.5 ^{13.51} _{13.51}				
	S16o	68.5 / 8.3 / 23.2	2.59	<0.5	20.0 ^{21.1} _{14.8}	64.5 ^{66.0} _{62.4}	>1.5	>1.4	<10.1	>10.8			
	H17o	79.1 / 0.0 / 20.9	1.77	0.4 ^{0.4} _{0.4}	<0.0	>9.8	<3.0	12.1 ^{12.8} _{11.4}	35.3 ^{35.9} _{34.9}	>-0.5	0.2 ^{0.2} _{0.2}	>0.7	
NGC4992	F06o	83.7 / 0.0 / 16.3	3.03	2.9 ^{2.8} _{2.6}	<0.0	>60.0	<0.0	<-1.0	<10.0	1.42 ^{1.44} _{1.41}			
	N08	57.4 / 24.8 / 17.8	3.98	1.9 ^{2.0} _{1.9}	<0.1	>14.8	>69.1	<5.0	0.5 ^{0.6} _{0.4}	20.0 ^{19.8} _{19.8}			
	H10o	55.7 / 9.6 / 34.7	2.74	2.5 ^{2.5} _{2.5}	30.3 ^{32.9} _{27.7}	5.0 ^{5.2} _{4.9}	>29.8 ^{27.2} _{27.2}	<2.0	>79.1				
	S15o	50.7 / 31.1 / 18.2	12.04	1.1 ^{1.1} _{1.0}	>85.9	<3.0	5.6 ^{12.7} _{4.9}	<0.0	13.5 ^{13.55} _{13.5}				
	S16o	65.9 / 19.6 / 14.6	4.84	2.6 ^{2.7} _{2.7}	<11.2	70.0 ^{70.4} _{69.6}	>1.5	>1.5	<10.0	<3.0			
	H17o	55.6 / 10.9 / 33.5	1.93	2.3 ^{2.3} _{2.2}	>89.8	<8.8	-2.75 ^{-2.71} _{-2.79}	>14.6	>44.3	<-2.5	<0.1	0.47 ^{0.62} _{0.45}	
IISZ010	F06o	97.9 / 2.1 / 0.0	11.89	0.1 ^{0.2} _{0.1}	<0.0	<20.0	4.0 ^{4.0} _{4.0}	>-0.0	<10.0	3.0 ^{3.0} _{2.99}			
	N08o	97.3 / 2.7 / 0.0	6.77	<0.5	>77.9	8.9 ^{8.6} _{8.6}	>67.3	<5.0	1.37 ^{1.44} _{1.24}	<10.0			
	H10o●	97.2 / 2.8 / 0.0	1.04	<0.5	77.6 ^{89.1} _{47.1}	>8.6	>45.8	-1.25 ^{-1.2} _{-1.31}	32.7 ^{35.0} _{31.5}				
	S15o	93.8 / 6.2 / 0.0	28.94	<0.5	>85.9	<3.0	<1.5	<0.0	13.5 ^{13.5} _{13.5}				
	S16o	98.6 / 1.4 / 0.0	10.69	<0.5	80.2 ^{81.5} _{79.4}	>79							

Obj.	Mod	A / S / I %	χ^2/dof	$E_{(B-V)}$	Parameters							
	F06			<i>i</i>	σ	Γ	β	Y	$\tau_{9.7\mu m}$			
	N08			<i>i</i>	N_0	σ	Y	q	τ_v			
	H10			<i>i</i>	N_0	θ	a	τ_{cl}				
	S15			<i>i</i>	R_{in}	η	τ_{ct}	τ_{disk}				
	S16			<i>i</i>	σ	p	q	Y	$\tau_{9.7\mu m}$			
	H17			<i>i</i>	N_0	a	σ	θ	a_w	h	f_w	
M-06-30-015	F06o	100.0 / 0.0 / 0.0	1.68	<0.5	56.6 _{54.0} ^{60.5}	39.4 _{39.0} ^{39.6}	<0.0	-0.91 _{-0.94} ^{-0.84}	<10.1	3.0 _{2.95} ^{3.03}		
	N08o	91.0 / 7.9 / 1.0	2.56	<0.5	>89.1	6.5 _{6.7} ^{8.1}	<31.1	>69.1	2.08 _{2.04} ^{2.13}	22.7 _{21.5} ^{25.4}		
	H10o	84.2 / 7.2 / 8.6	2.56	<0.5	<11.3	6.2 _{5.7} ^{6.1}	38.0 _{36.6} ^{40.0}	-0.3 _{-0.4} ^{-0.2}	>79.4			
	S15o	80.3 / 10.1 / 9.7	7.06	<0.5	>85.9	<3.0	5.9 _{5.6} ^{6.1}	<0.0	13.5 _{13.5} ^{13.54}			
	S16o	89.9 / 6.2 / 3.8	1.73	<0.5	55.6 _{54.5} ^{56.5}	40.0 _{38.9} ^{40.6}	>1.4	0.5 _{0.3} ^{0.7}	<10.3	6.7 _{6.3} ^{7.2}		
	H17o•	91.4 / 2.1 / 6.6	0.95	0.1 _{0.1} ^{0.1}	16.9 _{14.2} ^{14.2}	>9.9	-2.3 _{-2.4} ^{-2.1}	>14.8	>44.7	>-0.5	>0.5	>0.7
NGC5252	F06o	85.4 / 11.4 / 3.2	3.45	<0.5	11.6 _{10.3} ^{13.1}	<20.2	>6.0	>0.0	<10.0	6.0 _{5.9} ^{6.7}		
	N08o•	85.3 / 12.5 / 2.2	1.65	<0.5	>67.6	8.1 _{7.1} ^{11.0}	>15.0	13.7 _{10.4} ^{22.0}	1.8 _{1.4} ^{2.1}	<10.8		
	H10	79.7 / 12.3 / 8.0	1.39	<0.5	53.5 _{51.3} ^{61.3}	<6.6	>5.0	-0.74 _{-0.8} ^{-0.69}	52.1 _{59.1} ^{59.1}			
	S15o	83.3 / 13.6 / 3.2	9.43	<0.5	>85.8	<3.0	<1.5	<0.0	13.5 _{13.5} ^{13.52}			
	S16o	85.4 / 10.7 / 3.9	3.20	<0.5	72.4 _{68.5} ^{81.1}	>79.4	>1.5	0.8 _{0.7} ^{0.9}	<10.0	<3.1		
	H17	85.2 / 8.4 / 6.4	1.28	<0.5	30.0 _{29.3} ^{31.1}	>9.6	-2.66 _{-2.76} ^{-2.65}	10.0 _{9.8} ^{13.2}	<30.3	>-0.5	0.31 _{0.27} ^{0.35}	>0.7
IC4329A	F06o	95.5 / 4.5 / 0.0	3.26	<0.5	<0.0	<20.1	4.0 _{3.99} ^{4.03}	<-1.0	<10.0	4.72 _{4.68} ^{5.23}		
	N08o	93.3 / 6.7 / 0.0	2.02	0.4 _{0.3} ^{0.5}	<16.0	>14.6	>68.0	6.1 _{5.9} ^{6.2}	2.2 _{2.1} ^{2.3}	16.1 _{15.3} ^{15.3}		
	H10o	87.8 / 6.4 / 5.8	1.49	0.3 _{0.2} ^{0.3}	32.0 _{21.0} ^{24.3}	>9.6	<6.6	-1.8 _{-1.83} ^{-1.77}	>78.8			
	S15o	88.5 / 8.9 / 2.6	39.40	<0.5	>86.0	<3.0	<1.5	<0.0	13.5 _{13.5} ^{13.51}			
	S16o	93.3 / 5.7 / 1.0	4.93	<0.5	>88.4	70.3 _{69.9} ^{73.7}	>1.5	>1.5	<10.0	4.62 _{4.59} ^{4.67}		
	H17o•	97.4 / 0.0 / 2.6	0.76	0.4 _{0.4} ^{0.4}	60.6 _{59.8} ^{61.5}	7.0 _{6.8} ^{7.1}	<3.0	10.0 _{9.6} ^{10.1}	>44.0	>-0.5	0.3 _{0.28} ^{0.31}	0.3 _{0.28} ^{0.31}
UM614	F06o	94.6 / 5.4 / 0.0	6.09	<0.5	22.7 _{22.3} ^{22.3}	<20.0	>6.0	>0.0	<10.0	>9.9		
	N08o	95.1 / 4.9 / 0.0	4.55	<0.5	>86.8	>12.9	<23.0	9.9 _{10.0} ^{10.0}	2.1 _{2.0} ^{2.2}	<10.1		
	H10o	93.3 / 5.0 / 1.6	1.88	<0.5	74.7 _{71.1} ^{77.8}	4.8 _{4.4} ^{5.1}	30.3 _{31.4} ^{32.8}	-1.5 _{-1.52} ^{-1.45}	>76.6			
	S15o	91.5 / 8.5 / 0.0	22.94	0.3 _{0.3} ^{0.3}	>86.0	<3.0	1.64 _{1.63} ^{1.65}	<0.0	13.5 _{13.5} ^{13.53}			
	S16o	96.6 / 3.4 / 0.0	6.22	<0.5	70.3 _{69.5} ^{71.4}	>79.9	>1.5	>1.5	<10.0	4.37 _{4.33} ^{4.42}		
	H17o•	100.0 / 0.0 / 0.0	1.36	0.2 _{0.2} ^{0.2}	45.2 _{44.7} ^{44.7}	>9.9	<2.9	10.0 _{9.9} ^{10.1}	>44.8	>-0.5	0.4 _{0.4} ^{0.42}	0.16 _{0.16} ^{0.16}
Mrk279	F06o	90.2 / 5.3 / 4.6	2.60	<0.5	<0.0	<20.1	>6.0	<-1.0	<10.0	8.2 _{8.3} ^{8.3}		
	N08o	89.1 / 6.5 / 4.4	2.32	<0.5	>86.0	5.0 _{4.8} ^{5.3}	38.9 _{38.8} ^{45.8}	7.9 _{7.8} ^{8.7}	>2.2	41.0 _{39.2} ^{43.7}		
	H10	86.8 / 4.8 / 8.4	2.30	<0.5	42.5 _{25.1} ^{45.5}	>9.7	39.0 _{34.7} ^{41.6}	-1.35 _{-1.39} ^{-1.31}	>78.9			
	S15o	84.9 / 8.7 / 6.4	26.65	0.4 _{0.4} ^{0.4}	>86.0	<3.0	1.76 _{1.75} ^{1.78}	<0.0	13.5 _{13.5} ^{13.53}			
	S16o	90.8 / 4.9 / 4.3	3.72	<0.5	10.0 _{10.6} ^{10.6}	>78.0	>1.5	>1.5	<10.0	9.7 _{9.8} ^{9.8}		
	H17o•	90.0 / 3.6 / 6.4	1.18	<0.5	>71.6	7.3 _{6.8} ^{7.8}	<3.0	>12.8	>43.8	-1.11 _{-1.16} ^{-1.07}	>0.4	>0.7
Circinus	F06o	64.4 / 0.0 / 35.6	129.50	0.8 _{0.8} ^{0.8}	<0.0	<20.0	2.0 _{1.99} ^{2.0}	>0.0	<10.0	6.0 _{6.0} ^{6.81}		
	N08o	64.5 / 0.0 / 35.5	107.88	2.8 _{2.8} ^{2.8}	>81.0	10.9 _{10.8} ^{11.0}	>69.4	10.0 _{9.8} ^{10.03}	1.5 _{1.49} ^{1.51}	<10.0		
	H10	30.8 / 0.0 / 69.2	121.99	4.3 _{4.3} ^{4.3}	75.1 _{74.9} ^{75.4}	<2.5	>59.7	-0.11 _{-0.12} ^{-0.11}	<30.0			
	S15o	66.6 / 7.1 / 26.3	192.57	2.7 _{2.7} ^{2.7}	80.0 _{79.98} ^{80.02}	<3.0	38.5 _{38.49} ^{38.51}	<0.0	13.5 _{13.5} ^{13.5}			
	S16o	59.0 / 0.0 / 41.0	119.08	1.7 _{1.7} ^{1.7}	>89.8	>79.9	>1.5	<0.0	<10.0	6.75 _{6.7} ^{6.81}		
	H17o	48.9 / 0.0 / 51.1	119.23	3.2 _{3.2} ^{3.2}	>90.0	7.1 _{7.0} ^{7.2}	-2.5 _{-2.5} ^{-2.51}	>14.9	>44.9	-0.99 _{-1.0} ^{-0.98}	<0.1	0.3 _{0.3} ^{0.3}
NGC5506	F06	58.2 / 15.9 / 25.9	1.22	1.1 _{1.1} ^{1.2}	16.5 _{15.7} ^{17.8}	<24.8	4.0 _{3.93} ^{4.02}	<-1.0	10.6 _{10.5} ^{14.3}	>9.7		
	N08	43.9 / 26.0 / 30.1	2.82	1.7 _{1.6} ^{1.7}	29.8 _{28.9} ^{30.1}	>15.0	>69.9	8.23 _{8.19} ^{8.37}	0.49 _{0.35} ^{0.55}	20.02 _{19.96} ^{20.06}		
	H10	46.0 / 20.0 / 34.0	1.93	1.9 _{1.9} ^{2.0}	<0.0	>9.8	30.4 _{27.7} ^{31.1}	1.19 _{1.21} ^{-1.21}	>78.2			
	S15	40.1 / 27.0 / 32.9	14.74	2.8 _{2.8} ^{2.8}	>86.0	<3.0	<1.6	30.0 _{29.7} ^{30.5}	>44.9			
	S16	51.1 / 19.2 / 29.7	2.11	1.6 _{1.5} ^{1.6}	49.0 _{46.2} ^{51.0}	69.6 _{68.5} ^{70.5}	>1.5	>1.5	<10.0	>10.7		
	H17o	75.2 / 0.0 / 24.8	3.23	2.0 _{1.9} ^{2.0}	<0.0	>9.8	<3.0	>14.6	43.5 _{42.7} ^{44.0}	-0.83 _{-0.87} ^{-0.79}	0.3 _{0.27} ^{0.34}	>0.7
NGC5548	F06o	95.6 / 2.4 / 2.1	2.22	<0.5	<0.0	<20.3	>6.0	>0.0	11.5 _{11.6} ^{11.6}	8.4 _{8.6} ^{8.6}		
	N08o	95.3 / 2.8 / 1.9	1.75	<0.5	>84.0	4.5 _{4.2} ^{4.8}	34.0 _{34.8} ^{43.8}	18.6 _{14.6} ^{30.1}	>2.3	55.9 _{52.3} ^{52.3}		
	H10o	91.3 / 1.7 / 7.0	1.95	0.0 _{0.0} ^{0.1}	52.5 _{48.4} ^{54.1}	>9.4	>58.5	-0.7 _{-0.9} ^{-0.6}	73.9 _{70.3} ^{79.3}			
	S15o	88.9 / 4.1 / 7.0	18.66	0.4 _{0.4} ^{0.4}	>86.0	<3.0	3.23 _{3.28} ^{3.28}	<0.0	13.5 _{13.5} ^{13.52}			
	S16o	96.0 / 1.3 / 2.7	2.75	<0.5	<0.1	>79.6	0.66 _{0.63} ^{0.63}	>1.5	<10.0	>10.7		
	H17o•	94.3 / 0.0 / 5.7	1.07	<0.5	78.6 _{74.1} ^{80.3}	>6.6	<2.9	<9.7	>39.4	>0.6	<0.2	0.5 _{0.4} ^{0.54}
E511-G030	F06o	91.2 / 8.8 / 0.0	7.21	<0.5	<0.0	<20.1	4.0 _{3.99} ^{4.01}	<1.0	<10.0	2.32 _{2.29} ^{2.35}		
	N08o	91.4 / 8.6 / 0.0	2.13	<0.5	<25.7	7.3 _{6.4} ^{8.8}	>60.4	<5.1	>2.4	<10.2		
	H10o•	90.9 / 7.3 / 1.9	1.12	<0.5	>75.6	3.1 _{2.8} ^{2.8}	45.2 _{41.9} ^{52.2}	-1.34 _{-1.37} ^{-1.3}	<39.3			
	S15o	83.0 / 17.0 / 0.0	23.98	<0.5	33.0 _{32.1} ^{33.1}	<3.0	<1.5	<0.0	13.5 _{13.5} ^{13.5}			
	S16o	90.3 / 9.7 / 0.0	8.45	<0.5	40.5 _{38.2} ^{42.8}	>79.8	>1.5	>1.5	<10.0	<3.0		
	H17o•	100.0 / 0.0 / 0.0	0.71	0.4 _{0.3} ^{0.3}	30.0 _{29.6} ^{29.6}	<5.0	<3.0	<7.1	30.45 _{30.35} ^{30.52}	-1.34 _{-1.38} ^{-1.3}	<0.1	>0.7
Mrk477	F06o	97.4 / 2.6 / 0.0	2.63	<0.5	9.9 _{7.5} ^{10.4}	<20.2	>5.9	>0.0	23.2 _{23.0} ^{23.5}	>9.9		
	N08o•	97.0 / 3.0 / 0.0	1.73	<0.5	>88.4	14.6	25.5 _{21.3} ^{27.8}	25.9 _{24.5} ^{29.2}	1.1 _{1.0} ^{1.2}	<10.6		
	H10o	78.7 / 4.7 / 16.6	2.37	<0.5	>89.0	3.06 _{3.01} ^{3.13}	>58.7	>0.0	>79.4			
	S15o	87.3 / 3.0 / 9.7	3.79	<0.5	>85.9	<3.0	9.8 _{10.0} ^{10.0}	29.9 _{28.5} ^{30.4}	13.5 _{13.6} ^{13.6}			
	S16o•	100.0 / 0.0 / 0.0	1.90	<0.5	33.7 _{32.7} ^{39.2}	69.5 _{67.0} ^{76.0}	0.9 _{0.7} ^{1.0}	<1.0	20.3 _{19.4} ^{23.4}	6.3 _{5.4} ^{8.0}		
	H17o•	86.4 / 0.0 / 13.6	1.54	0.3 _{0.3} ^{0.3}	27.1 _{26.4} ^{37.4}	>9.8	<3.0	>14.9	>44.6	>0.5	0.26 _{0.22} ^{0.31}	>0.7
IC4518A	F06o	33.3 / 0.										

Obj.	Mod	A / S / I		χ^2/dof	$E_{(B-V)}$	Parameters									F06 N08 H10 S15 S16 H17	i σ N_0 θ η p a q σ θ	$\tau_{9.7\mu m}$ τ_v τ_{cl} τ_{disk} Y θ $\tau_{9.7\mu m}$ a_w	h	f_w
		i	σ			Γ	β	Y	$\tau_{9.7\mu m}$	τ_v	N_0	σ	θ	a	q	τ_{cl}	τ_{disk}	Y	θ
Mrk1392	F06o	97.0 / 3.0 / 0.0	3.46	<0.5	<0.2	<20.2	>6.0	>-0.0	12.4 _{12.2} ^{12.5}	>9.9									
	N08o•	93.9 / 3.5 / 2.6	1.47	<0.5	>86.7	6.8 _{6.3} ^{8.5}	<25.6	10.0 _{9.7} ^{10.2}	1.0 _{1.2} ^{1.2}	26.8 _{21.9} ^{30.2}									
	H10o	84.0 / 3.9 / 12.1	2.01	<0.5	52.0 _{46.1} ^{55.3}	>8.9	>53.0	>-0.0	35.1 _{32.9} ^{32.8}										
	S15o	90.6 / 4.5 / 4.9	14.44	0.4 _{0.4} ^{0.5}	>86.0	<3.0	<1.5	<0.0	36.9 _{36.4} ^{37.5}										
	S16o	93.0 / 2.4 / 4.7	2.69	<0.5	60.1 _{62.7} ^{62.7}	>79.4	<0.0	>1.2	<10.0	6.0 _{5.8} ^{6.5}									
	H17o•	90.3 / 0.5 / 9.2	1.04	<0.5	45.2 _{43.7} ^{43.7}	<5.3	<-2.9	>14.0	38.8 _{37.9} ^{40.2}	>-0.5	0.33 _{0.28} ^{0.43}								
	F06o	94.7 / 5.3 / 0.0	6.43	<0.5	11.5 _{11.3} ^{11.3}	<20.0	>6.0	>-0.0	<10.0	>9.8									
Mrk290	N08o	94.3 / 5.7 / 0.0	3.14	<0.5	>88.6	11.1 _{10.9} ^{11.4}	34.5 _{29.6} ^{38.8}	10.0 _{9.9} ^{10.1}	1.56 _{1.5} ^{1.6}	<10.1									
	H10o	88.9 / 5.7 / 5.4	1.52	<0.5	75.5 _{73.9} ^{87.9}	3.5 _{3.3} ^{4.0}	45.4 _{43.8} ^{53.8}	-0.98 _{-1.01} ^{-0.91}	56.5 _{52.5} ^{59.0}										
	S15o	91.3 / 8.1 / 0.6	31.96	0.6 _{0.5} ^{0.6}	>86.0	<3.0	2.13 _{2.12} ^{2.15}	<0.0	13.5 _{13.5} ^{13.51}										
	S16o	96.5 / 3.5 / 0.0	5.38	<0.5	70.0 _{69.9} ^{70.7}	>79.9	>1.4	>1.3	<10.0	5.3 _{5.0} ^{5.5}									
	H17o•	92.5 / 3.4 / 4.0	0.93	0.1 _{0.1} ^{0.1}	53.1 _{51.9} ^{53.7}	6.1 _{5.9} ^{6.6}	-2.5 _{-2.5} ^{-2.5}	10.0 _{9.7} ^{10.2}	>44.1	>-0.5	0.33 _{0.28} ^{0.43}								
E138-G001	F06o	92.0 / 3.3 / 4.8	2.55	<0.5	11.7 _{11.2} ^{12.4}	<20.1	>6.0	>-0.0	<10.0	>9.9									
	N08o•	93.1 / 2.6 / 4.3	1.30	0.4 _{0.3} ^{0.5}	>72.4	7.5 _{6.8} ^{8.1}	>37.8	10.7 _{9.5} ^{12.0}	>2.3	20.0 _{16.8} ^{21.2}									
	H10	84.2 / 3.7 / 12.1	1.64	0.1 _{0.1} ^{0.1}	75.2 _{72.6} ^{79.1}	>9.5	44.9 _{41.5} ^{47.6}	-1.5 _{-1.5} ^{-1.47}	56.7 _{52.8} ^{60.6}										
	S15o	88.7 / 4.8 / 6.5	21.46	<0.5	>85.8	<3.0	<1.5	<0.0	13.5 _{13.5} ^{13.51}										
	S16o	92.4 / 1.4 / 6.2	2.94	<0.5	80.0 _{78.5} ^{84.5}	>79.6	>1.5	>1.4	<10.0	5.03 _{4.95} ^{5.67}									
	H17	90.9 / 0.0 / 9.1	1.00	0.3 _{0.2} ^{0.3}	60.3 _{58.1} ^{61.3}	7.0 _{6.7} ^{7.4}	<-3.0	>14.2	37.1 _{35.5} ^{39.4}	>-0.5	0.81 _{0.8} ^{0.84}								
	F06	87.3 / 7.0 / 5.7	1.59	<0.5	<56.7	<20.8	<0.0	<-1.0	<10.1	>2.5									
Mrk501	N08	80.7 / 11.3 / 7.9	1.65	<0.5	>85.3	13.8 _{12.6} ^{14.5}	<17.0	<5.1	>2.5	<11.1									
	H10	80.2 / 9.1 / 10.7	1.36	<0.5	45.0 _{39.1} ^{50.7}	>9.5	45.6 _{43.0} ^{49.4}	-1.88 _{-1.92} ^{-1.84}	>78.9										
	S15	78.6 / 15.7 / 5.6	7.72	<0.5	33.0 _{32.1} ^{33.3}	<3.0	<1.5	<0.0	13.5 _{13.5} ^{13.52}										
	S16	82.5 / 10.8 / 6.7	2.12	<0.5	67.5 _{63.6} ^{71.4}	70.3 _{69.3} ^{71.6}	>1.5	>1.5	<10.0	<3.1									
	H17	85.4 / 6.0 / 8.6	1.04	<0.5	<0.0	>8.4	<-3.0	9.9 _{8.9} ^{10.7}	37.7 _{35.8} ^{40.3}	-1.73 _{-1.77} ^{-1.67}	<0.1	>0.7							
	F06o	25.4 / 0.0 / 74.6	8.54	2.4 _{2.4} ^{2.4}	>89.7	<20.1	<0.0	-0.33 _{-0.34} ^{-0.31}	<10.0	>10.0									
	N08o	25.7 / 3.0 / 71.2	6.17	4.3 _{4.3} ^{4.4}	<16.5	>13.9	34.8 _{33.4} ^{36.6}	7.3 _{7.0} ^{7.7}	<0.0	63.6 _{56.0} ^{69.4}									
NGC6300	H10o	32.0 / 0.0 / 68.0	10.63	3.7 _{3.7} ^{3.7}	<0.0	>10.0	45.0 _{44.5} ^{45.4}	>0.0	>79.2										
	S15o	44.9 / 11.7 / 43.4	20.35	1.0 _{1.0} ^{1.0}	<19.4	<3.2	>77.6	>996.3	22.5 _{20.5} ^{23.4}										
	S16o	36.8 / 0.0 / 63.2	10.29	1.4 _{1.4} ^{1.4}	>90.0	<10.0	>1.5	>1.5	<10.1	5.9 _{5.8} ^{6.1}									
	H17o	27.6 / 0.0 / 72.4	9.16	4.2 _{4.2} ^{4.2}	<0.0	>10.0	>-0.5	>7.0	>41.7	-1.9 _{-2.0} ^{-1.8}	>0.5	>0.32	>0.16						
	F06o	79.3 / 5.8 / 14.9	0.91	<0.5	10.0 _{13.8} ^{13.8}	<22.8	4.9 _{4.6} ^{5.0}	<-1.0	<10.2	>8.7									
	N08o	74.1 / 9.4 / 16.6	1.49	<0.5	<22.2	>12.9	61.0 _{69.6} ^{69.6}	6.9 _{6.6} ^{7.3}	1.7 _{1.5} ^{1.9}	20.1 _{18.3} ^{21.9}									
	H10o	74.7 / 6.4 / 18.9	1.17	0.3 _{0.2} ^{0.3}	<0.0	>9.6	31.5 _{25.1} ^{25.1}	-1.23 _{-1.28} ^{-1.19}	>77.8										
Fairall49	S15o	71.5 / 10.2 / 18.3	11.58	1.0 _{1.0} ^{1.1}	>85.9	<3.0	3.6 _{3.4} ^{3.7}	<0.0	13.5 _{13.5} ^{13.52}										
	S16o	78.5 / 6.2 / 15.4	1.36	0.1 _{0.1} ^{0.2}	39.1 _{33.7} ^{41.8}	70.0 _{69.6} ^{70.6}	>1.5	>1.5	<10.0	>9.9									
	H17o	79.1 / 4.4 / 16.5	0.87	0.4 _{0.4} ^{0.4}	75.0 _{74.5} ^{74.5}	>9.5	<-3.0	10.1 _{9.5} ^{10.8}	>43.0	-0.9 _{-1.0} ^{-0.8}	>0.5	>0.5	>0.32	>0.16					
	F06o	100.0 / 0.0 / 0.0	3.06	0.3 _{0.3} ^{0.3}	47.8 _{46.8} ^{48.3}	<20.1	1.3 _{1.1} ^{1.7}	>-0.0	<10.2	>10.0									
	N08o•	93.8 / 6.2 / 0.0	0.74	1.2 _{1.2} ^{1.4}	29.9 _{29.0} ^{30.3}	>15.0	>69.9	9.3 _{9.1} ^{39.9}	0.5 _{0.4} ⁵¹	20.0 _{19.9} ^{20.04}									
	H10o	80.6 / 5.4 / 14.0	1.26	1.4 _{1.4} ^{1.4}	>83.3	>9.7	>38.6	-1.25 _{-1.3} ^{-1.25}	69.1 _{64.7} ^{64.7}										
	S15o	85.5 / 6.5 / 8.0	13.60	1.9 _{1.9} ^{1.9}	>86.0	<3.0	9.3 _{9.4} ^{9.4}	<0.0	13.5 _{13.4} ^{13.52}	<10.0	>10.0								
E103-035	S16o•	93.8 / 0.0 / 6.2	0.91	1.0 _{1.0} ^{1.0}	80.2 _{78.1} ^{81.2} </td														

Table 4. Spectral fit results (continuation).

Obj.	Mod	A / S / I %	χ^2/dof	$E_{(B-V)}$	Parameters							
	F06				i	σ	Γ	β	Y	$\tau_{9.7\mu m}$		
	N08				i	N_0	σ	Y	q		τ_v	
	H10				i	N_0	θ	a	τ_{cl}			
	S15				i	R_{in}	η	τ_{cl}	τ_{disk}			
	S16				i	σ	p	q	Y	$\tau_{9.7\mu m}$		
	H17				i	N_0	a	σ	θ	a_w	h	f_w
NGC7130	F06o	32.9 / 0.0 / 67.1	3.28	<0.5	<0.2	<21.0	3.5 _{3.3} ^{4.1}	-0.4 _{-0.5} ^{-0.3}	66.4 _{64.2} ^{68.2}	6.0 _{5.8} ^{6.1}		
	N08o	40.9 / 2.3 / 56.8	2.63	1.5 _{1.4} ^{1.6}	>88.3	13.1 _{12.6} ^{14.3}	<26.6	>96.1	0.8 _{0.7} ^{0.9}	<10.3		
	H10o	24.5 / 5.9 / 69.6	6.61	1.1 _{1.0} ^{1.4}	>87.6	>10.0	<5.7	>-0.0	>79.9			
	S15o	40.5 / 0.0 / 59.5	3.09	1.2 _{1.1} ^{1.3}	67.0 _{67.0} ^{67.03}	>15.3	<2.4	>998.6	>4.0			
	S16o	19.8 / 0.0 / 80.2	3.19	0.0 _{0.1} ^{0.1}	>89.2	50.5 _{44.5} ^{51.7}	0.48 _{0.29} ^{0.51}	<0.0	>29.7	>10.8		
	H17o	12.0 / 5.2 / 82.8	6.67	3.2 _{3.2} ^{3.9}	45.0 _{34.0} ^{45.9}	>10.0	>-0.5	>15.0	>45.0	>-0.5	>0.5	>0.7
Mrk520	F06	50.9 / 0.0 / 49.1	1.40	<0.5	14.8 _{10.4} ^{10.4}	>59.9	<0.0	<-1.0	134.0 _{129.4} ^{138.2}	2.0 _{2.0} ^{2.01}		
	N08	7.8 / 6.5 / 85.7	1.59	1.5 _{1.4} ^{1.7}	<10.1	>14.7	>68.8	15.1 _{14.6} ^{15.7}	<0.5	40.0 _{38.9} ^{41.4}		
	H10	14.2 / 6.0 / 79.8	1.83	1.0 _{0.8} ^{1.0}	<0.1	>9.7	20.9 _{16.6} ^{32.2}	>-0.0	>70.2			
	S15	10.6 / 6.4 / 83.0	1.87	<0.5	<22.1	<3.0	>70.3	>961.2	13.5 _{12.8} ^{13.8}			
	S16	27.4 / 0.0 / 72.6	1.70	0.7 _{0.7} ^{1.0}	88.9 _{88.6} ^{89.3}	<10.0	>1.4	<0.0	>29.4	4.4 _{4.2} ^{4.7}		
	H17	8.1 / 7.2 / 84.7	1.73	1.8 _{0.8} ^{0.8}	>89.7	>9.7	>-0.6	>8.9	>40.4	<-2.1	<0.2	>0.6
NGC7172	F06	4.0 / 1.1 / 94.9	13.52	10.2 _{10.3} ^{10.6}	70.0 _{69.2} ^{70.9}	<20.3	<0.5	>-0.0	<10.0	<0.1		
	N08	5.2 / 5.9 / 88.9	13.77	9.2 _{9.1} ^{9.3}	>86.9	1.3 _{2.0} ^{2.0}	37.9 _{36.6} ^{39.3}	<5.0	>2.5	<14.2		
	H10	1.4 / 0.0 / 98.6	14.63	10.2 _{10.3} ^{10.6}	60.4 _{58.5} ^{61.5}	5.0 _{4.8} ^{4.8}	45.0 _{44.1} ^{46.6}	<-2.0	>78.6			
	S15	13.5 / 61.5 / 25.0	38.82	4.2 _{4.0} ^{4.1}	<33.8	6.8 _{6.5} ^{6.5}	>77.6	>984.3	13.5 _{13.49} ^{14.19}			
	S16	30.1 / 69.9 / 0.0	22.16	6.0 _{6.1} ^{6.1}	70.1 _{69.6} ^{70.7}	<10.0	>1.5	>1.3	>29.9	<3.0		
	H17	1.8 / 0.0 / 98.2	11.87	9.7 _{9.6} ^{9.6}	>89.6	7.0 _{6.8} ^{7.1}	<-3.0	>14.7	>44.6	<-2.1	<0.1	>0.7
NGC7212	F06o	95.5 / 0.0 / 4.5	2.84	<0.5	60.0 _{59.4} ^{60.8}	<20.2	<0.0	>-0.0	<10.0	5.5 _{5.2} ^{5.8}		
	N08o•	88.5 / 5.0 / 6.5	1.36	<0.5	>77.5	>13.7	46.9 _{40.2} ^{54.6}	19.9 _{18.8} ^{20.3}	1.02 _{1.09} ^{1.09}	<10.3		
	H10o	67.8 / 6.7 / 25.5	2.15	<0.5	>88.7	>9.2	>59.6	>-0.0	33.8 _{32.8} ^{34.8}			
	S15o	87.3 / 3.7 / 9.0	6.77	<0.5	>85.9	<3.0	8.9 _{8.8} ^{9.0}	30.0 _{29.2} ^{30.4}	13.5 _{13.6} ^{13.6}			
	S16o	87.0 / 2.7 / 10.3	2.03	<0.5	80.0 _{73.9} ^{86.9}	>78.1	<0.1	0.5 _{0.25} ^{0.25}	11.6 _{11.5} ^{11.5}	6.9 _{6.6} ^{7.4}		
	H17o•	83.0 / 0.0 / 17.0	1.80	0.4 _{0.3} ^{0.4}	53.7 _{53.6} ^{53.6}	>9.4	<-3.0	>14.9	>44.8	>-0.5	<0.2	0.6 _{0.58} ^{0.63}
NGC7213	F06o	96.3 / 3.7 / 0.0	6.95	<0.5	10.6 _{10.2} ^{10.2}	<20.1	>6.0	-0.09 _{-0.13} ^{-0.06}	<10.0	6.02 _{5.97} ^{6.4}		
	N08o•	96.4 / 3.6 / 0.0	1.46	0.6 _{0.5} ^{0.6}	65.4 _{64.1} ^{65.9}	12.9 _{11.1} ^{13.9}	17.0 _{15.2} ^{18.3}	9.98 _{9.8} ^{10.04}	0.64 _{0.58} ^{0.72}	<10.1		
	H10	89.0 / 4.9 / 6.0	1.51	<0.5	<2.9	3.0 _{2.7} ^{3.7}	>58.2	>-0.0	35.7 _{33.6} ^{39.7}			
	S15o	92.9 / 6.1 / 1.0	8.15	<0.5	>85.8	<3.0	1.66 _{1.63} ^{1.68}	<0.0	13.5 _{13.5} ^{13.5}			
	S16o	96.3 / 3.7 / 0.0	6.61	<0.5	>88.0	>79.6	<0.0	>1.4	<10.0	<3.0		
	H17o•	90.7 / 4.3 / 5.0	1.37	0.2 _{0.1} ^{0.2}	<0.1	<5.1	-1.21 _{-1.25} ^{-1.15}	<9.2	>33.1	>-0.6	<0.1	<0.2
NGC7314	F06	72.0 / 0.0 / 28.0	1.72	<0.5	61.8 _{60.7} ^{62.3}	<20.3	0.26 _{0.19} ^{0.34}	>-0.0	<10.0	>9.8		
	N08	62.5 / 5.9 / 31.6	0.85	1.0 _{0.8} ^{1.1}	<61.8	>3.9	>45.0	<5.5	>0.2	137.5 _{105.1} ^{186.3}		
	H10	67.4 / 1.4 / 31.1	1.98	1.3 _{1.0} ^{1.4}	30.7 _{22.2} ^{37.4}	>9.6	>56.2	>-0.0	71.5 _{63.4} ^{76.0}			
	S15	64.8 / 4.3 / 30.9	4.75	0.9 _{0.8} ^{1.0}	>85.9	<3.0	2.4 _{2.2} ^{2.5}	<0.0	>44.7			
	S16	66.9 / 0.0 / 33.1	1.60	0.5 _{0.4} ^{0.5}	49.8 _{41.7} ^{53.0}	69.6 _{65.5} ^{71.5}	>1.2	<0.1	<10.4	>10.6		
	H17	58.5 / 6.3 / 35.3	1.07	0.1 _{0.0} ^{0.2}	>88.7	>9.0	>-0.7	>12.9	>43.2	-2.01 _{-2.05} ^{-1.98}	<0.1	>0.7
Mrk915	F06o	97.6 / 1.4 / 0.9	3.90	<0.5	<0.0	<20.4	>5.9	>-0.2	11.9 _{11.7} ^{12.4}	>9.9		
	N08o•	91.5 / 3.9 / 4.6	1.77	<0.5	>65.5	5.6 _{5.3} ^{6.0}	>61.0	10.0 _{9.0} ^{10.3}	>2.5	78.0 _{73.8} ^{88.3}		
	H10	79.2 / 3.4 / 17.5	2.74	<0.5	71.1 _{66.2} ^{73.1}	3.9 _{3.3} ^{4.3}	>52.0	>-0.0	40.4 _{38.5} ^{43.8}			
	S15o	87.9 / 3.1 / 9.0	10.13	<0.5	>85.9	<3.0	7.69 _{7.54} ^{7.73}	<0.0	13.5 _{13.5} ^{13.5}			
	S16o	95.7 / 1.5 / 2.8	3.43	<0.5	20.0 _{19.8} ^{21.1}	>79.7	<0.0	1.32 _{1.25} ^{1.35}	<10.0	>10.4		
	H17	82.1 / 3.2 / 14.8	1.33	<0.5	44.6 _{39.2} ^{42.8}	>9.8	<-3.0	9.7 _{8.9} ^{11.0}	>44.2	>-0.5	<0.1	0.18 _{0.17} ^{0.19}
M+01-57-016	F06o	76.4 / 6.1 / 17.5	1.99	<0.5	10.2 _{10.2} ^{10.7}	<20.7	>5.9	>-0.0	17.6 _{15.6} ^{17.9}	>9.7		
	N08o•	74.6 / 6.6 / 18.8	1.65	<0.5	>87.7	6.7 _{5.8} ^{8.6}	<31.5	17.9 _{15.6} ^{20.3}	1.5 _{1.0} ^{1.0}	36.2 _{28.0} ^{43.2}		
	H10	64.0 / 7.3 / 28.7	1.68	0.1 _{0.3} ^{0.3}	70.9 _{66.0} ^{74.4}	3.2 _{2.7} ^{3.8}	>54.7	>-0.0	>72.5			
	S15	71.0 / 7.3 / 21.7	3.87	0.5 _{0.4} ^{0.5}	>85.9	<3.0	<1.5	2.5 _{2.0} ^{3.2}	>44.6			
	S16	72.3 / 5.9 / 21.8	1.69	<0.5	40.4 _{36.6} ^{42.8}	59.7 _{57.8} ^{60.6}	<0.0	<0.0	<10.3	6.7 _{6.1} ^{7.1}		
	H17	67.1 / 4.8 / 28.0	1.36	<0.5	30.3 _{33.0} ^{33.0}	7.4 _{6.9} ^{7.8}	<3.0	13.5 _{11.9} ^{14.8}	>43.2	>-0.5	0.3 _{0.2} ^{0.4}	>0.7
UGC12282	F06	84.1 / 3.2 / 12.7	2.39	0.3 _{0.3} ^{0.3}	9.9 _{7.1} ^{9.7}	<20.2	5.61 _{5.57} ^{5.65}	>-0.0	<10.0	>9.9		
	N08	81.0 / 5.5 / 13.5	1.35	<0.5	>74.8	>14.0	>56.1	<5.1	>2.4	24.2 _{22.6} ^{26.2}		
	H10	78.5 / 2.3 / 19.1	2.29	0.4 _{0.3} ^{0.4}	>88.0	>9.8	<5.8	-1.8 _{-1.82} ^{-1.79}	>78.8			
	S15	78.1 / 6.5 / 15.4	8.83	0.9 _{0.9} ^{0.9}	>85.9	<3.0	2.6 _{2.5} ^{2.7}	<0.0	13.5 _{13.5} ^{13.54}			
	S16	84.1 / 1.4 / 14.5	3.05	<0.5	>76.6	>79.4	>1.5	1.2 _{1.1} ^{1.4}	<10.0	5.0 _{4.9} ^{6.1}		
	H17	81.5 / 0.0 / 18.5	1.09	0.3 _{0.4} ^{0.4}	45.4 _{44.8} ^{50.0}	<5.1	<3.0	>13.6	>44.6	-1.51 _{-1.53} ^{-1.4}	<0.1	0.45 _{0.41} ^{0.49}
NGC7603	F06	91.1 / 5.1 / 3.8	11.93	0.8 _{0.8} ^{0.8}	40.0 _{35.4} ^{44.5}	<20.1	<0.0	<-1.0	<10.0	0.46 _{0.45} ^{0.46}		
	N08	87.4 / 8.4 / 4.2	13.79	<0.5	>89.6	4.9 _{4.8} ^{5.0}	34.8 _{30.4} ^{35.2}	<5.0	>2.5	<10.0		
	H10	88.7 / 4.0 / 7.3	2.61	<0.5	44.9 _{44.1} ^{45.4}	<2.5	29.9 _{29.2} ^{29.7}	<-2.0	76.7 _{74.6} ^{78.5}			
	S15o	81.1 / 17.8 / 1.1	82.28	<0.5	33.0 _{32.6} ^{33.0}	<3.0	<1.5	<0.0	13.5 _{13.5} ^{13.5}			
	S16o	86.8 / 10.3 / 2.9	25.30	<0.5	<10.3	70.0 _{69.9} ^{70.1}	>1.5	>1.5	<10.0	<3.0		
	H17	91.1 / 2.3 / 6.6	1.26	<0.5	74.8 _{70.0} ^{75.9}	<5.2	<-3.0	<7.3	>42.3	-2.26 _{-2.28} ^{-2.24}	<0.1	0.56 _{0.47} ^{0.62}
UGC488	F06	88.0 / 5.4 / 6.6	4.85	<0.5	<0.0	<20.1	4.0 _{3.8} ^{4.01}	<-1.0	<10.0	3.46 _{3.43} ^{3.49}		
	N08	84.2 / 7.2 / 8.6	1.59	<0.5	>76.9	>14.6	40.0 _{31.3} ^{31.3}	<5.1	>2.5	<10.8		
	H10	82.5 / 5.5 / 12.0	1.72	<0.5	15.0 _{14.7} ^{48.0}	>9.8	<5.7	<-				

Obj.	Mod	A / S / I %	χ^2/dof	$E_{(B-V)}$	Parameters						
	F06				i	σ	Γ	β	Y	$\tau_{9.7\mu m}$	
	N08				i	N_0	σ	Y	q	τ_v	
	H10				i	N_0	θ	a	τ_{cl}		
	S15				i	R_{in}	η	τ_{cl}	τ_{disk}		
	S16				i	σ	p	q	Y	$\tau_{9.7\mu m}$	
	H17				i	N_0	a	σ	θ	a_w	h
											f_w
NGC3147	F06	49.2/ 15.9/ 34.9	1.94	<0.5	>0.0	<43.5	>3.4	>-0.1	50.4 _{42.6} ^{61.1}	<0.1	
	N08	53.0/ 13.8/ 33.3	1.35	<0.5	<75.2	<1.6	<17.4	9.9 _{6.8} ^{11.7}	<1.7	<11.8	
	H10	51.5/ 12.8/ 35.7	1.48	<0.5	<19.3	<2.7	>56.7	-1.25 _{-1.39} ^{-1.17}	<31.7		
	S15	45.6/ 19.7/ 34.7	2.58	<0.5	33.1 _{31.1} ^{37.6}	<3.0	<1.5	<0.0	13.51 _{13.5} ^{13.66}		
	S16	48.9/ 15.5/ 35.6	2.17	<0.5	<21.5	59.2 _{57.2} ^{66.3}	>1.4	>1.4	<10.5	<3.1	
	H17	52.7/ 11.6/ 35.7	1.60	<0.5	<23.4	<5.8	-2.39 _{-2.49} ^{-2.37}	<12.8	<31.9	>-2.5	<0.1 <0.2
E439-G9	F06o	100.0/ 0.0/ 0.0	2.63	0.5 _{0.5} ^{0.6}	<0.0	<21.6	4.76 _{4.68} ^{4.8}	-0.25 _{-0.27} ^{-0.21}	10.5 _{10.4} ^{10.7}	>10.0	
	N08o●	93.1/ 2.7/ 4.3	0.70	0.5 _{0.6} ^{0.4}	>78.5	>14.6	>64.7	7.5 _{6.9} ^{8.0}	1.5 _{1.4} ^{1.6}	20.5 _{19.5} ^{23.0}	
	H10o	80.7/ 0.0/ 19.3	1.88	0.5 _{0.4} ^{0.4}	67.6 _{60.5} ^{72.3}	>8.4	>56.1	>-0.5	<36.7		
	S15o	94.6/ 0.6/ 4.8	6.85	1.3 _{1.3} ^{1.3}	>85.9	<3.0	<1.5	0.4 _{0.3} ^{0.5}	>44.8		
	S16o	94.2/ 0.0/ 5.8	1.49	<0.5	22.5 _{17.1} ^{28.7}	>79.4	>1.2	<0.1	<10.0	>10.1	
	H17o●	84.4/ 0.0/ 15.6	0.89	0.5 _{0.4} ^{0.6}	>87.8	<5.3	-1.66 _{-1.75} ^{-1.61}	>14.3	>44.3	-0.99 _{-0.03} ^{-0.87}	<0.1 0.45 _{0.42} ^{0.48}
Mrk273	F06o	100.0/ 0.0/ 0.0	8.63	1.5 _{1.4} ^{1.7}	1.9 _{1.2} ^{11.6}	>59.9	4.1 _{4.0} ^{4.2}	>-0.0	>149.6	7.3 _{7.6} ^{7.6}	
	N08o	34.7/ 14.6/ 50.7	11.03	4.4 _{4.4} ^{4.5}	<0.0	>15.0	55.0 _{54.9} ^{55.1}	80.2 _{79.6} ^{81.9}	<0.1	60.0 _{59.4} ^{60.7}	
	H10	3.2/ 14.7/ 82.1	20.26	8.0 _{8.0} ^{8.0}	<0.0	>10.0	<5.1	>-0.0	>80.0		
	S15o	31.1/ 5.5/ 63.3	11.39	5.4 _{5.3} ^{5.9}	43.2 _{42.0} ^{48.5}	>15.4	>77.4	>990.1	7.45 _{7.36} ^{7.61}		
	S16o	28.3/ 0.0/ 71.7	12.46	4.1 _{4.2} ^{4.2}	>89.9	20.6 _{20.5} ^{20.7}	<0.0	<0.0	>29.9	>11.0	
	H17o	1.9/ 0.0/ 98.1	22.92	10.0 _{9.9} ^{10.0}	22.1 _{21.8} ^{22.7}	>10.0	>-0.5	>14.9	>44.9	>-0.5	>0.5 >0.7

Table 4. Spectral fit results (continuation).**B. PARAMETERS FOR THE FULL SAMPLE**

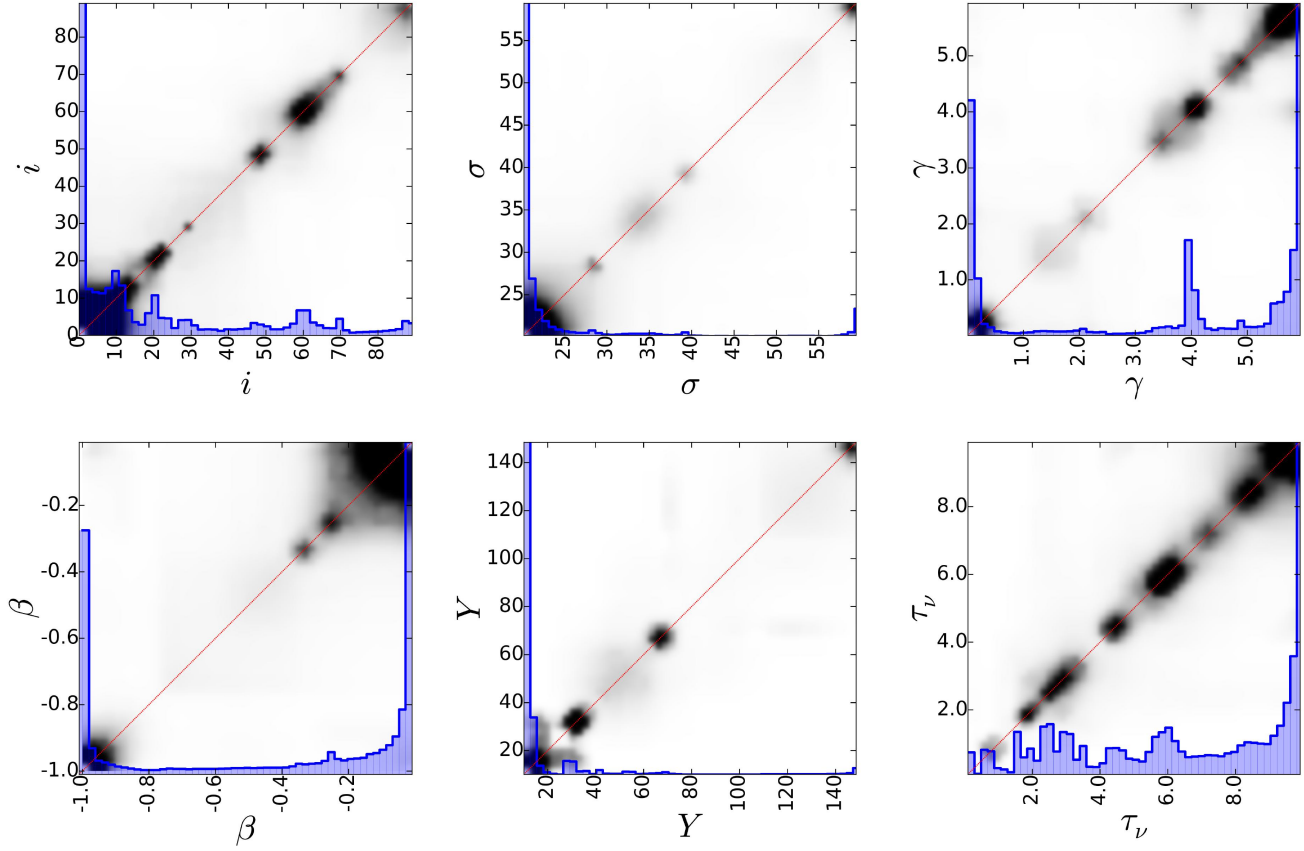


Figure 14. Parameter versus parameter estimated from the sample drawn from the PDF (see text) for the model [Fritz06]. The blue histogram shows the total distribution for each parameter.

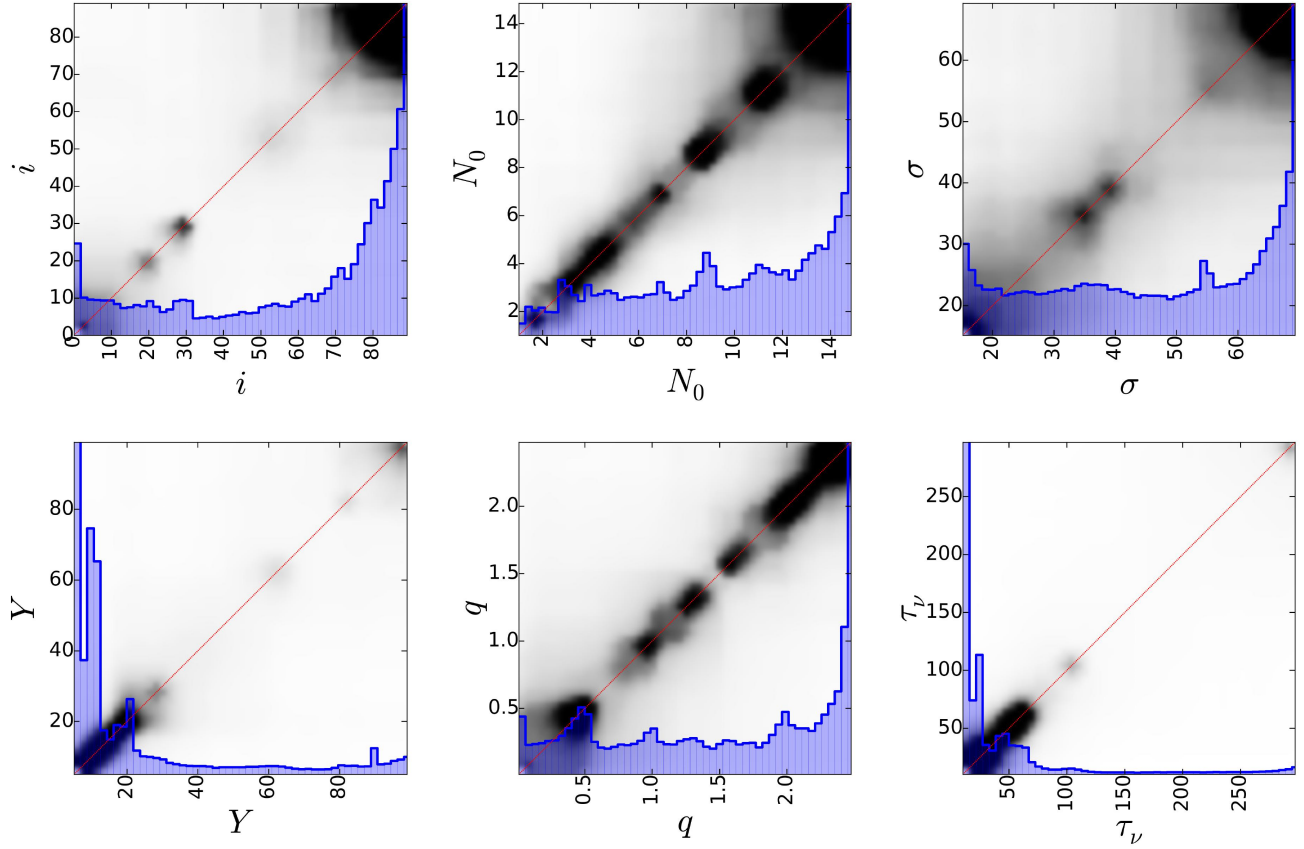


Figure 15. Parameter versus parameter estimated from the sample drawn from the PDF (see text) for the model [Nenkova08]. The blue histogram shows the total distribution for each parameter.

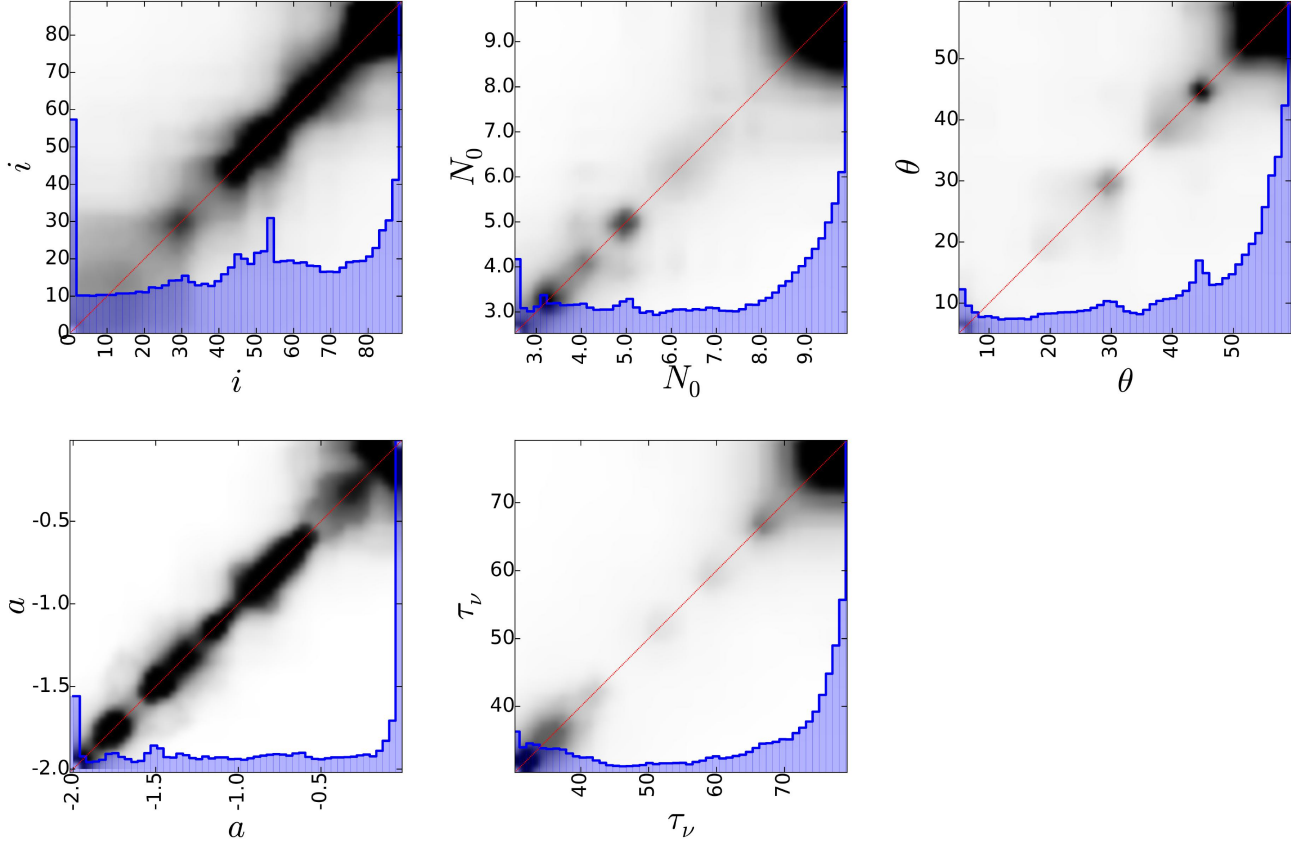


Figure 16. Parameter versus parameter estimated from the sample drawn from the PDF (see text) for the model [Hoenig10]. The blue histogram shows the total distribution for each parameter.

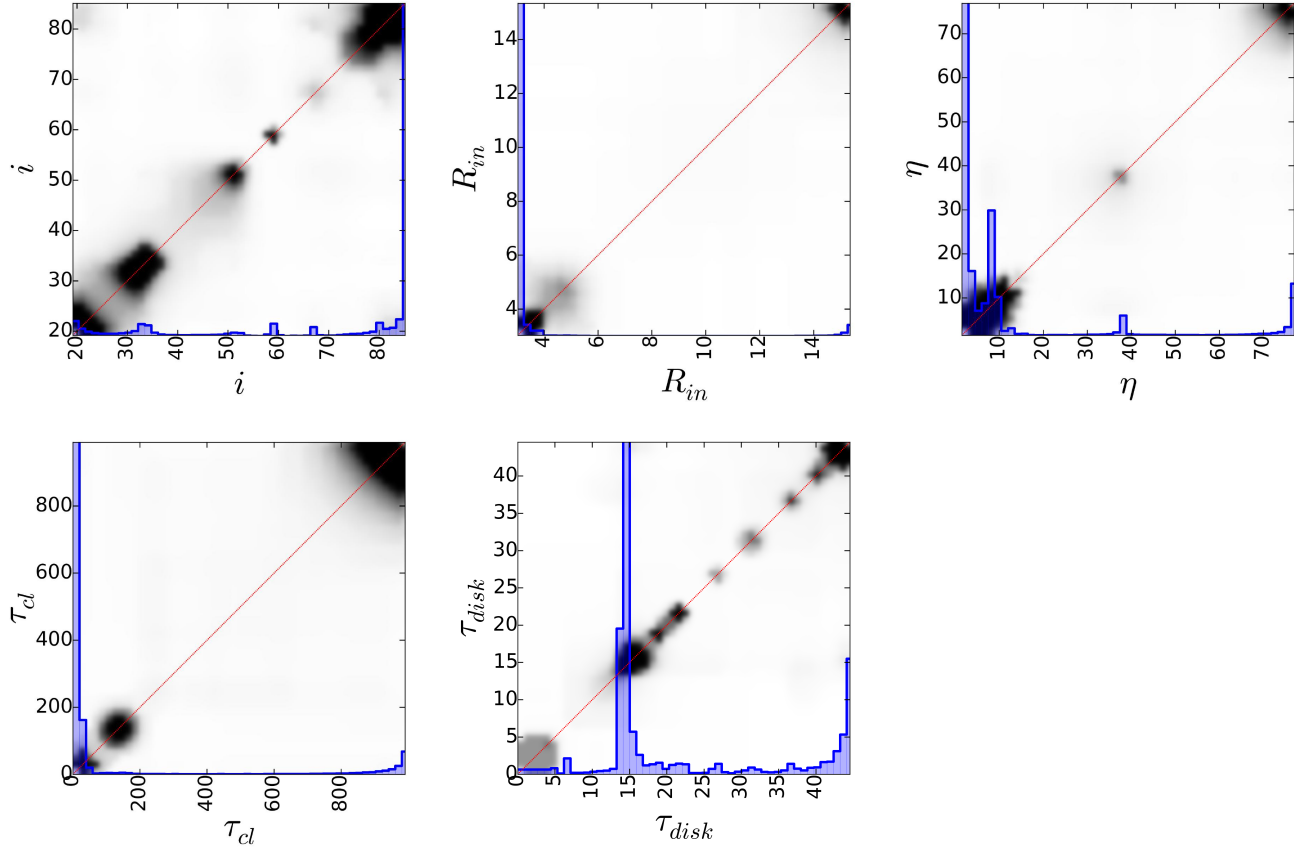


Figure 17. Parameter versus parameter estimated from the sample drawn from the PDF (see text) for the model [Sieben15]. The blue histogram shows the total distribution for each parameter.

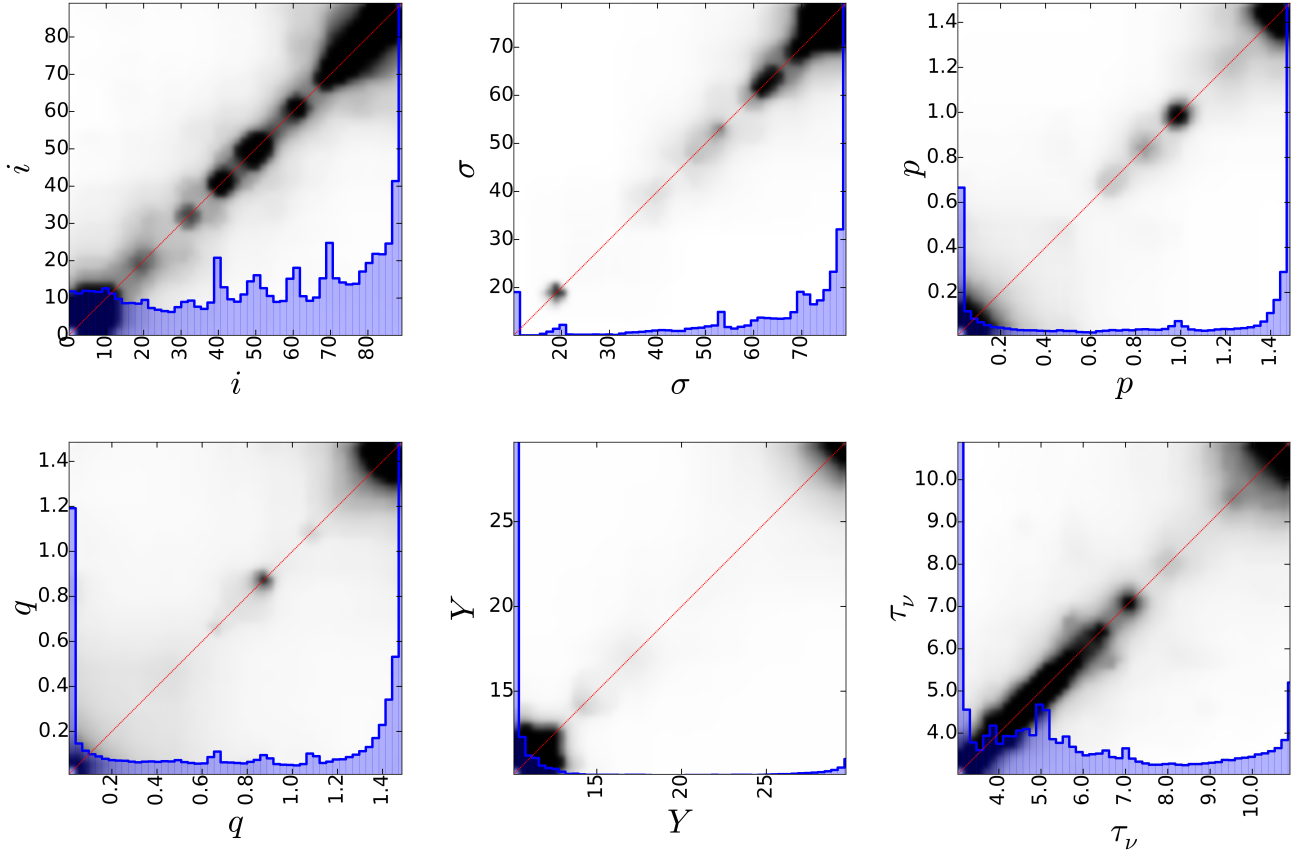


Figure 18. Parameter versus parameter estimated from the sample drawn from the PDF (see text) for the model [Stalev16]. The blue histogram shows the total distribution for each parameter.

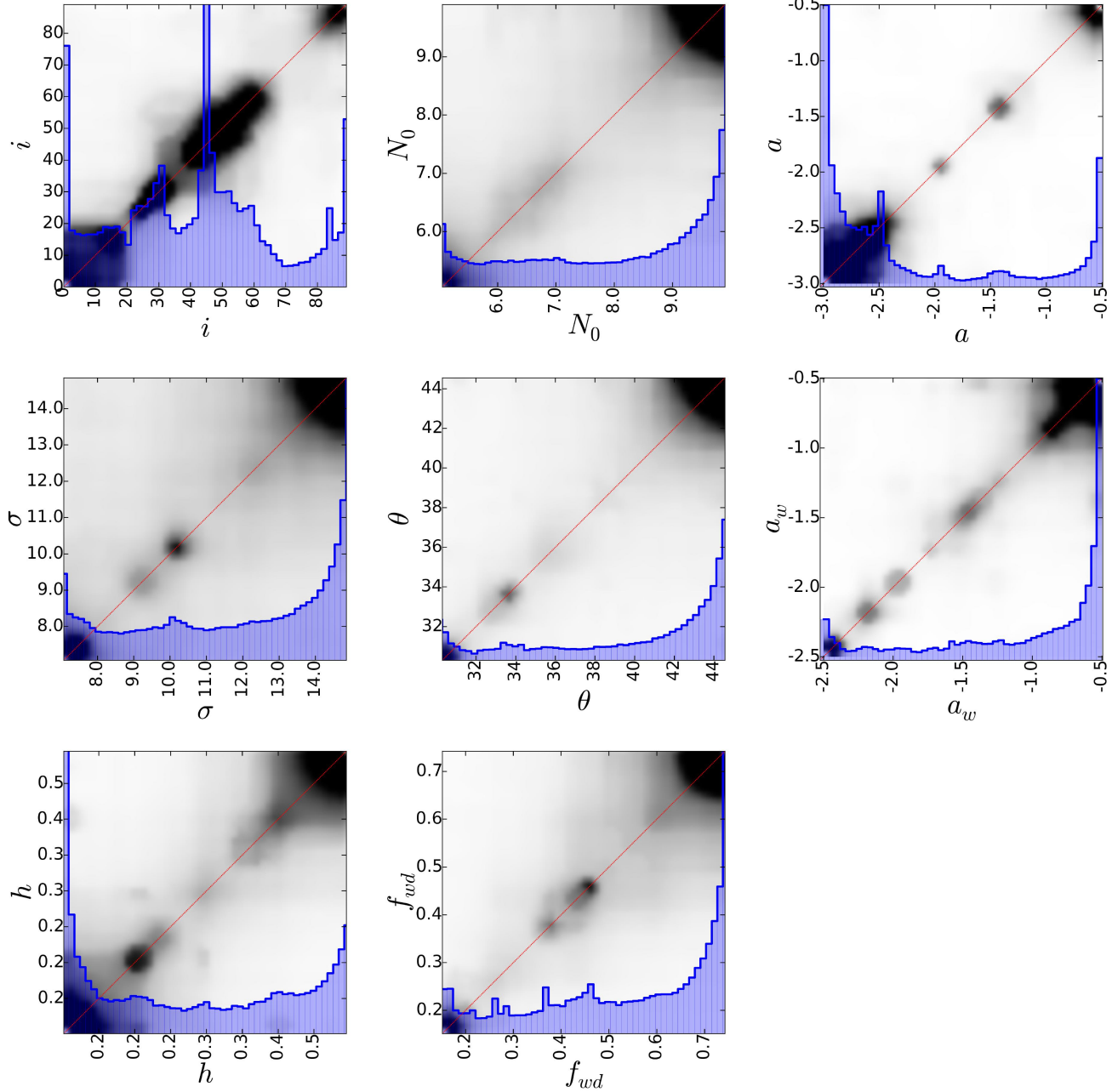


Figure 19. Parameter versus parameter estimated from the sample drawn from the PDF (see text) for the model [Hoenig17]. The blue histogram shows the total distribution for each parameter.